5-2024

Harnessing Nature's Building Blocks: Exploring Sustainable Biomass for Polymer and Composite Materials

Kavan Sheth
kavans@clemson.edu

HARNESSING NATURE'S BUILDING BLOCKS: EXPLORING SUSTAINABLE BIOMASS FOR POLYMER AND COMPOSITE MATERIALS

A Dissertation
Presented to
the Graduate School of
Clemson University

In Partial Fulfillment
of the Requirements for the Degree
Doctor of Philosophy
Automotive Engineering

---

by
Kavan Sheth
May 2024

Accepted by:
Dr. Srikanth Pilla, Committee Chair
Dr. James Sternberg
Dr. Craig Clemons
Dr. Morteza Sabet
Dr. Hongsoek Choi

ABSTRACT

The automotive industry has been actively pursuing lighter and more fuel-efficient vehicles to address rising emissions and challenges associated with global warming. Polymers such as polyamides, polyolefins, and polyesters play a crucial role in reducing the weight of structural components while maintaining required safety standards. However, this transition has inadvertently made the automotive sector one of the largest contributors to plastic waste generation. Plastic waste presents a significant challenge due to its chemically inert nature, leading to its persistence in the environment and the leaching of toxic chemicals over hundreds of years. Scientists and lawmakers have been tackling this issue through research and policy initiatives. Additionally, the source of these polymers has come under scrutiny due to depleting petroleum reserves and growing health hazards associated with the chemicals used in their synthesis.

To address these concerns, researchers have explored sustainably sourced feedstocks for polymer synthesis and composite fillers. One promising feedstock is lignocellulosic biomass, which consists of lignin, cellulose, and hemicellulose. By carefully modifying these feedstocks chemically, it is possible to obtain high-value fillers and polymeric materials.

This research focuses on utilizing biobased feedstocks, like cellulose for polymer filler applications, and specifically lignin extracted directly from wood, as a precursor for polyamides and polyesters. The study centers on functionalizing lignin to create polymer precursors and modifying cellulose to generate fillers for composites. The resulting polymers and composites are then subjected to thermal, chemical, viscoelastic and morphological testing, allowing for a comparison with commercially available counterparts.

Central to this work is the integration of green chemistry principles at every stage of the chemical process, aiming for a sustainable future in polymer synthesis. By adopting this approach,

the research seeks to contribute towards a more environmentally friendly and responsible automotive industry.

ACKNOWLEDGEMENTS

In the crafting of this dissertation, my heartfelt appreciation first and foremost goes to Dr. Srikanth Pilla, whose unwavering support and motivation have been pivotal throughout this journey. His patience, guidance, and encouragement have not only shaped this research but have also been a source of personal inspiration.

I extend my sincere thanks to the members of my dissertation committee: Dr. James Sternberg, Dr. Craig Clemons, Dr. Hongseok Choi, and Dr. Morteza Sabet. Their insightful feedback and guidance were instrumental in deepening and broadening the scope of my research, pushing me to explore and engage with my subject matter in more meaningful ways.

I am equally grateful to current and past members of Dr. Pilla's research group - Kavya, Vitasta, Dr. Ting Zheng, Amit, Dr. James Sternberg, and Olivia. Their theoretical insight and practical assistance have been invaluable at every stage of my work. The camaraderie and support of these fellow lab members have been essential to my progress, and it is fair to say that the completion of this project would have been much more challenging without their contributions.

On a personal note, the enduring support and motivation from my family have been the backbone of my resilience and persistence throughout this academic endeavor. Their belief in me has been a constant source of strength and encouragement.

To all mentioned and unmentioned who contributed to this journey, I extend my deepest gratitude. Your collective wisdom and support have been the pillars upon which this work stands.

TABLE OF CONTENTS

LIST OF FIGURES

LIST OF TABLES

CHAPTER ONE:

BIOMASS FOR THE SYNTHESIS OF POLYMERS AND COMPOSITES

1.1 Introduction

Petroleum based fuels and chemicals have taken a toll on the environment not just in terms of global warming, but also in terms of the harmful effects of the toxic substances involved [1]. The world heavily relies on these chemicals and materials to meet the ever-increasing performance requirements of modern applications. It is imperative that the world will continue relying on products of the chemical industry be it for advancement or comfort. In order to meet this necessity and reliance, it is becoming increasingly important to develop a chemical industry that not only thinks about the final properties of synthetic materials, but also incorporates thoughts into the production process of these chemicals, while keeping in mind the adverse consequences of the said chemicals. In today's chemical industry, manufacturing is conducted in a linear model where feedstocks, primarily sourced from fossil fuels and limited in quantity [2]. This manufacturing process relies on the use of toxic and reactive reagents that endanger not only the workers but also the environment if they are ever released. These manufacturing processes are prone to waste production which can be toxic in nature, environmentally persistent, and prone to bioaccumulation [3]. Specialty chemicals and pharmaceuticals produce waste many time in excess of the desired product (up to 100-fold) [4]. Moreover, the resulting chemical products are typically engineered for their intended use without comprehensive assessments of potential hazards, relying instead on situational controls. This lack of assessment tools and models has historically led to numerous unintended negative consequences (endocrine effects of BPA,

bioaccumulation of PFAS, etc.). The polymer industry is a subset of the larger chemical industry that is plagued by the exact same set of problems.

The touted alternative to liner processes lies in 'Circular Processes' which essentially are products designed for end-of-life recyclability creating an endless loop of use-recycle instead of use-throw [5–8]. There are multiple ways in which the current plastics industry can be challenged and improved in terms of sustainability. The most important change required for a sustainable plastics industry is the switch from petroleum-based feedstocks to renewable feedstocks. The use of benign and non-toxic chemicals should accompany the use of renewable feedstocks. The chemical processes/reactions should follow the principles of green chemistry focusing on atom, step and solvent economy [9]. The end goal of such a plastic industry is maximizing performance by minimizing hazards and maximizing function.

Table 1 Linear vs Circular Plastics Industry [10]

Linear Plastics Industry	*Circular Plastics Industry*
Fossil feedstocks	Renewable feedstocks
Reactive, persistent, or toxic chemical reagents and products	Benign chemical reagents and products
Covalent bonds	Weak, noncovalent interactions
Catalysis using rare metals	Catalysis using abundant metals, enzymes, photons, or electrons
Conventional solvents	Low toxicity, recyclable, inert, abundant, easily separable green solvents or solventless
Large "waste" volume	Atom-, step-, and solvent-economical processes
Material- and energy-consuming isolation and purification	Self-separating systems
"Waste" treatment	"Waste" utilization
Design exclusively for use phase with reliance on circumstantial control	Intentional molecule design for full life cycle

Performance = maximize function	Performance = maximize function + minimize hazards
Maximum chemical production for increased profit	Maximum performance with minimal benign material uses for increased profit

This body of work addresses the highlighted solutions in order to achieve a sustainable plastics economy. In order to move to a circular economy, especially for polymers, a lot of focus should be placed on the feedstocks necessary to produce the chemicals. The challenge of producing materials not sourced from petroleum in addition to meeting high performance requirements for modern applications is a challenge in itself [11]. Modern policy and research discourse has been shifting towards a more sustainable future with reduced emissions, sustainably sourced feedstocks, non-toxic chemicals, and end of life waste management strategies [12]. There have been efforts to replace petroleum-based fuel with biomass-based fuel, and efforts to replace combustion completely [13]. In the field of polymeric materials, there has been a steady increase in the demand and supply for biobased polymers. Global bioplastics production capacities are set to increase by 386% over the next 5 years [7]. There are multiple ways of harnessing biobased chemicals included but not limited to Lignocellulosic biomass feedstock is one of the most promising sources of carbon to replace petroleum [14]. There is around 180 million tons of lignocellulosic feedstock available yearly. However, the current state of refining biomass does not allow completely and efficient utilization of the biomass [15,16]. The historical background of biologically producing commodity chemicals is significant. From 1945 to 1950, a substantial portion of n-butanol (66%) and acetone (10%) in the United States were manufactured through fermentation of molasses and starch. Additionally, various other commodity products like acetic acid, citric acid, lactic acid, and itaconic acid were also

produced through fermentation during the first half of the 20th century. However, the practice of fermentative production declined due to the rise in sugar feedstock prices and the decrease in petrochemical feedstock prices. On top of economics, there are multiple reasons for incomplete and inefficient use of biomass, namely, lack of an integrated petroleum like refinery, complex chemical structure of the three biopolymers (Cellulose, Hemicellulose, and Lignin). Setting up a biorefinery is a huge technical challenge that would require significant capital investment and research efforts [6].

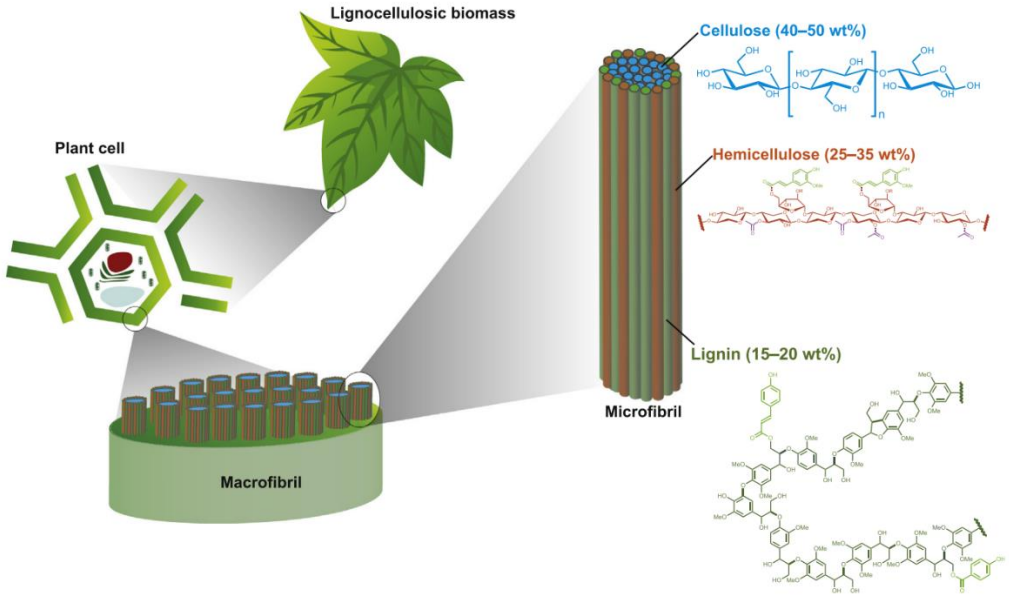

Figure 1. Lignocellulosic Biomass [17]

The biomass valorization research community has been focusing on creating fuels and chemicals from cellulose and hemicellulose for the purpose of transportation and other industries [18–21]. An ideal biomass valorization would ensure complete utilization of the building blocks of biomass including cellulose, hemicellulose and lignin.

There are numerous processes (chemical, enzymatic, and thermal) that can transform cell-wall polymers like lignin, cellulose, and hemicellulose into value-added small molecule compounds including aromatic compounds and carbohydrate derivatives [14]. Cellulose and hemicellulose can be valorized to sugars which can be further

chemically modified to yield valuable chemicals like glycerol, ethanol, fumaric acid, furfural and gluconic acid.

To foster a truly global bio-based circular economy that leverages lignocellulosic biomass as a resource, it is essential to tap into the value of lignin not only for energy production but also for chemical production [15]. Despite extensive research over the years, fully realizing the potential of lignin remains a formidable challenge but is increasingly critical for sustainability. The global research community is vigorously exploring various methodologies to valorize lignin, motivated by the pressing need for a sustainable carbon economy. A focal point of interest is the development of "lignin-first" biorefining techniques, which emphasize the valorization of lignin alongside carbohydrates during the processing of lignocellulosic biomass [16,22].. This approach involves the use of active stabilization methods to dissolve lignin from the biomass without causing condensation reactions that produce more resistant lignin polymers. The objective of lignin-first strategies is to optimize the use of lignocellulose by integrating lignin valorization from the outset of biorefining process design. Achieving this through solvolysis, catalytic conversion, or the application of protection-group chemistry to lignin oligomers or reactive monomers is pivotal for the economic success of lignocellulosic biorefineries, ensuring a more comprehensive utilization of biomass.

1.2 Overview of Research Tasks

This dissertation aims to tackle the challenges identified earlier by leveraging the valorization of lignocellulosic biomass, guided by lignin-first principles. This novel approach encompasses the utilization of cellulose-based fillers for polymers and the incorporation of lignin as a pre-polymeric material in the synthesis of diverse polymer

classes. Such materials are anticipated to have significant implications for high-value applications, particularly within the automotive sector.

In Chapter 3, the focus shifts to the development of a hybrid filler for a specific biopolymer, PHBV, and introduces the pioneering effort of foaming PHBV using nitrogen gas within a batch foaming setup. The preparation of hybrid nanofillers through the functionalization of crystalline nanocellulose is detailed, alongside a comprehensive analysis of the fillers' chemical properties utilizing XPS and FTIR techniques. Additionally, the influence of these fillers on the thermal, mechanical, viscoelastic, and morphological properties of PHBV is investigated through TGA, DSC, tensile testing, rheology, and SEM analyses. Both neat PHBV and its composites are subjected to foaming using supercritical nitrogen to assess the effects.

Following the innovative creation of cellulose-based fillers, Chapter 4 delves into the extraction and functionalization of lignin to forge a pre-polymeric material suitable for polyamide synthesis. Utilizing reductive catalytic fractionation—a cornerstone method of lignin-first biorefining—the extracted lignin is functionalized employing eco-friendly reagents and solventless processes. This functionalization process is thoroughly examined through NMR, GPC, GC, FTIR, DSC, and TGA. Subsequently, the functionalized lignin oil undergoes polymerization via direct solvent-based polycondensation, with the resultant polymers analyzed for their thermal, chemical, and viscoelastic properties.

Chapter 5 expands on the successful application of functionalized lignin oil by exploring a new class of polymers: unsaturated polyester resins. Given lignin oil's high monomer content alongside a significant fraction of dimers and oligomers—endowing it with polyfunctional capabilities—this chapter posits its suitability for forming polymeric

thermosetting networks. Polyurethanes and epoxies have been extensively explored in literature as thermosetting polymers from lignin. The study aims to introduce unsaturated polyesters as another class of thermosetting polymers derived from lignin. The functionalization process mirrors that of Chapter 4 but employs ethylene carbonate as the reagent. The analysis of this functionalization, as well as the properties of the cured polyester, is conducted using NMR, GPC, FTIR, DSC, TGA, and DMA.

Collectively, these research chapters underscore the potential of lignocellulosic biomass in the synthesis of polymers and composites, leveraging biorefinery products. The literature review that follows provides an in-depth examination of functionalization techniques for cellulose, the effects of hybrid cellulose fillers on PHBV, and the innovative utilization of lignin in the synthesis of polyesters and polyamides. This body of work advocates for the direct use of lignin in polymer synthesis, exploring a variety of chemical methodologies.

CHAPTER TWO:

LITERATURE REVIEW

2.1 Chemical Structure of Lignocellulosic Biomass

Before understanding the use of lignocellulosic biomass in polymeric materials, it is necessary to understand the chemical structure of lignocellulosic biomass. As stated earlier, it is primarily comprised of plant cell walls. Three biopolymers in varying ratios make up almost all lignocellulosic biomass. Namely, cellulose, hemicellulose, and lignin [23]. Cellulose is a carbohydrate network that forms the structural framework for plant cell walls. Hemicellulose is also a carbohydrate polymer, while lignin is an aromatic polymer. Depending on the species, the ratios of these building blocks change, and the ratio of the sub-building blocks[24] .

Cellulose is the largest available source of biocarbon on earth. Lignocellulosic biomass can be viewed as a composite with hemicellulose and lignin as the matrix and the cellulose as the reinforcement. Cellulose is a homopolymer of β-d-glucopyranose ($C_6H_{12}O_6$) units that are interconnected through β-(1–4)-glycosidic linkage [21]. The chemical structure of cellulose exists in the chair conformation with three equatorial hydroxyl groups. The condensation of β-d-glucopyranose molecules with the elimination of water, leads to the formation of the monomeric cellulose unit ($C_{12}H_{22}O_{11}$). The monomeric unit contains three hydroxyl groups capable of being functionalized. These hydroxyl bonds are also responsible for strong hydrogen bonding with the matrix as well amongst the cellulose chains itself. These hydrogen bond linkages are what cause cellulose to exhibit a crystalline character.

Hemicellulose is a complex group of polysaccharides that, along with cellulose and lignin, is one of the main components of plant cell walls. Unlike cellulose, which is composed solely of glucose units, hemicellulose consists of a mix of different sugars, making it heterogeneous in structure. The composition and structure of hemicellulose can vary significantly between different types of plants, but it generally serves to cross-link cellulose fibers, contributing to the structural integrity and flexibility of the cell wall. Hemicellulose, a crucial component of plant cell walls, exhibits a complex mix of polysaccharides that significantly varies in structure and composition among different plant species and environmental conditions. This diversity is essential for the functionality and interaction of hemicellulose within the cell wall, influencing plant physical properties and their utility in industrial applications, notably in bioproduct development from lignocellulosic biomass. Among the four principal hemicellulose compositions—xylans, mannans, β-glucans, and xyloglucans—xylans and mannans stand out for their relevance in lignocellulosic bioproducts. Xylans, predominantly found in hardwood and herbaceous plants, feature a β-1→4 D-xylopyranose backbone with branches containing various sugars and modifications, enabling diverse interactions within the cell wall. Mannans, prevalent in softwoods, vary more in their backbone composition, with galactomannans and glucomannans presenting backbones of D-mannopyranose and mixed D-glucopyranose and D-mannopyranose, respectively. These mannans often feature branching with galactose as a primary component. Within the lignocellulosic matrix, hemicellulose chains form a network structure through random coil configurations and interpolymer contacts, embedding cellulose and lignin components.

To produce high-quality, high-performance materials from lignin, a detailed understanding of the chemical structure of both lignin and lignin oil is crucial. Lignin is considered a redox biopolymer composed of aryl propane structural units [25]. Specifically, lignin is formed through the oxidative coupling of three major hydroxycinnamic alcohols (p-coumaryl, coniferyl, and sinapyl). The phenyl propane units within the lignin molecule differ in terms of the quantity and nature of substituents in aromatic rings and are classified as H, G, and S units, representing p-hydroxyphenyl, guaiacyl, and syringyl units, respectively [26]. These aromatic units are linked by various chemical linkages, with the β-O-4 linkages being the most prevalent and extensively studied in the context of lignin depolymerization.

Table 2 Chemical Linkages in Lignocellulosic Biomass [27]

	Lignin	*Hemicellulose*	*Cellulose*
Subunits	Guaiacylpropane (G), Syringylpropane (S), p-Hydroxyphenylpropane (H)	D-Xylose, mannose, L-arabinose, galactose, glucuronic acid	D-Pyran glucose units
Bonds between the subunits	β-O-4 ether bond, β- β carbon bond, β-5 ether linkage, 4-O-5 ether bond	β-1,4-Glycosidic bonds in main chains; β-1.2-, β-1.3-, β-1.6-glycosidic bonds in side chains	β-1,4-Glycosidic bonds

2.2 Functionalization of Cellulose

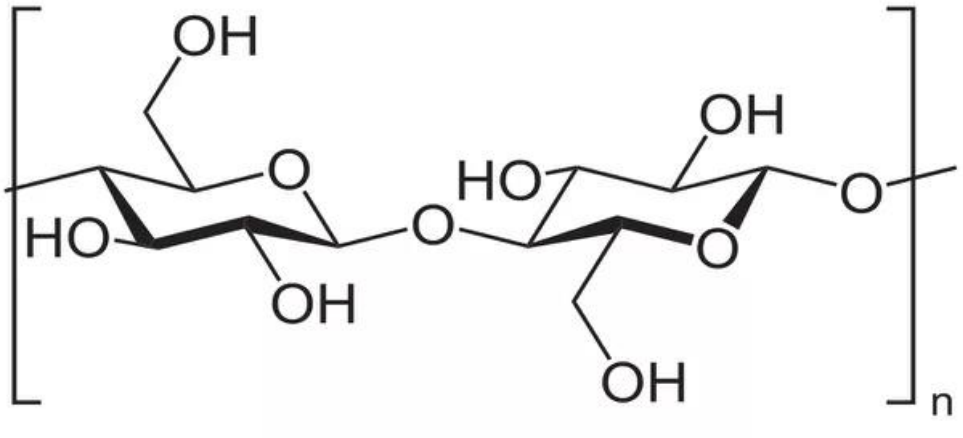

Figure 2 Chemical Structure of Cellulose

Keeping these chemical properties in mind, the extraction and purification of cellulose is a field in itself [28]. Nanocelluloses extracted from bacterial and lignocellulosic sources have lengths varying in the micro and nano scale and a diameter ≤ 100 nm [29]. The source and method of nanocellulose extraction influences the final properties including chemistry, aspect ratio, crystallinity, and surface morphology [30].

Despite varying extraction methods nanocellulose shows very interesting properties like biocompatibility, renewability, and reactivity towards functionalization. Mechanically it has been shown to be lightweight, possess tensile strength, high stiffness, strength to weight ratio, low thermal expansion coefficient, and optical transparency [31].

Nanocellulose that is synthesized by the top-down approach can generally be classified into cellulose nanocrystals (CNCs) and cellulose nanofibers (CNFs) [32]. It has been reported that the physical and mechanical properties of CNCs are superior to CNFs. The figure below shows all possible methods for functionalization of CNCs. Below is a review of surface modifications of CNCs that have been used as filler and reinforcements in polymer matrices.

Figure 3 Surface modification of cellulose nanocrystals [33]

2.2.1 Acetylation

Acetylation is a process of introducing acetyl groups via ester bonds onto hydroxyl groups of CNCs. Acetyl are used to improve the hydrophobicity of the CNCs in order to improve compatibility with polymer matrices. Lee and co-workers carried out acetylation by introducing acetic anhydride in a solution of well dispersed powdered CNCs in DMF. [34].

On the other hand, another team, led by Xu, tried a different method that accomplishes two things at the same time: it breaks down the cellulose into nanocrystals and makes them water-repellent. They started with a type of cellulose that had been treated with an alkali solution (referred to as Na-Cellulose) and applied a traditional acetylation technique directly to it. This resulted in the creation of rod-shaped particles, with lengths varying from 21 to 140 nanometers and widths from 12 to 20 nanometers. These dimensions were confirmed using a technique called TEM. After this process, the CNCs not only became more resistant to water but also showed an improvement in their ability to withstand heat [34].

2.2.2 Carbamation

Carbamation using isocyanates can be an effective way of utilizing and functionalizing the hydroxyl groups on CNCs. Depending on the nature of the isocyanate utilized, they can either be used to graft hydrophobic aliphatic chains via single isocyanate bonds. Utilizing diisocyanates as linkers any species of choice can be grafted onto CNCs. Chemicals with single isocyanate groups like 3,5-dimethylphenyl isocyanate, n-octadecyl isocyanates (OI) can be utilized as surface modifying agents to incorporate hydrophobicity onto CNC surfaces [35]. Toluene diisocyanate (TDI), methylene dipheyl diisocyanate (MDI), isophorone diisocyanate, Methylenebis(Cyclohexyl Isocyanate) have been utilized as diisocyanates to graft reactive isocyanate groups on CNCs. Abushammala et al employed 2,4-toluene diisocyanate as a modifier and linkers, along with triethylamine (TEA), for the carbamation of CNCs. They observed a higher reactivity of the para-isocyanate group with the groups of CNCs compared to the ortho-isocyanate group present on 2,4-TDI. These free isocyanate groups could be utilized further to graft hybrid species

on to the surface of the CNCs. They have also published a highly impactful review on the carbamation of cellulose [36,37]. Further modifications to cellulose nanocrystals (CNCs) reportedly enhanced their dispersion within a polyurethane matrix, as observed through polarized microscopy. In parallel, Guo and colleagues functionalized CNCs with OI, facilitating their application as emulsifiers for water/oil mixtures. The biggest drawback to utilizing isocyanates along with CNCs is the detrimental effect of water on the carbamation reactions.

2.2.3 Esterification

Esterification is a versatile process used to introduce organic functional groups onto CNCs. The hydroxyl groups on the CNCs can be used in an esterification/acetylation reaction using carboxylic acids, acid anhydrides and acid chlorides. Because of the low reactivity of carboxylic acid groups towards esterification reactions at mild conditions, acid derivatives like acid chlorides and acid anhydrides are used to introduce ester bonds on the CNC hydroxyl groups. For instance, Cellante et al. used Fischer esterification to link a chlorotoxin-Cyanine peptide, resulting in excellent biocompatibility [38]. Similarly, Leszczyńska et al. surface-modified CNCs using succinic anhydride, leading to improved surface characteristics, dimensions, and thermal properties [39]. Shen et al. esterified CNCs with diethylenetriamine pentaacetic dianhydride to enhance the anchoring rate of Mn2+ for MRI tumor detection, offering higher biocompatibility and specific area compared to conventional manganese particles doped nanomaterials [40]. In composite materials, esterification with fatty acid chains made the CNCs hydrophobic and improved dispersion. However, due to the lack of strong covalent interactions with the matrix, the tensile properties did not show significant improvement. In summary, esterification, primarily

utilizing anhydrides, has been applied for various purposes, including hydrophobicity, biocompatibility, and dispersion in composites [41].

2.2.4 Silanization

Silane coupling agents are widely used in composites for their adhesive properties and commercial availability. These agents contain active chemical functionalities capable of forming covalent or van der Waals interactions with different chemical groups in polyme composites. Silanization imparts hydrophobic characteristics to the CNCs' surface, enhancing their dispersibility in low-polarity organic solvents, and in hydrophobic polymer matrices. Silanization typically involves two stages: hydrolysis of the silane coupling agent to silanol and subsequent condensation with OH groups on CNCs. However, silanization has drawbacks such as low graft percentage and limited improvement in mechanical properties [42].

2.2.5 Hybrid Fillers in context of PHBV

Hybridization via graft copolymerization is a highly effective strategy for enhancing interfacial interaction and dispersion between nanocellulose and the polymer matrix. By carefully selecting graft species and lengths, favorable outcomes can be achieved in the final polymer [43]. Numerous studies have focused on grafting polymers onto the surface of nanocellulose to limit phase separation, enable stress transfer, improve dispersion, and enhance miscibility. For example, Chen et al. grafted epsilon Caprolactone and palmitoyl chloride, resulting in two different fillers [44]. Nanocellulose grafted with caprolactone increased the tensile strength of the composite at a 1% loading [45]. My research group grafted glycidyl methacrylate onto PHBV but observed minimal improvements in tensile strength [46]. Yu et al. attempted grafting PHBV onto cellulose

using carbamation chemistry, reporting improvements in thermal degradation and hydrophobicity [47]. In a recent study, Han et al. grafted hyperbranched polyesters onto nanocellulose, leading to significant enhancements in toughness and tensile strength for PHBV/PEBE blends [48]. Another study grafted PHBV onto cellulose nanocrystals, resulting in improved tensile strength, stiffness, elongation at break, and thermal degradation [49]. Grafting graphene oxide onto CNCs also improved the tensile strength and elongation at break of PHBV composites [50]. Additionally, bifunctional rosin-nanocellulose fillers showed a 108% increase in tensile strength and a 44% improvement in elongation at break for PHBV composites [51]. In conclusion, selecting a graft polymer that improves dispersion and interacts well with the matrix is crucial. Hybrid fillers have been shown to improve PHBV performance considerably and choosing the right filler and right chemistry might be key to making PHBV a viable biopolymer alternative. The chemistry of graft polymerization plays a key role in producing high-value fillers from nanocellulose. There are opportunities to incorporate synthetic polymerization techniques onto nanocellulose's hydroxyl groups for grafting high-performance polymers onto cellulose.

Table 3 Hybrid nanocellulose fillers for PHBV composites

Polymer	Graft Species	Graft Chemistry	Tensile Strength	Modulus	Elongation at Break	Reference
PHBV	polycaprolactone	Ester	26%	-	-	[44]
PHBV	GMA	Free radical	-4.5%	-3%	13%	[46]
PHBV	PHBV	Isocyanate	-	-	-	[47]
PEBE	HBP	Esterification	31.8%	-	210%	[48]
PHBV	PHBV	Isocyanate	113%	95%	17%	[49]
PHBV	GO	Isocyanate	170%	137.5	52.1%	[50]
PHBV	Rosin	Ester	107.9%	79%	43.9%	[51]

2.3 Condensation Polymers from Lignin

The primary challenge associated with lignin utilization is its large macromolecular structure, which makes it resistant to depolymerization. Despite having reactive groups, the steric hindrance caused by lignin's structure poses difficulties [52]. Moreover, the structure of lignin varies significantly depending on the type of wood it is extracted from. Softwood, for instance, contains a higher lignin content but yields lower monomer content upon depolymerization [53]. Nonetheless, isolated lignins contain both aliphatic and aromatic hydroxyl groups. These hydroxyl groups after adequate characterization can serve as polymerization sites to create lignin-based macromonomers.

Lignin has been successfully employed as a macromonomer in the synthesis of various polymers, including polyurethanes, polyesters, epoxies, vinyl resins, and phenolic [54–59]. With advancements in depolymerization techniques, the utilization of lignin as a starting point offers an interesting strategy to simultaneously extract, depolymerize, and stabilize lignin monomers. The resulting product is commonly known as lignin oil, a hydrophobic, brown viscous liquid that is soluble in common organic solvents. Furthermore, a significant fraction of lignin oil comprises phenolic monomers. The choice of catalyst in the process can influence the nature of the final monomers. For example, a study by Van den Bosch et al. demonstrated that switching the catalyst from Ru/C to Pd/C led to the formation of monomers with two hydroxyl groups, which can be further functionalized for polymerization [60].The same functionalization techniques applied to macromolecular lignin can be applied to monomeric lignin oil.

Upton and Kasko published a significant review on polymeric materials derived from lignin [61], which has served as a foundation for subsequent studies that have

expanded on their work to develop polymeric materials from lignin and lignin oil. The sections below focus on the synthesis of polyesters and polyamides from lignin and other biomass sources.

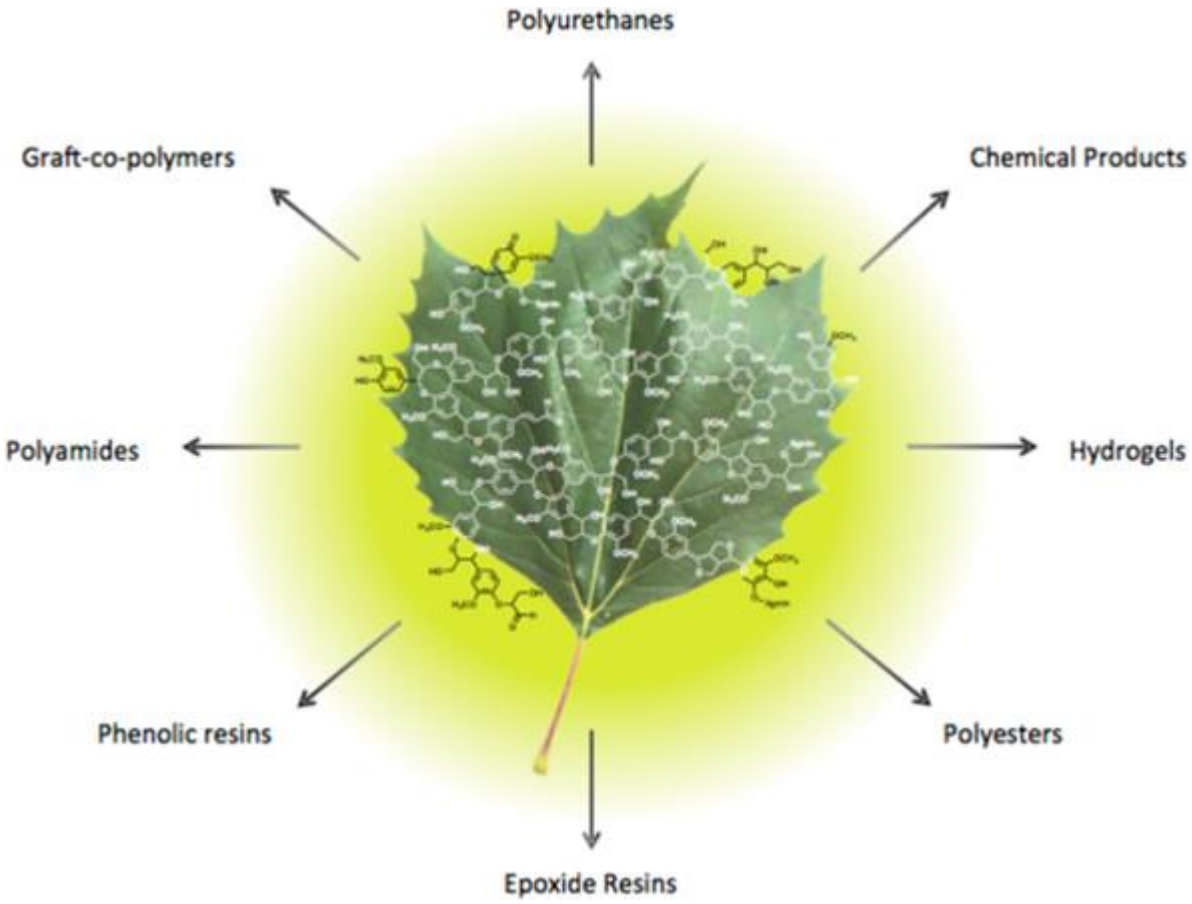

Figure 4 Polymeric Materials from Lignin Adapted with permission from Upton and Kasko Strategies for the Conversion of Lignin to High-Value Polymeric Materials: Review and Perspective. Copyright 2016 American Chemical Society [61]

2.3.1 Aromatic Polyamides from Biomass

Polyamides are a crucial class of engineering thermoplastics known for their extensive range of applications. Recognizing their importance, there has been a shift towards developing biobased alternatives to traditional polyamides. Notably, PA11 and

PA10, produced from castor oil, have emerged as industrially significant aliphatic biobased polyamides. However, the availability of aromatic biobased polyamides remains limited.

Table 4 Aromatic Polyamides from Biomass

Reference	Monomers	Synthesis Methodology	Temperature (°C)	Time (hrs)	M_w	Processing Method	T_g (°C)	T_m(°C)	T_{d5}(°C)	Tensile Strength (MPa)	Modulus (GPa)	Elongation (%)
[62]	2,5-furandicarboxylic acid (2,5-FDCA) based diamine, aromatic dianhydride	Two-step polycondensation	-	-	-	Solvent casting	270-350	-	400-450	80-140	2.5-5.4	3-12%
[63]	Fatty dimer amine and azelaic acid	One-pot melt polycondensation	220	24	84800	Solvent casting		83.6 °C	434 °C	31.8	-	1220%
[64]	Dimethyl 9-octadecenedioate and p-xylylenediamine, diethyltriamine	Polycondensation	160	4	-	Compression Molding	78	154-201	355	18.45	-	22.11
[65]	2,5-furan dicarboxylic acid, aromatic diamines	Interfacial polymerization			10,000–70,000		90-280	-	270-360	-	-	-
[66]	2,5-furan dicarboxylic acid, Decamethylene diamine	Solventless condensation with TBD catalyst	190-200	6	60000-70000	Not specified	100-105	-	400-450	54.46	1.45	138
[67]	diglycerol dicarbonate (DGDC) and diamino-telechelicoligoamides (DAPAhs)	Melt aminolysis copolymerization	120	1	-	Hot compression 120 C	0	94-110		12.12	-	373.32
[68]	Bisfuran and dicarboxylic acid	Interfacial polymerization	RT	1	34000	Not specified	120-160	186	250-316	-	-	-
[69]	dimethyl furan-2,5-dicarboxylate and 1,3-cyclohexanedimethanamine	Melt polymerization	1. 120 2. 240	60-180	-	Not specified	155-181		286-391	-	-	-
[70]	Divanillin based diamine and divanillin based dicarboxylic acid	Polycondensation	130	overnight	50000-60000	Solvent casting/ Hot pressing	207-262		268-301	40	1	8
[71]	Silk inspired; 3,6-dioxa-1,8-octanedithiol, UDA derivatives	Thiol-ene addition polymerization	70	12	23000-32000	Solvent cast	-32.6	35-139	-		0.04-0.2	78-710
[72]	Divanillin based dicarboxylic acid with commercial diamine	Polycondensation	120	10	-	-	-	-	-	-	-	-
[73]	Divanillic acid with commercial aromatic diamines	Polycondensation	130	overnight	47000 - 112000	Solvent Cast/Hot press	162-300		380-420	13-46	0.48 - 1.34	3 to 6
[74]	Monolignol based	Interfacial Polymerization	RT	-	4700 - 27000	-	67 - 126		203-264	-	-	-
[75]	Hydroxycinnamates	Interfacial Polymerization	RT	-	3800 - 28000	-	66 - 124		121-243	-	-	-

A primary area of focus has been the use of furfural as a precursor for aromatic rings, which is then oxidized to furan dicarboxylic acid (FDCA). A noteworthy study by Ma et al. explored the synthesis of polyamide-imides from FDCA [62]. The incorporation of aromatic rings led to polymers exhibiting an exceptionally high glass transition temperature of 364°C and remarkable thermal stability. In a different approach, another research effort utilized esters derived from canola oil to synthesize unsaturated polyamides. Although the diamines in this study were not biobased, the investigation revealed that aromatic polyamides possess higher moduli than their aliphatic counterparts under both microwave-assisted and conventional polycondensation conditions[63] .

Additional studies on furan-based polyamides have consistently reported high glass transition temperatures and excellent thermal stability, underscoring the potential of aromatic structures in enhancing polymer properties [62,65,66,69,76,77]. Vanillin, a monomer that can be derived from lignin, represents another avenue for developing aromatic biobased polyamides. Yagura et al. demonstrated the synthesis potential of divanillin, a dimer of vanillin, with commercial diamines, achieving polymers with high thermal stability [73]. Their subsequent work involved converting divanillin into an aromatic diamine, setting the stage for the creation of fully biobased aromatic polyamides from lignin [70]. Another study explored the incorporation of lignin into aliphatic polyamides with the aim of enhancing stiffness and hydrophobicity [78]. This approach not only contributes to the diversification of biobased polyamides but also highlights the versatility of lignin as a sustainable resource in polymer science. Two important studies utilized monolignols and hydroxycinnamates to form BPA alternatives for polyamide

synthesis. The first study utilized ether bonds to link hydroxycinnamates to form a diacid, while the second study utilized ester bonds to link monolignols to form a diacid [74,75]. The polymers were synthesized with a wide variety of diamines ranging from short chain aliphatic diamines to aromatic diamines. An important takeaway was the improved thermal stability of the polyester amides over polyether amides. Reasons for this were not provided but a possible explanation could be the relatively low molecular weights for polyether amides compared to polyester amides.

2.3.2 Polyesters from Lignin

Table 5 Literature Review on Lignin Based Polyesters

Reference	Lignin Prepolymeric Material	Functionalization	Reaction Conditions	Glass Transition / Melting (°C)	Processing
[79]	Kraft Lignin	-	Polycondensation with acid chlorides	T_g = -50	-
[59]	Kraft Lignin	-	Polycondensation with acid chlorides	T_g = 70	Melt processing 120-140 C
[80]	Sulfuric Acid Lignin and PCL	-	ROP for caprolactone	Tm = 46-61	-
[81]	Vanillin pendant group monomers	Methyl Acetate	Melt Polycondensation with ethylene glycol	Tg = 31-51	-
[82]	Phloretic acid - Lignin Monomer	Ethylene Carbonate	Melt polycondensation	Tm = 6-32	Extrusion/Injection Molding
[83]	Ester containing monomer from vanillin	Tischenko reaction with allyl bromide	Thiolene polymerization	Tg = -18 - 31	-
[84]	Phloretic acid dimers and trimers	Acetic Anhydride	Solvent Polycondensation	Tg = 41-105 Tm = 197-265	-
[85]	Bisguaiacol	-	Polycondensation with acid chlorides	Tg = 42-164	
	Vanillin	1,3-chloropropanol	Melt Polycondensation	Tg = 68 C Tm = 200	Solvent casting
[86]	Divanillic ester monomers	-	Polycondensation	Tg = 60-120	Solvent casting
[87]	Divanillic acid monomers	-	Polycondensation	Tg = 19-89	Solvent Casting/Thermopressing
[88]	Divanillic acid monomers	-	Polycondensation with adipic acid / hexanediol	Tg = 48-111	Solvent Casting
[89]	Divanillic acid monomers	-	Polycondensation with hexanediol	Tg = 108	Solvent Casting
[90]	Pyridine Dicarboxylic Acid from Lignin	-	Polycondensation / Enzymatic Condensation	Tg = -30-30 Tm = 100-185	-
[90]	BisIsoeugenol	Hydrogenation	Interfacial polycondensation	Tg = 19 - 108 C Tm = 106 – 259	Solvent Casting

[91]	Kraft Lignin	-	Melt polycondensation with PEG and Citric acid	Tg = 4-10	Solvent Casting
[92]	Organsolv Lignin		Melt polycondensation with acid chlorides and PEG	Tg = =36 to -58	-
[93]	BisIsoeugenol	Epoxidation	Interfacial polycondensation followed by crosslinking	Tg = 19-105	Solvent cast
[94]	Steam exploded lignin	-	Solvent Polycondensation	-	-
[95]	Vanillin	4-BromoButyrate	Copolymerization with DMT, BDO and DEG	Tm = 164	
[96]	Vanillin	Vanillyl Alcohol by reduction	Polycondensation with diacid chloride	Tg = 16-81	-

This review outlines the evolution and various methodologies of synthesizing polyesters from lignin or lignin-derived monomers, highlighting key innovations and findings in the field. The initial endeavors involved utilizing kraft lignin directly as a macromonomer, predominantly reacting with acid chlorides to produce polymers of low molecular weight and glass transition temperatures. It was observed that aliphatic OH groups were more reactive in these polymerization reactions compared to aromatic OH groups.

A significant advancement was noted by Gandini et al., who introduced oxypropylation to modify sterically hindered lignin hydroxyl groups into more accessible aliphatic hydroxyl groups, although this modification wasn't explored for polyester synthesis [79]. Incorporating aromatic linkers emerged as a technique to enhance the glass transition temperatures of the polymers significantly, from as low as -60°C to as high as 155°C [59]. This finding underscores the principle that more rigid aromatic rings can elevate the glass transition temperatures of polymers. Subsequent research shifted towards utilizing technical lignins in copolymers with synthetic polymers, demonstrating improvements in properties such as hydrophobicity—attributed to the aromatic content from lignin—and melting behavior similar to caprolactone [97].

The focus on lignin-based monomers marked a pivotal direction in research, with phloretic acid drawing significant attention. Phloretic acid, derivable from lignin, was utilized in innovative ways to yield polyesters. For instance, Winfield et al. functionalized this monomer using ethylene carbonate, transforming an aromatic hydroxyl group into an aliphatic one, subsequently polymerizing it to form a polyester [82]. Similarly, Ren et al. engaged the Tishchenko reaction to introduce ester linkages into allyl bromide functionalized vanillin, facilitating further polymerization to a polyester through thiolene polymerization [83]. Efforts to enhance molecular weights in polyesters derived from lignin involved acetylation of phloretic acid to mitigate sublimation during melt polycondensation, showcasing a strategic approach to overcome limitations associated with direct melt polycondensation. The development of polypropylene vanillate as a semicrystalline polyester, through the functionalization of the aromatic hydroxyl group with chloropropanol and subsequent melt polymerization, represents another notable achievement in the field [98]. This approach mirrors that used with phloretic acid, yielding a monomer with distinct acid and alcohol functionalities conducive to polyester synthesis. Diverse studies involving divanillic acid have explored the synthesis of polyesters by varying the monomers, including cyclic, aromatic, and aliphatic ones. These studies have indicated potential for biodegradability and adhesive applications, significantly broadening the scope of lignin-derived polyesters [86–89,99]. Innovations continue with the exploration of bisisoeugenol, derived from the reductive catalytic fractionation of wood, showcasing the synthesis of polyesters with tunable glass transition temperatures and the integration of epoxy networks for enhanced mechanical properties [90,93]. This trajectory of research not only emphasizes the versatility of lignin and its derivatives in polymer

science but also underscores the ongoing potential for new material development with improved or novel properties.

2.3.3 Lignin Oil Based Polymers

There have been a few studies attempting to synthesize epoxies and polyurethanes from lignin oil. A study attempted to create epoxy resins by modifying pine wood lignin oil with epichlorohydrin. In a follow up study, hardwood lignin oil was utilized in a similar protocol to form epoxy resins. The resins were cured with diethylene triamine and BPA based diglycidyl ether to yield cured thermosets [170,171]. In a similar study, lignin oil was used as one of the polyols along with polyethylene glycol to form polyurethane foams [172].

Given the burgeoning interest in lignin-derived materials, it's pivotal to acknowledge that, to date, lignin oil—a rich source of aromatic biocarbons—has been underutilized in the synthesis of both polyesters and polyamides. While compounds derivable from lignin have demonstrated potential for polyester and polyamide synthesis, the direct utilization of lignin or its oil for polyamide production could significantly mitigate the low yield issue inherent to pure lignin-derived monomers in biorefineries.

A notable gap exists in the application of lignin for polyamide synthesis, particularly because previous efforts often resorted to employing toxic acid chlorides. Chapter 4 of this dissertation directly addresses this challenge by employing lignin oil in a solvent-based polycondensation pathway for polyamide production. This approach not only circumvents the low yield dilemma but also leverages a more environmentally friendly synthesis process.

On the polyester front, the abundant hydroxyl functionalities of lignin have captivated considerable research interest. Yet, the domain of unsaturated polyesters remains largely unexplored with respect to lignin or lignin oil. Chapter 5 seeks to bridge this gap by pioneering the synthesis of unsaturated polyesters from lignin oil, followed by curing with various acrylates. This venture into uncharted territory aims to expand the repertoire of lignin-based materials, potentially leading to new applications and sustainability benefits in the field of polymer science.

CHAPTER THREE:

HYBRID NANOCELLULOSE-HYPERBRANCHED POLYMER FILLERS FOR PHBV

3.1 Introduction

Due to increasing public awareness of the depletion of natural resources and concern about pollution associated with petroleum-based plastic products, the development of sustainable plastics has drawn considerable attention from consumers, manufacturers, policymakers, and institutions [12]. Accordingly, significant progress has been made in recent decades toward synthesizing bio-based and biodegradable plastics with performance competitive with large-volume plastics while having a smaller carbon footprint [100].

Polylactic acid (PLA) has the largest market share of all biobased plastics. It has been incorporated into the food and beverage industry to replace single-use plastics with requisite mechanical and thermal performance [101]. Another bio-based polymer of interest, poly (3-hydroxybutyrate-co-3-hydroxyvalerate) (PHBV), is a bacteria-derived linear polyester containing randomly arranged 3-hydroxybutyrate (HB) and 3-hydroxyvalerate (HV) segments [102]. The market share of PHBV is expected to increase from 1.8% to 6.4% over the next five years, making it the third largest biobased biodegradable polymer in the market [103]. PHBV exhibits several advantages, such as biodegradability in multiple mediums, high biocompatibility with a wide variety of cells, and scalable production [104]. Despite its advantages, PHBV exhibits a high brittleness associated with large spherulites and high glass transition temperature. An increase in the HV segment content can reduce the brittleness of PHBV but at the expense of tensile strength and modulus. Various properties of PHBV, such as mechanical properties,

crystallinity, degradation rate, thermal stability, and hydrophilicity, need to be tailored to achieve a plastic with balanced properties appropriate for real-world applications [105].

Adding functional fillers to PHBV is a feasible and effective way to overcome its shortcomings. For example, nanomaterials such as graphene, reduced graphene oxide, and carbon nanotubes have been shown to reinforce PHBV [106–108]. For example, a study on graphene/PHBV nanocomposite films showed a 25% increase in tensile strength [107]. Another study showed that functionalized carbon nanotubes increase the tensile strength and Young's modulus of PHBV by up to 88% and 172%, respectively [108]. However, formidable cost limits its application in many plastics, including PHBV. On the other hand, low-cost natural plant-based fibers such as jute, flax, pineapple, hemp, and oak wood have also been incorporated into PHBV to improve its mechanical properties while maintaining its sustainability and biodegradability [42,109–112].

Among plant-based fibers, cellulose nanocrystals (CNCs) are an exciting choice because of their exceptional mechanical properties, high aspect ratio, and high purity [113]. Because of their interesting properties, CNCs can be utilized in a wide variety of applications, like biomedical, Pickering emulsifiers, adsorption, adhesives, and in polymer composites [114]. Primarily CNCs are prepared from cellulose-rich sources like wood, cotton, hemp, linen, and flax via chemical methods like acid hydrolysis and oxidation. CNCs can also be prepared via mechanical defibrillation. Biologically CNCs can be synthesized from bacteria [114]. CNCs are crystalline in nature with rod like structures with common aspect ratios of 4–20 nm in width and 100–500 nm in length [115]. Like most plant-based fibers, CNCs are highly hydrophilic due to the abundant hydroxyl groups, resulting in a strong tendency for irreversible agglomeration [116] and poor compatibility

with hydrophobic biopolymers, both of which are deleterious to the mechanical properties of the final composite. To address this, the CNCs have been chemically modified to mitigate their hydrophilicity and improve compatibility [37,117–119]. Consequently, CNCs have been incorporated into bio-based polymers such as PLA, polycaprolactone (PCL), and PHBV to improve mechanical properties [113,120–123]. Previous studies on incorporating CNC in PHBV showed mixed results with improved stiffness at the cost of elongation at break [21–23,28].

PHBV and many other biodegradable bioplastics have insufficient strength and low toughness; thus, simultaneous enhancement of both properties is highly desirable. However, achieving this is considerably challenging. In previous attempts, a hyperbranched polymer (HBP) was incorporated into PHBV to improve the toughness and elongation at break, but it also reduced tensile strength and modulus [124]. In recent work, phenyl-terminated HBP was compounded with PHBV, increasing elongation at the break and impact strength by 400% and 158%, respectively. However, stiffness was reduced [125] This is a common trend while incorporating toughening agents/tough polymers into biobased polymer matrices. In many cases, fillers capable of improving strength and stiffness usually fail to enhance the toughness and impact strength [46,102,122,124,125].

Li et al. proposed a strategy of "soft-rigid" reinforcements, in which “soft" amorphous polycarbonate (PC) and “rigid” modified CNCs were incorporated into PHBV by dissolving PC and PHBV in chloroform and emulsifying the blend with CNCs dispersed in water [126]. Films made from the blends had improvements in tensile strength and toughness of up to 273.8% and 821.9%, respectively, over the initial PHBV. In our previous study, the research group grafted “soft” poly(ethylene glycol) (PEG) segments

onto the surfaces of "rigid" CNCs to create a hybrid particle filler [43]. The study involved meticulously adjusting the PEG length in order to enhance the stiffness and toughness of PVA composite films simultaneously.

Keeping the soft-rigid architecture in mind, I have selected HBP as the hybridization agent and PHBV as the matrix for the following reasons (1) HBP is commercially available and has been shown to act as a toughening agent in the co-author's previous studies [127] (2) CNC and HBP both have an abundance of hydroxyl groups that can be easily linked using isocyanate chemistry at low temperatures (3) Utilizing hybridized CNC aimed to draw the toughening properties of HBP along with the stiffening properties of CNC to improve the properties of PHBV. In this study, I investigated a hybrid filler prepared by conjugating HBP with CNC ("soft" and "stiff" components, respectively) through isocyanate chemistry. The study attempts to relate the chemical structure and surface properties of the hybrid filler with polymer crystallinity as well as the thermal, mechanical, viscoelastic, and morphological properties of the PHBV composites.

Foaming biopolymers through physical and chemical blowing methods is another strategy for mitigating brittleness and improving toughness while also lowering bulk density and often improving economics [128,129]. Currently, there are only a few studies on batch foaming of PHBV; most, if not all, use supercritical CO_2 as the blowing agents [130,131]. However, in studies on polypropylene and polylactic acid, N_2 led to a higher cell density, less shrinkage of foams, and a higher expansion ratio than CO_2, despite its lower solubility [132]. The same may be true for PHBV, but this has not yet been studied. Here, I investigate supercritical batch foaming of PHBV alone, as well as with our hybrid fillers, using supercritical N_2.

3.2 Materials and Methods

3.2.1 Materials

PHBV pellets (ENMAT Y1000P, 8% HV content, injection molding grade) were purchased from Tianan Biological Materials, China. The CNCs were prepared by the USDA Forest Products Laboratory in Madison, WI, via sulfuric acid hydrolysis and had a length of 271±47 nm and a width of 6.17±2.00 nm. CNCs were freeze-dried before dispersion in solvent and HBP conjugation. Toluene diisocyanate (Sigma Aldrich) and the HBP Boltorn™ H30 Regular (Polymer Factory) were commercially available and were used without purification. Tetrahydrofuran (THF), Toluene, and Acetone were purchased from Sigma Aldrich.

3.2.2 Synthesis of fillers

Two types of CNC-HBP fillers were synthesized through similar chemistry but different protocols (Fig 1). The filler prepared by treating CNC first and then adding HBP for conjugation was termed CH; the other, made by first treating HBP and then adding pristine CNC, was termed HC. Details of the synthesis are presented below.

CH – The freeze-dried CNCs were dispersed in toluene under ultrasonication. The concentration of the CNC was kept at 1g per 50 ml of toluene. The dispersion quality of the sonicated suspension was qualitatively assessed using cross polarizers for shear birefringence according to a procedure specified by Foster et al [133]. The suspension was heated to 90 °C and held for an hour to eliminate any water in the solution. The temperature was then reduced to 45 °C, and three equivalents (eq.) of toluene diisocyanate were introduced into the system. The reaction was carried out for 5 hours. The suspension was centrifuged at 6000 rpm (4427 g) for 10 mins, and the precipitated product was washed

with dry toluene four times to eliminate unreacted isocyanates and other side products. Following this, the isocyanate functionalized nanocellulose was dispersed in 50 ml tetrahydrofuran (THF) under ultrasonication. The suspension was heated to 60 °C. One eq. of HBP was added to the suspension and reacted for 5 hours. After the conjugation reaction, the product was washed with THF four times.

HC – 1g HBP was first dissolved in 50 ml THF and heated to 60 ℃. 3 eq. of toluene diisocyanate (32 OH groups per molecule of THF) was added and reacted for 5 hours. After the reaction, the product was recovered using a rotary evaporator and washed with acetone to remove unreacted isocyanates. 1g of freeze-dried CNCs were suspended in 50 ml THF using ultrasonication, and the dried modified HBP was added to the suspension. The solution was reacted at 60 ℃ for 5 hours. Following the reaction, the suspension was centrifuged, and the sediment product was washed with THF four times to eliminate unbonded HBP. The schematics of these two procedures are presented in Fig 5.

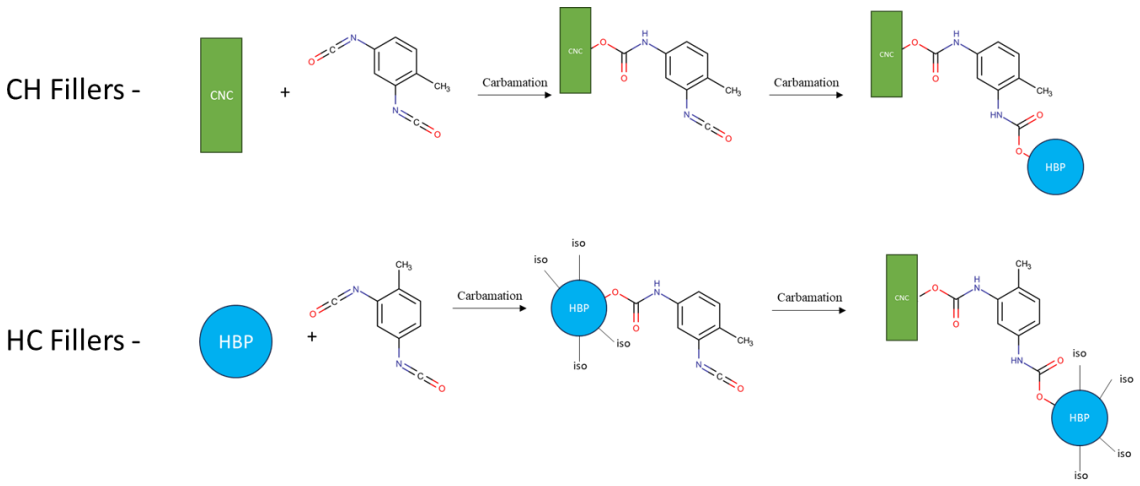

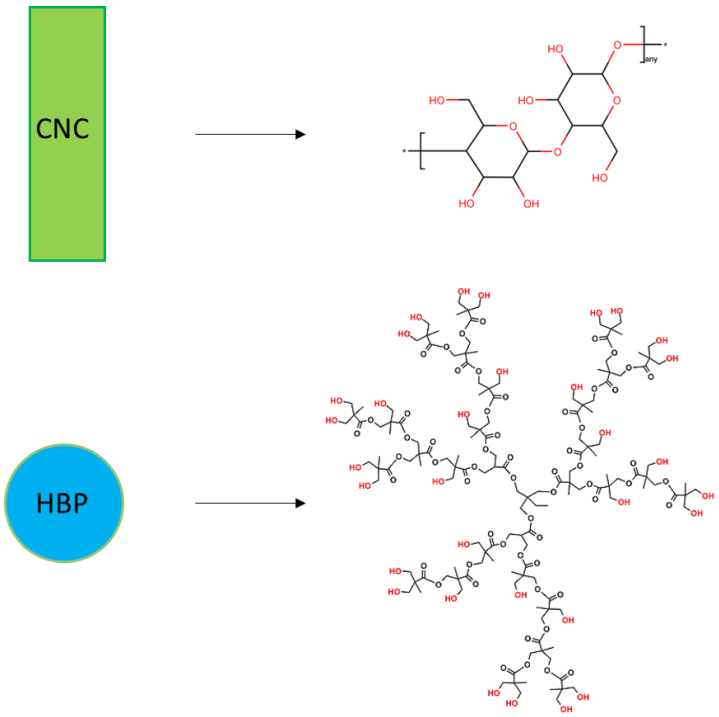

Figure 5 Schematic of CH (upper) and HC (lower) synthesis via two procedures.

3.2.3 Chemical characterization of hybrid fillers

Fourier transform infrared spectroscopy (FTIR, Thermo-Nicolet is 50) was used to determine the chemical nature of the fillers. Spectra were collected in transmittance mode from 4000 to 400 cm^{-1} at a resolution of 2 cm^{-1}. A VersaProbe III (Physical Electronics, USA) with a monochromatic Al X-ray source operating at 15 kV, 25W, with a beam spot of ~100 μm in diameter, was used for X-ray photoelectron spectroscopy (XPS).

3.2.4 Preparation of nanocomposites (CH and HC)

The CNC-HBP nanostructures were dispersed in chloroform using ultrasonication. After ultrasonication, PHBV pellets were added to the suspension and heated to 60 °C. The mixture was stirred for 4 hours before being cast in a 5 cm × 5 cm square silicon container. After complete drying under the ambient condition, the solvent-cast specimens were ground into granules for subsequent injection molding.

3.2.5 Injection molding

Before injection molding, CH and HC composites were vacuum-dried at 70 ℃ for 4 hours to remove moisture. A DSM Xplore micro-injection molding unit with a barrel temperature of 170 ℃ and a mold temperature of 60 ℃ was used to injection mold Standard type-V tensile specimens (ASTM D638, thickness=1.12 mm). The injection and holding pressures were both 4.5 bar, and the holding time was 15 s.

The names of the composites are denoted as xCH and yHC, where x and y are the filler contents (x, y = 1, 3, 5, 10). The filler content is by weight% of CNC in the final composite. It is noted that, when denoting the concentration of fillers in the composites, it only considered the weight of CNC core, excluding the mass of HBP. This method makes the measurements easy.

3.2.6 Mechanical properties of composites

The tensile properties of the injection-molded type-V specimens were determined as per ASTM D638-14 using an Instron universal testing machine (Model 1125), which was equipped with a load cell of 50 N and a cross-head speed of 1 mm/min with 7.62 mm initial gage length. The dimensions were based on Type V ASTM D638-14 samples. Overall length was 63.5 mm. The width of the narrow section was 3.18 mm, and the length of the narrow section was 9.52 mm. The strain rate of 0.1312/min was chosen based on a previous study. The sample thickness was measured at 1.1 mm. The force vs displacement data was through the crosshead speed.

3.2.7 Thermal characterization of the PHBV composites

For differential scanning calorimetry (DSC, DSC250, TA Instruments) measurements, each sample (≈5mg) was subjected to a heating-cooling-heating cycle in

N_2 from -50 to 200 ℃ at the rate of 20 ℃/min, -5 ℃/min, and 10 ℃/min, respectively. The melt temperatures (T_m) and the enthalpy (ΔH_m) were determined from the second heating scan. The crystallization temperature (T_c) and enthalpy (ΔH_c) were determined from the cooling scan. The degree of the crystallinity (χ_c) was calculated by:

$$\chi_c(\%) = \Delta H_m/\Delta H_m^0 \times 100/a,$$

where the ΔH_m^0 is the melting enthalpy for 100% crystalline PHBV, taken as 146.6 J/g [134], and a is the weight fraction of the PHBV in the composites. For thermogravimetric analysis (TGA, TGA250, TA Instruments), samples (≈8.0 mg) were analyzed from 25 to 600 ℃ at 10 ℃/min under N_2 flow.

3.2.8 Foaming

The procedure involved saturating the sample at 4000 psi at 175 ℃ for 30 mins and then reducing the temperature to 80 ℃ for 3 hours to complete the dissolution. These samples were then depressurized rapidly to induce cell nucleation, foamed in an oil bath at varying temperatures (160-180 ℃) and times to induce cell growth, and finally submerged in a water bath to stabilize the cells. To observe the cell morphology, foams were treated with liquid nitrogen and broken. After sputter coating with platinum, the exposed foamed cross-sections were observed using scanning electron microscopy with an accelerating voltage of 15 kV (SEM, Hitachi-S3400).

A quantitative analysis of the average cell size and cell density was performed using an image analysis tool (ImageJ). The cell density was calculated using the following formula where N is the number of cells, L is the linear length of the area, and M is a unit conversion resulting in the number of cells per unit volume. –

$$\text{Cell Density} = \left(\left(\frac{N}{L^2}\right)^{3/2}\right) M$$

3.2.9 Scanning Electron Microscopy Fracture Analysis

The fractured surfaces after tensile testing were sputter coated with platinum. The morphologies were analyzed under an SEM (Hitachi-S3400) under high-vacuum with an accelerating voltage of 5 kV.

3.2.10 Rheological Characterization

A parallel plate rheometer (Discovery HR-2, TA Instruments) was used to determine dynamic rheoloical properties of CH and HC composites. The measurements were performed at 176 °C using stainless steel plates with a diameter of 25 mm. The trim gap was set at 1000 μm between the two plates. Samples were equilibrated at 176 °C for 5 min before tests. A strain sweep test was first performed to determine the linear viscoelastic region of the composites, and a shear strain of 0.5% was chosen for all subsequent frequency sweep tests. The frequency was varied from 0.1 to 628 rad/s.

3.3 Results and Discussions

3.3.1 Chemical analysis

For this study, toluene diisocyanate was used to modify CNCs due to its selectivity of the para-substituted isocyanate over the ortho-substituted isocyanate. The para-substituted isocyanate is more reactive and can selectively react with the substrate's hydroxyl groups. This allows me to carry out a two-step functionalization [36]. The suspensions of isocyanate-modified CNCs are more stable in many solvent systems than unmodified CNCs [36,113,135] due to their increased hydrophobicity and solvent compatibility. FTIR spectra and XPS graphs were recorded to evaluate the chemical

linkage between CNC and HBP designed for the hybrid fillers. Fig 6(a) shows the spectra of the pristine CNC and HBP. The peak at 1160 cm^{-1} can be assigned to the presence of a sulphated group formed due to the sulphonation of CNC while performing acid hydrolysis [136]. The band at 1060 cm^{-1} represents the stretching of the C–O bond in the glucose unit in the CNC. The band at 2833 cm^{-1} corresponds to the aliphatic C-H stretching in the CNC units. The peak at 1428 cm^{-1} can be assigned to CNC's CH_2 symmetrical bending and scissoring motion. A peak at 1722 cm^{-1} represents the prominent carbonyl in its backbone for the HBP unit (see Fig 5). The terminal hydroxyl groups show a broad hydrogen bonding peak between 3000-3500 cm^{-1}.

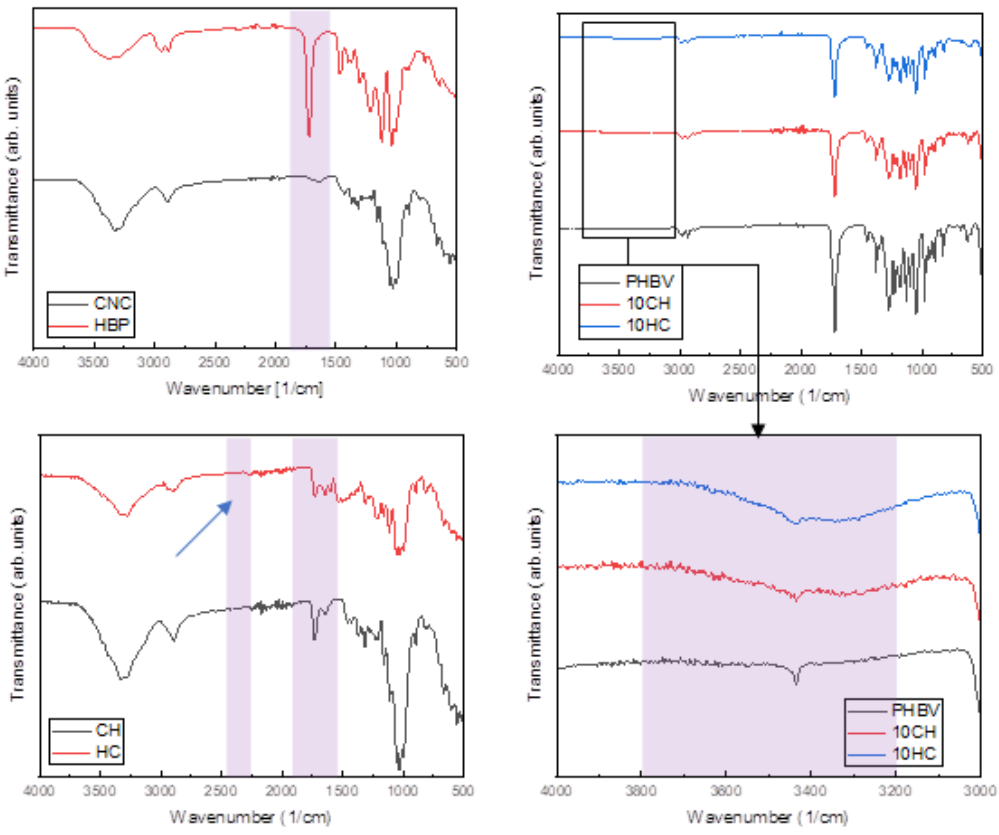

Figure 6 FTIR spectra of (a) pristine CNC and HBP, (b) fillers CH and HC, (c) and (d) 10CH and 10HC composites.

Fig 6(b) shows the FTIR spectra of the two-hybrid fillers. Both fillers show characteristic peaks from the CNC as well as HBP. For example, the C-O stretching peak (1060 cm^{-1}) from the CNC and the backbone carbonyl (1722 cm^{-1}) from the HBP peak were observed in both fillers. The fillers showed a broad peak associated with the intramolecular hydrogen bonding of the -OH groups in the CNC between 3000-3500 cm^{-1}. A critical distinction is the free isocyanate peak (2276 cm^{-1}) visible in the FITR spectra of HC filler (arrow in Fig 6(b)) while not seen for CH. This can be attributed to the abundance of hydroxyl groups on HBP, which extended to excessive isocyanate and were left unreacted after the CNC conjugation. Previous studies on surface modification of CNC with isocyanates have reported the carbonyl peak corresponding to the urethane linkage between 1700-1720 cm^{-1} [113]. Isocyanate functionalization of CNC is a challenge as the isocyanates are sensitive to moisture. The presence of moisture leads to the self-polymerization of the toluene diisocyanate, forming an inactive polyurea [137]. The FTIR spectra of PHBV and PHBV/CNC-HBP composites were also analyzed, as shown in Fig 6 (c,d). A broad peak between 3000-3500 cm^{-1} was observed for both CH and HC composites while not evident for neat PHBV. This peak is characteristic of hydrogen bonding of hydroxyl groups [138]. Upon closer inspection of the peaks of HC and CH composites, the peaks in the composites are broader than in neat PHBV, without any evidence of peak shifting. Moderate hydrogen bonding leads to this phenomenon in FTIR spectra [139]. This can confirm the existence of hydrogen bonds between the carbonyl groups in the PHBV matrix and the terminal hydroxyl groups in the filler. Hydrogen bonding is thus the primary matrix filler interaction observed here.

Since isocyanate modifications and CNC-HBP conjugation occur preferably on the surface, XPS is an appropriate method to analyze the chemistry in these near-surface regions. The reaction however favors surface hydroxyl groups C2-OH groups versus C6-OH and C3-OH groups. C6-OH groups are sulphonated during acid hydrolysis and C3-OH groups are sterically hindered [43]. The XPS survey spectra show evidence of carbon, nitrogen, and oxygen in both CH and HC nanostructures as seen in Fig 7(a), with a higher nitrogen element content (N%), found in HC (9.25%) than in CH (5.51%). The nitrogen element can primarily be attributed to the chemical urethane linkages introduced by the isocyanate reaction. Higher N% implies a higher isocyanate graft in HC, which can be explained by more available terminal hydroxyl groups on the HBP than CNC, and is in agreement with the observation of the FTIR spectrum (Fig 6(a))

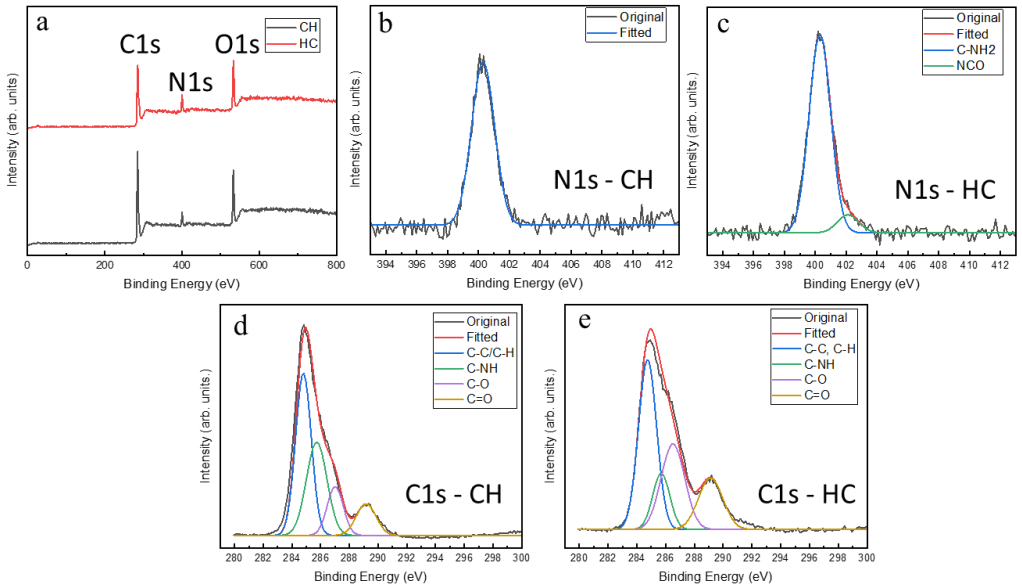

Figure 7 (a) Survey spectra of CH and HC filler, (b) N1s spectra of CH filler, (c)N1s spectra of HC filler, (d) C1s spectra of CH filler, and (e) C1s spectra of HC filler.

High-resolution XPS spectra were recorded for the two hybrids to understand the nature of the bonding (Fig 7(b-e)). The high-resolution spectra for C1s and N1s were

analyzed, and peaks were fitted using PeakFit with an R^2 value of at least 0.99. On nitrogen analysis, both CH and HC show a peak at 400 eV, corresponding to the C-NH bond found in urethanes. The HC sample shows an additional peak at 402.1 eV, which corresponds to free isocyanates N-C=O on the surface of the linked HBP (Fig 7(c)) and is consistent with the FITR results. The C1s spectra for CH and HC showed C-C, C-H linkages at 284.8 eV, C-N linkages at 285.7 eV, C-O linkages at 286.4 eV, and C=O linkages at 289.0 eV; this is in agreement with previous literature for urethane linkages [140]. These particular linkages confirm the formation of the urethane bond. Thus, the chemical linking of the HBP and CNC and the existence of free isocyanate on the HC surface were confirmed.

3.3.2 Thermal analysis

Understanding the thermal, crystallinity, and degradation behavior of the composites is critical to understanding the properties of the composites. The thermal properties and crystallinity were assessed using DSC and TGA. PHBV is a semi-crystalline thermoplastic with sharp melting and crystallization peaks in its thermogram. The crystallinity of the composites was estimated using the second heating curve and melting enthalpies. Table 4 highlights the DSC thermal behaviors of the composites and the crystallinities.

Table 6 Thermal behavior of the CH and HC composites.

Sample	***1st Heating Melting temperature (°C)***	***2nd Heating Melting temperature (°C)***	***2nd Heating Melting Enthalpy (J/g)***	***Crystallization Temperature (°C)***	***Crystallization Enthalpy (J/g)***	***Degree of Crystallinity, PHBV (%)***
PHBV	174.10	174.37	89.446	126.2	83.136	61.01
1CH	174.37	172.83	88.013	119.2	82.450	60.60

3CH	175.89	174.14	87.354	122.94	80.589	61.43
5CH	173.40	174.15	84.007	124.00	78.057	60.31
10CH	173.05	174.85	85.917	127.24	79.880	65.11
1HC	173.51	174.96	91.062	126.04	84.035	62.74
3HC	174.27	173.79	85.752	120.57	79.350	60.30
5HC	174.40	173.83	85.408	119.82	79.297	61.32
10HC	174.64	173.77	87.844	123.27	81.150	66.57

For both CH and HC composites, the degrees of crystallinity were relatively unchanged, up to 5% filler loadings, and notably increased at 10% loading. Generally, CNC fillers have two opposing effects on the crystallization of the polymer. On one hand, the filler provides additional sites for nucleation, induces heterogeneous nucleation, and thus increases the crystallinity. On the other hand, the filler reduces the polymer chain's mobility inhibiting its crystallization [113]. Both effects on crystallization are comparable for the two samples at lower concentrations, up to 5% filler loading. However, the 10CH and 10HC samples show an increased crystallinity compared to the rest and can be attributed to a significant increase in heterogeneous nucleation sites.

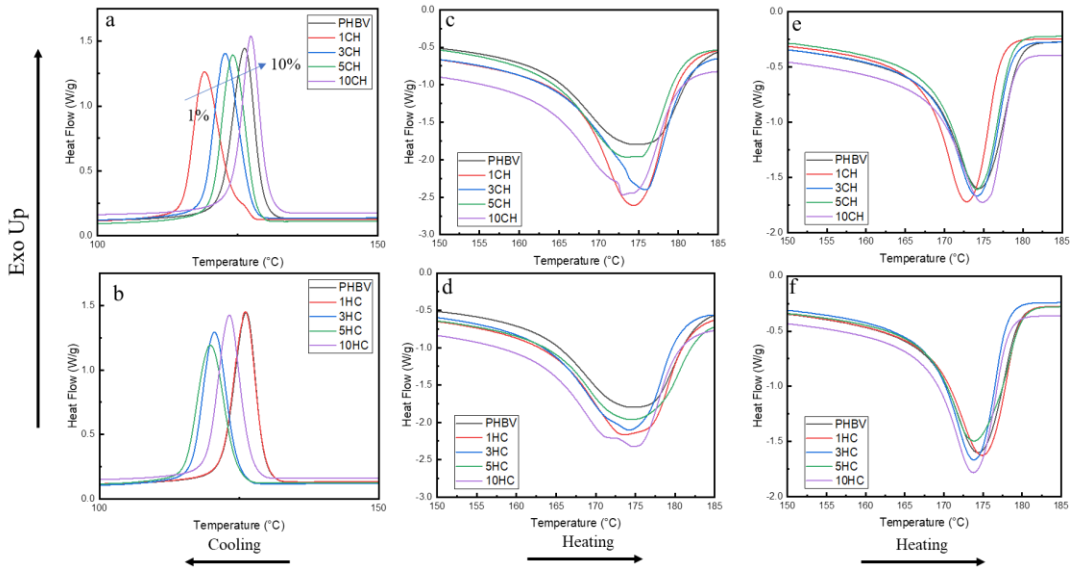

Figure 8 *DSC thermograms for cooling (a) CH (b) HC, 1st heating (c) CH (d) HC, and 2nd heating (e) CH (f) HC.*

Fig 8 shows the DSC thermograms for the cooling, 1st and 2nd heating cycles of the CH composites. Upon inspecting the cooling behavior, adding 1% of CH filler retarded crystallization, but the crystallization temperature recovered as more filler was added. The CH filler with its complex molecular arrangement involving branched HBP at its terminals can cause further entanglement with PHBV molecular chains. This entanglement can cause the crystallization process to lag and cause a decrease in crystallization temperature. However, the addition of filler reversed the trend. For the HC composites, the trend appears similar, except that more filler was required before a minimum crystallization temperature was reached, and the temperature had not yet fully recovered with the addition of 10% filler. The 2nd heating thermogram showed a single melting peak for all the composites. The melting temperatures followed a similar pattern to the crystallization temperatures. The 1st heating thermograms show the thermal history related to the processing conditions of the composites. Higher ramp rate and higher filler loadings for both CH and HC composites led to the broadening of the melting peak. I hypothesized that the more

complicated filler surface interaction might mitigate the heterogenous nucleating effects and further chemical and imaging investigation of the surface of the fillers was needed to understand the crystallization behavior of the composites.

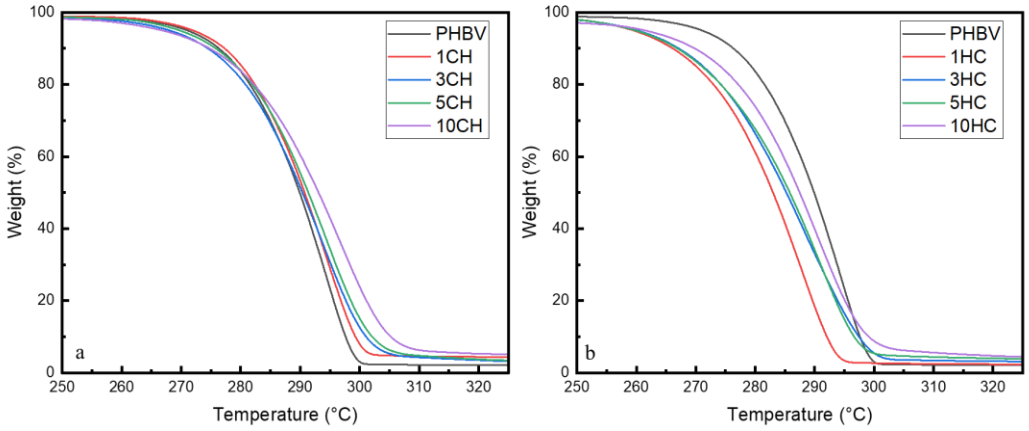

Figure 9 TGA degradation curves for the (a) CH and (b) HC composites.

TGA thermograms of CH and HC composites are shown in Fig 9(a, b). Table 5 highlights 5% ($T_{5\%}$) and 95% ($T_{95\%}$) weight loss for the composites under a N_2 atmosphere. All thermal degradation appeared to be single-step processes between 250-340 °C. Both the CH and HC fillers decreased the $T_{5\%}$ and showed a reduction in thermal stability compared to neat PHBV. It has been reported that nanocellulose slightly accelerates the thermal degradation of PHBV because of impurities or absorbed water. PHBV has been shown to degrade undergoing random chain scission via the mechanism of cis-elimination [141,142]. While little difference in the $T_{5\%}$ temperatures was found for the CH composites, there were notable reductions for the HC composites. This could be due to the additional degradation sites resulting from the free isocyanate groups on the surface of the HC filler [143]. However, the effect is not proportional to filler content, and more investigation is required to better understand the source of this reduced thermostability. The $T_{95\%}$ for both

CH and HC composites generally increased with filler content, as has been found in similar investigations [116,123].

Table 7 TGA degradation temperatures for CH and HC composites.

Composite	$T_{5\%}$ (°C)	$T_{95\%}$ (°C)
0	271.04	299.01
1CH	271.99	302.44
3CH	265.24	299.17
5CH	269.75	308.24
10CH	266.82	327.7
1HC	259.49	293.79
3HC	260.16	300.43
5HC	259.84	301.18
10HC	261.64	312.65

3.3.3 Mechanical properties

The tensile properties are shown in Fig 10. Fig. 11 shows representative stress-strain curves for the composites. The HC composites showed an increase in stiffness with increased filler loading from 1-5%. A similar increase was not observed for CH samples. Maximum moduli increases were observed in 5% filler addition, with 34% and 19% increases for HC and CH composites, respectively. The improvement in stiffness came at the cost of reducing the elongation at break for the HC and CH fillers, which is commonly seen in many composites, including those made with CNCs [144]. The 5HC sample showed a 48% reduction in elongation at break compared to neat PHBV. The partial recovery in elongation at break of 10 % loading is can explained by the agglomeration of CH/HC at high concentration leading to a reduction in reinforcement compared to a well-dispersed filler. No significant improvements were observed in the tensile strength of either our CH or HC-reinforced composites. The lack of CH/HC reinforcement was disappointing and indicated an inability of the fillers to transfer stress from the matrix effectively. This may

be attributed to a number of factors including suboptimal dispersion of the CH composites as seen in the SEM images in Fig 12., inadequate HBP linkage to CNCs in both CH and HC composites, or lack of adequate covalent bonds between the PHBV matrix and the isocyanate from the HC filler. Compared to conventional fillers reported in literature like CNTs, the reinforcement is rather subpar. Previous studies on functionalized CNTs showed an increase in tensile strength of up to 88% and increase in stiffness up to 172% [108]. Compared to CNTs, graphene on the other end had rather poor reinforcement ability in this particular study [145] with an increase of up to 25% in tensile strength.

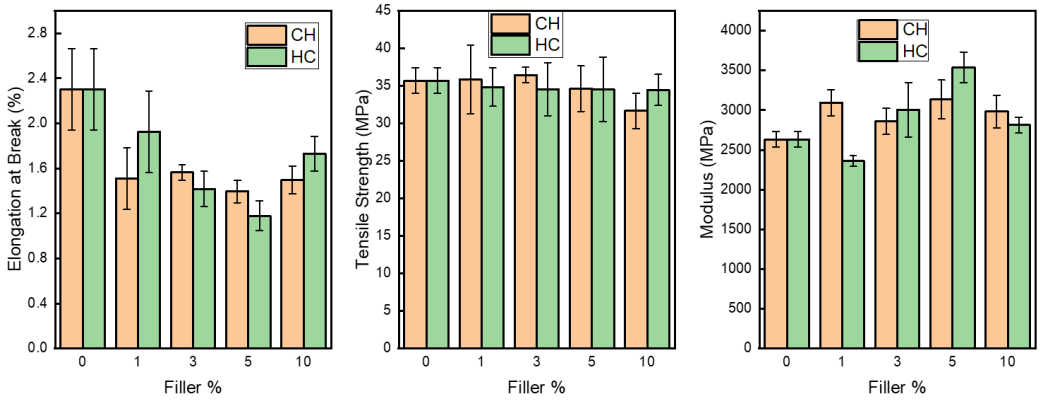

Figure 10 Mechanical properties of the CH and HC composites

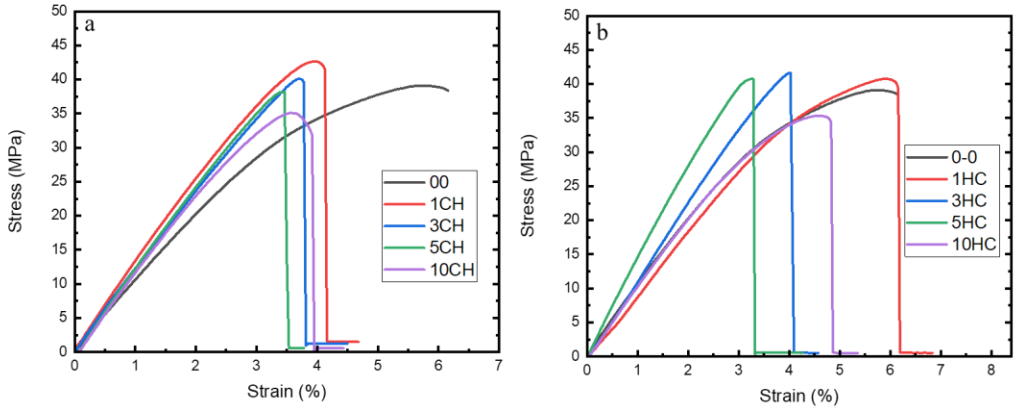

Figure 11 Representative stress-strain curves of the CH and HC composites

3.3.4 Fracture Morphology

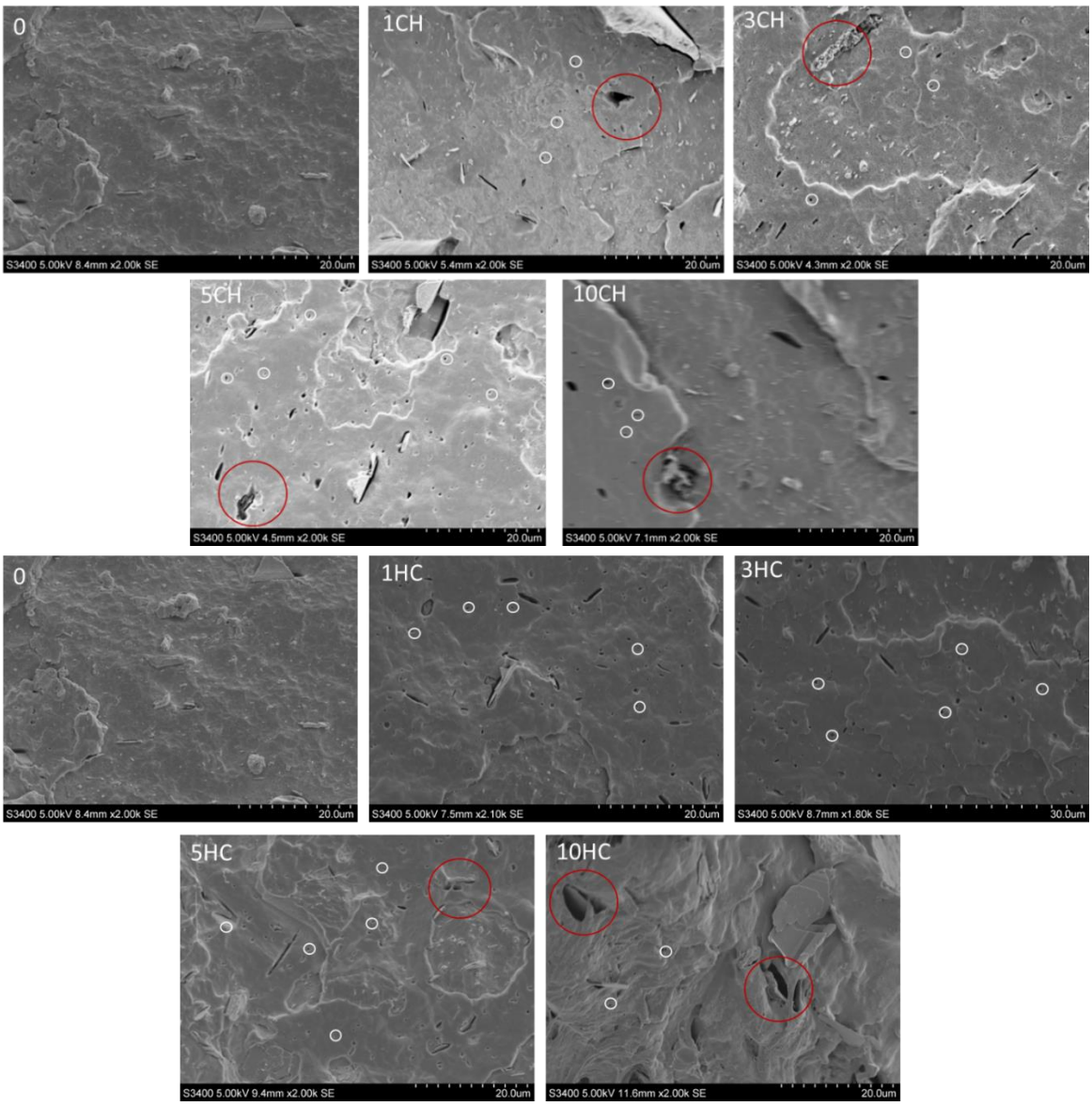

Figure 12 SEM images of fracture morphologies of the CH (top) and HC (bottom) composites.

The fracture surfaces of both neat PHBV and the composites exhibited a characteristic smoothness, indicative of brittle failure in the composite materials [130,146]. Upon closer examination of the SEM images, distinct features were identified on the surfaces of CH and HC composites. Both composites revealed an even distribution of tiny holes, marked by white circles, suggesting filler pullout occurring in various orientations

[146]. The uniformity in hole distribution in both CH and HC composites implies a consistent pullout phenomenon. Notably, the SEM analysis revealed signs of filler agglomeration in the CH composites, as indicated by red circles, even at lower filler loadings. The uneven size of the observed holes in CH composites was attributed to this filler agglomeration, potentially influencing the mechanical properties and fracture behavior of the composites. The surface chemistry of the HC fillers facilitated easier dispersion compared to CH fillers, evident in the absence of voids and the uniform distribution of the fillers. Despite the favorable dispersion, the surface chemistry of the HC fillers did not contribute to strong adhesion with the PHBV matrix, resulting in limited improvements in tensile strength. However, the even dispersion did contribute to improved stiffness in the composites. Conversely, CH fillers showed a slight improvement in tensile strength, but the relatively uneven distribution of the filler particles resulted in suboptimal performance enhancements. The SEM analysis indicated that the addition of CH and HC fillers did not alter the brittle failure mode of PHBV; the composites retained characteristics of brittle failure despite the variations in filler content and distribution.

3.3.5 Foaming of the composites

The CH and HC composites were saturated with N_2 using a high-pressure Parr reactor using N_2. Despite having lower solubility than CO_2, N_2 as a blowing agent has been shown to have higher cell densities, less foam shrinkage and higher expansion ratios [132]. Xu, et al. developed a two-step batch foaming procedure incorporating a melting step at 176 °C during gas absorption [131]. This was done in order to overcome PHBV crystallization effects on N_2 solubility. The second step in the study carried out a depressurization at 145-165 °C to induce foaming with increased melt strength [131].

However, in the case of N_2, depressurization at a high temperature led to poor results. Consequently, in our procedure, I also incorporated a melting step but depressurized at 80 °C to prevent premature foaming in the pressure vessel. After N_2 saturation, the PHBV sample was immersed in an oil bath at temperatures from 160-180 °C, which reduced stiffness and triggered the nucleation of the dissolved N_2 and bubble growth.

Immersion time and oil bath temperature were first optimized with pure PHBV to yield high bubble density and low bubble diameter. The foaming processing window was very narrow. The samples did not foam at temperatures below 165 °C due to their high stiffness inhibiting cell expansion, but they melted at temperatures over 180 °C resulting in bubble collapse. Samples foamed for less than 30 s showed no cellular structure, and those foamed for 40-60 s deformed. Consequently, the optimal foaming temperature and time for PHBV were 170 °C for 30 s (Fig 13(a)). The PHBV samples showed a cell density of 5.26 x 10^5 cells/m^3. Previous reports have shown that addition of filler leads to an increase in melt stiffness and reduction of cell size. Unfortunately, when I applied these foaming conditions to the CH and HC composites, little evidence of foaming was observed (Fig 7(b)). Incorporating CH/HC fillers in PHBV may have increased melt stiffness, reduced gas solubility, or increased gas loss during foaming [124]. To understand the failure in foaming, melt rheological studies were carried out for the composites.

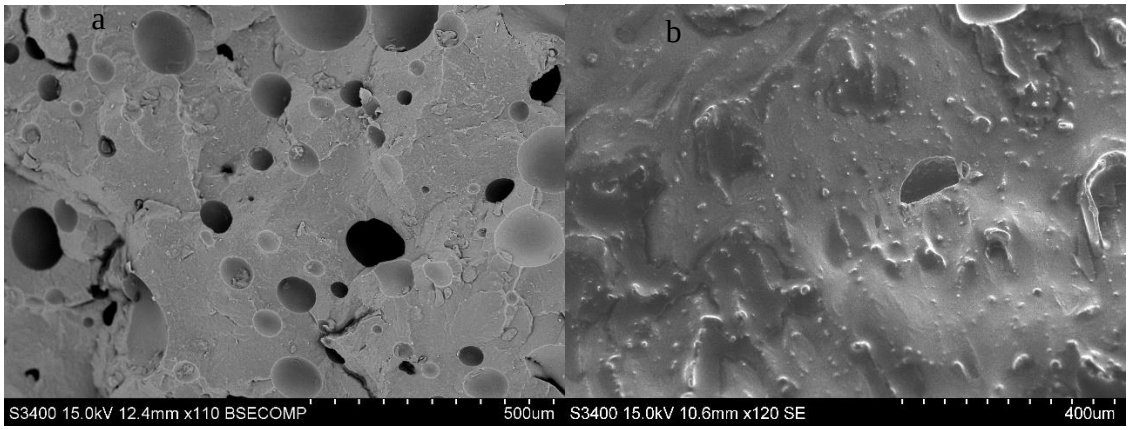

Figure 13 SEM Micrographs of neat PHBV (a) and 1CH composite (b) foamed at 170 ℃ for 30 s.

3.3.6 Rheological Properties

Melt strength, as determined by rheological properties, is a pivotal factor influencing the foaming behavior of composites. Lower melt strength promotes larger cell sizes due to increased cell growth, while higher melt strength impedes cell expansion, preventing cell rupture and collapse [147]. The storage and loss moduli for the CH and HC composites have been shown in Fig. 14. In examining the control sample of PHBV, observable polymer melting characteristics were noted, with an elevation in both storage and loss moduli corresponding to an increase in angular frequency. The heightened loss modulus of pure PHBV suggests a prevalent viscous nature under the specified conditions. Conversely, CH composites exhibited amplified storage and loss moduli, indicating enhanced melt strength and foaming prevention. At higher angular frequencies, the composites displayed shear-thinning behavior while maintaining consistent storage and loss moduli. The inclusion of CH fillers resulted in composites that were less sensitive to angular frequency, indicative of solid-like material behavior in rheology. Additionally, CH composites exhibited a higher degree of elastic behavior relative to viscous behavior under the specified conditions, a phenomenon previously observed in cellulose nanowhisker-PHBV composites [148]. In contrast, HC composites displayed lower storage and loss

moduli compared to CH composites. HC composites exhibited a higher storage modulus at lower angular frequencies but displayed non-terminal behavior at higher frequencies. The intricate interactions between isocyanate and the polymer matrix may contribute to this behavior, distinguishing it from CH composites. The rheological behavior of the composites can give us some insights into the dispersion of fillers. A previous study on PLA/CNC composites showed improved storage moduli with incorporation of CNCs in the polymer matrix under oscillatory load. The stronger polymer-filler interactions for CH composites led to an improvement in the storage modulus and more solid like behavior. The fillers with good adhesion led to the formation of a network like structure in the composites leading to an increased storage modulus.

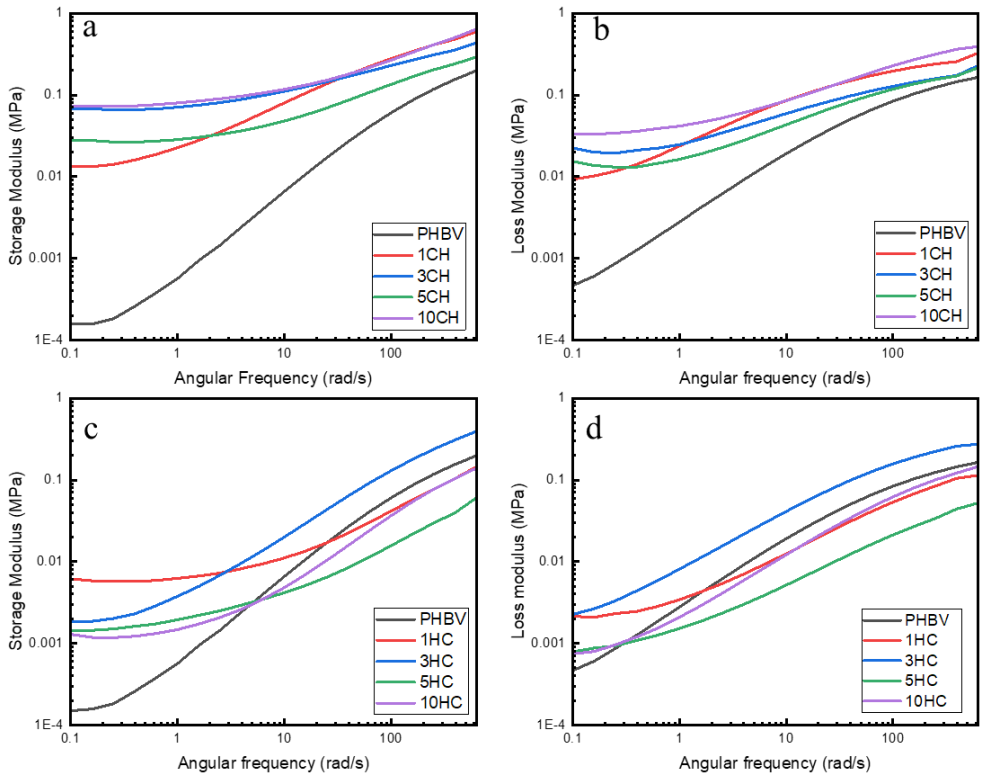

Figure 14 Storage modulus for the CH (a) and HC (c) composites and loss modulus for the CH(b) and HC(d) composites.

3.4 Conclusions

This study attempted to combine the benefits of CNC and HBP to construct hybrid fillers to reinforce yet improve (or at least maintain) the toughness of PHBV. Isocyanates were chosen as the linkage because of their high reactivity with hydroxyl groups of CNCs and HBPs. Two types of fillers were constructed using similar isocyanate chemistry but different procedures. The FTIR results identified the urethane linkages between the HBP and CNC and free isocyanate on HC, both of which were further confirmed by XPS. The DSC results showed that reduced molecular mobility dominated at low CH and HC loading, while nucleation dominated in 10CH and 10HC composites. The TGA analysis showed that HC composites were thermally less stable than CH composites as well as pure PHBV. This can be attributed to the free isocyanates on the HC filler degrading earlier than the constituents. The moduli for HC composites increased up to 34% but at the cost of elongation at break. The tensile strength remained relatively unchanged for all fillers, suggesting unsatisfactory reinforcement by the new hybrid nanostructure. The HC filler showed better dispersion but did not show any improvement in tensile strength. This was attributed to the surface chemistry of the HC filler. The CH filler showed marginal improvement in tensile strength but showed signs of agglomeration. A notable drawback of the study was that the workflow involved multiple steps, which can be technically demanding and cost inefficient, and use of toxic solvents for solvent casting. Possible factors associated with the failure of reinforcement include 1) Agglomeration of the CH fillers 2) surface chemistry of the HC fillers, 3) the crystallization kinetics of PHBV with CH/HC fillers, and the effect of chain entanglement on crystallization. I also attempted batch foaming of the samples using N_2. For unmodified PHBV, a narrow range of foaming

temperatures (170-175 °C) and time (30 s) were found. The composites, however, did not foam at these optimized conditions. Rheological investigations revealed an increased melt stiffness of the composites, and more elastic behavior in the composites.

CHAPTER FOUR:

SYNTHESIZING POLYAMIDES FROM LIGNIN – LINKING THE STRUCTURE OF LIGNIN OIL TO POLYMER PROPERTIES

4.1 Introduction

With the depletion of petroleum reserves and the escalating global temperatures, the demand for sustainable polymers has become increasingly crucial [149]. To address this need, current research endeavors are centered around employing the principles of green chemistry in polymer synthesis and manufacturing [10]. One particular area of focus is the exploration of alternative feedstocks for polymers [150]. Nature offers a plethora of potential feedstocks such as starch, soluble sugars, polysaccharides, cellulose, pectin, hemicellulose, and lignin, which have garnered significant attention in research [11]. Among these feedstocks, lignin has emerged as a subject of particular interest. As the second most abundant biopolymer attainable from non-food-based sources, lignin exhibits a complex and heterogeneous structure composed of three aromatic monomers: coniferyl, p-coumaryl, and sinapyl alcohols [151]. Extracting and functionalizing these monomers holds the promise of yielding high-value polymers, serving as a viable substitute for petroleum-derived feedstocks [52].

Conventionally, lignin is commercially isolated through sulfite, kraft, organosolv, and soda pulping methods, with the final properties of the lignin contingent upon the specific process employed [152]. At the laboratory scale, alternative approaches such as enzymatic hydrolysis, wet oxidation, pyrolysis, ionic liquids, and reductive catalytic fractionation have been explored [153–156]. Extensive efforts have been devoted to functionalizing lignin, leading to the formation of polyols, epoxies, and improved

compatibility with polymer matrices [52,58,157–161]. Notably, the field of lignin functionalization has progressively embraced the principles of green chemistry [162]. For instance, organic carbonates have been proposed as substitutes for allyl bromides in the production of epoxy precursors, and isocyanates in the production of polyols [159,160,163]. Recent studies have even demonstrated the use of organic carbonate functionalized lignin for the development of chemically recyclable non-isocyanate polyurethanes, as well as the replacement of bisphenol A (BPA) in epoxy resins [55,56,164]. Furthermore, the scalability of the process from lab to pilot scale has been demonstrated [57]. Reductive catalytic fractionation, a "lignin-first" process, enables the solubilization, fractionation, and extraction of lignin directly from wood. Traditionally conducted under catalytic pressure in a hydrogen atmosphere, this process yields small lignin monomers [16,22]. The choice of catalyst employed influences both the chemical composition and the molecular weight distribution of the resulting product. For instance, while Ru/C lacks selectivity toward a specific monomer, Pd/C selectively yields bifunctional monomers [60]. The resulting product, referred to as RCF Lignin or lignin oil, comprises a mixture of monomers, dimers, and oligomers derived from the lignin's molecular structure. This oil possesses abundant aliphatic and aromatic hydroxyl groups, which present opportunities for further functionalization [17]. Research has been carried out in trying to understand the constituents of lignin oil. Lignin oil produced by Pd/C catalysis tends to favor the formation of bifunctional monomers with an aliphatic as well as aromatic hydroxyl group [60]. Lignin oil is comprised of up to 49% monomers for hardwood [165].

Lignin oil, a relatively novel material, has garnered significant research interest for its potential in polymer production and as a precursor material [166,167]. Prior to the

emergence of lignin oil, lignin-based polyamides were synthesized using vanillin. A recent study highlighted the synthesis of high molecular weight and thermally stable polymers from divanillin acid using a solvent-based polycondensation method[168,169]. Other studies have explored the use of furan dicarboxylic acid and its derivatives to form high molecular weight polyamides with commendable thermal and mechanical properties [62,65,66,76,77]. A previous study incorporated lignin into biobased polyamides to increase crosslinking and improve mechanical properties and hydrophobic behavior [78] Two important studies utilized monolignols and hydroxycinnamates to form BPA alternatives for polyamide synthesis. The first study utilized ether bonds to link hydroxycinnamates to form a diacid, while the second study utilized ester bonds to link monolignols to form a diacid. The polymers were synthesized with a wide variety of diamines ranging from short chain aliphatic diamines to aromatic diamines [74,75].

There have been a few studies attempting to synthesize epoxies and polyurethanes from lignin oil. A study attempted to create epoxy resins by modifying pine wood lignin oil with epichlorohydrin. In a follow up study, hardwood lignin oil was utilized in a similar protocol to form epoxy resins. The resins were cured with diethylene triamine and BPA based diglycidyl ether to yield cured thermosets [170,171]. In a similar study, lignin oil was used as one of the polyols along with polyethylene glycol to form polyurethane foams [172]. The addition of lignin oil improved mechanical properties of these systems.

This present study focuses on the chemical modification of lignin oil generated from the reductive catalytic fractionation process to produce a prepolymeric material for the synthesis of polyamides. The modification process occurs in two steps involving organic carbonates and maleic anhydride. The modified lignin oil was extensively

characterized to determine its thermal and chemical properties. Subsequently, the prepolymeric material was polymerized using polycondensation with various diamines, and the resulting polymer was subject to thermal, chemical, and dynamic mechanical analysis. The results revealed the formation of polyamides with varying glass transition temperatures and thermal degradation behaviors. These prepared polyamides could be processed via solvent casting and molding into samples for mechanical testing in a similar process to divanillic acid based polyamides [70,73].

This study demonstrates the ability to chemically functionalize lignin oil with the green class of chemicals known as organic carbonates, and studies their polymerization to a high-value class of polymers, polyamides. Through the utilization of sustainable feedstocks and green chemistry principles, the study aims to enhance the understanding and development of lignin-based polymers with desirable properties and potential applications as semi-aromatic and aromatic elastomers with good thermal resistance.

4.2 Materials and Methods

4.2.1 Chemicals

Poplar wood was purchased from Home Depot. Methanol, Acetone, and Dichloromethane (DCM) were purchased from Fischer Scientific. Triphenyl phosphite (TPP), lithium chloride (LiCl), n-methyl pyrrolidone (NMP), pyridine, d-DMSO, d-Chloroform, p-Phenylenediamine (PPD), 1,10-diaminodecane (DAD), propylene carbonate (PC), Pd/C, and maleic anhydride (MA) were purchased from Sigma Aldrich. Lignin Oil (RCF) was provided by NREL for the preparation of DMA testing samples.

4.2.2 Reductive Catalytic Fractionation of Wood

The poplar wood was converted into sawdust using an electric saw. The sawdust was then sieved through a 0.5mm sieve to remove larger chips. The experiment was conducted in a 500 ml high-pressure batch reactor (Parr Instruments). To set up the reactor, 30 g of poplar wood, 3 g of Pd/C catalyst, and 300 ml of methanol were loaded into the reactor under a constant nitrogen environment. The reactor was sealed and flushed three times with N2 (10 bar). Subsequently, the reactor was pressurized with H2 (30 bar at room temperature). The reaction mixture was stirred at 750 rpm while being heated to 250°C for approximately 30 minutes. The reaction was allowed to proceed for 3 hours. This procedure was adapted from Bosch et al. [60]. After the reaction time, the reactor was cooled and depressurized at room temperature. The contents of the reactor were collected quantitatively by washing the reactor with methanol. The solid pulp obtained was then stirred with acetone for 3 hours. The mixture was filtered, and the solid residue was washed with acetone. The resulting filtrate was subjected to a threefold liquid-liquid extraction using dichloromethane (DCM) and distilled water. The DCM-extracted phase, containing the RCF lignin oil (RCF), was dried in an oven at 80 °C. It is important to note that the procedure involves a highly flammable solvent and catalyst mixture and should be handled safely.

4.2.3 Functionalization of RCF Lignin

1 g of RCF lignin oil was weighed and 5 ml of propylene carbonate was added to it. 0.095g of K2CO3 was added to the reaction mixture. The reactants were reacted at 170 °C after flushing with nitrogen in a condenser setup for 1 hour. The product was

subjected to a threefold liquid-liquid extraction using DCM and distilled water. The DCM extracted phase (RCFPC) was dried in an oven at 80 °C overnight.

1 g of RCFPC was weighed and 5g of maleic anhydride was added to the reaction mixture. The mixture was heated to 130 °C and reacted for 5 hours under a condenser set up. The product was subjected to a threefold liquid-liquid extraction using DCM and distilled water. The DCM extracted phase (RCFPCMA) was dried in an oven at 80 °C overnight.

4.2.4 Polymerization

RCFPCMA (1 g) was dissolved in NMP (10 mL), then an equimolar amount (Based on ^{31}P N NMR calculations) of diamine, 2 equivalents of TPP, and pyridine (1.2ml). were slowly dripped into the flask, which was filled with nitrogen and heated for varying temperatures and times. Following the reaction, the product was precipitated in water and washed with methanol followed by deionized water. Finally, the product was dried overnight under vacuum at 80 °C. The polyamides were named RCFPA-Aromatic and RCFPA-Aliphatic for PPD and DAD based polymers respectively.

4.2.5 FTIR Spectroscopy

Fourier transform infrared spectroscopy (FTIR, Thermo-Nicolet is50) was used to determine the chemical nature of the fillers. Spectra were collected in ATR mode from 4000 to 400 cm^{-1} at a resolution of 2 cm^{-1} with 64 scans.

4.2.6 NMR Spectroscopy

^{31}P NMR spectroscopy was conducted to elucidate the phosphorylation status of lignin samples. The experiments utilized a Bruker Avance Neo III 300 MHz spectrometer, equipped with a phosphorus-optimized pulse program to ensure accurate quantification and

resolution of phosphorus-containing species. An internal standard solution was prepared by dissolving cholesterol in a mixed solvent of pyridine and deuterated chloroform (CDCl3) at a ratio of 1.6:1 (v/v), achieving a concentration of 40 mg/ml. Using the same solvent mixture, a relaxation agent solution of chromium acetylacetonate was prepared at 10 mg/ml. For the sample preparation, approximately 40 mg of lignin was precisely weighed and combined and dissolved in 500 µL of the solvent solution. To this, 100 µL of the internal standard solution and 50 µL of the relaxation agent solution were added. 100 µL of 2-chloro-4,4,5,5-tetramethyl-1,3,2-dioxaphospholane was added to the prepared solution. A standard phosphorus pulse program was employed, with the spectral acquisition consisting of 256 scans. Topspin 4.2 software was used for data processing and volume integration. HSQC 2D NMR was carried out on the Bruker Avance Neo III 300 MHz NMR. 40-50 mg of sample was dissolved in d-DMSO.

4.2.7 Gel Permeation Chromatography

The molecular weight of lignin precursors was measured using GPC (Waters) with a Styragel HR1. The lignin oil was dissolved in THF at a concentration of 5 mg/ml. 0.22 um PTFE filters were used for the solvent as well as samples. PS calibration standards were used at 1 mg/ml. The flow rate was fixed at 1 ml/min. Lignin samples were detected by a UV-Vis detector at 210 nm. All molecular weight calculations were carried out after calibration using Empower software.

4.2.8 Thermal Analysis

Thermogravimetric analysis of the cured resins was performed while heating under N_2 using a TA instruments Discovery TGA 5500. About 5 mg of the dried sample was heated at 10 °C/min to 700 °C at a flow rate of 25 mL/min. TGA allows determination of

the degradation temperature and simultaneously indicated the absence of residual solvents. Differential Scanning Calorimetry (DSC) measurements were performed on a DSC 250 (TA Instruments) by using a heat-cool-heat cycle from -50 to 200 °C. The glass transition temperatures were reported from the second heating cycle.

4.2.9 Dynamic Mechanical Analysis

Dynamic Mechanical Analysis (DMA) was conducted using a Mettler Toledo DMA (SDTA 861) instrument. The samples were prepared by solvent casting of the samples, utilizing a solution of formic acid and DCM spread onto PTFE dishes. The polymers were then allowed to dry overnight at a temperature of 80 °C. Subsequent to drying, the samples were molded into discs with a diameter of 7.5 mm. These discs were affixed to a shear fixture, and the sample thickness was determined by measuring the difference in the fixture's thickness before and after the samples were clamped. A dynamic force of 35 N was applied. The strain was set at 1%, corresponding to an amplitude of 6.1 μm. Temperature sweeps were conducted for the RCFPA-Aliphatic samples over two distinct ranges: from -50°C to 60°C and from 20°C to 120°C. Additionally, the frequency of the sweeps was adjusted between 0.5 Hz and 5 Hz. Specifically, the storage modulus, loss modulus, and tan delta values, were plotted to assess the materials' mechanical behaviors over the specified temperature and frequency ranges.

4.3 Results and Discussion

4.3.1 Functionalization of Lignin Oil

The lignin oil was obtained through reductive catalytic fractionation/hydrogenolysis. This process resulted in a brown viscous liquid. The lignin oil is a mixture of monomers, dimers, and oligomers. This was evident in Fig. 17 which

highlights the GPC chromatogram of RCF. The highest peak on the GPC chromatogram corresponds to 4-propanolsyringol and 4-propanolguaiacol. The lignin oil had a 40.35% bifunctional monomer content by mass based on the GPC chromatogram areas. Hardwood upon reductive catalytic fractionation leads to a high monomer content in the lignin oil, compared to softwood. Hence, poplar wood, a cheap easily renewable hardwood was chosen as a starting material for the production of lignin oil [173]. The lignin oil has a mixture of aliphatic as well as aromatic hydroxyl groups which can be functionalized to form polymerizable reaction sites.

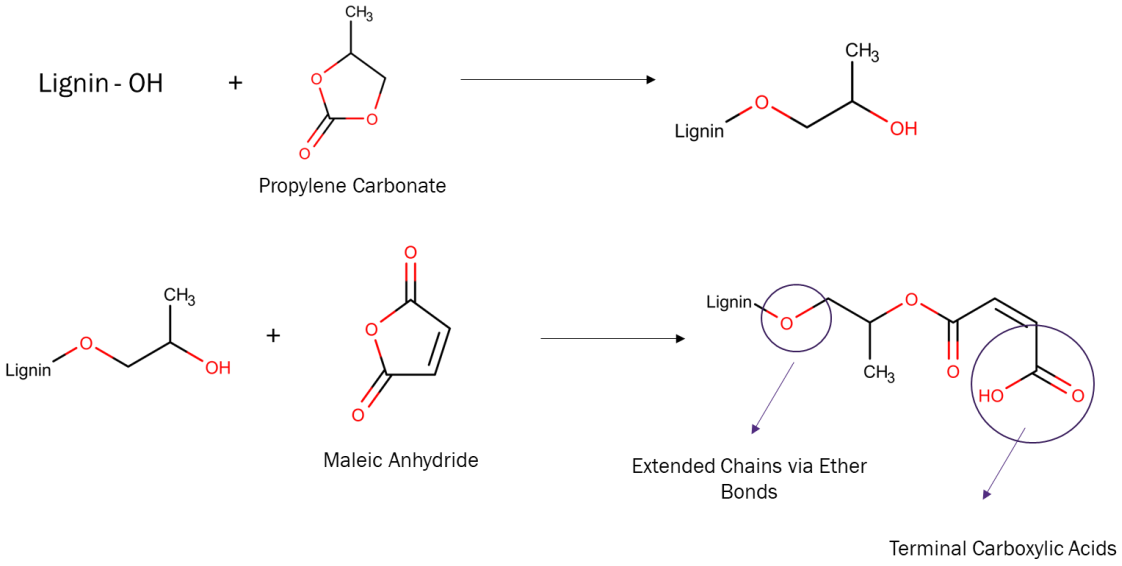

Figure 15 Reaction Scheme for Functionalization of Lignin Oil

To functionalize the lignin oil, the first step involved using propylene carbonate as a solvent and reagent for oxyalkylation. Propylene carbonate was chosen as an alternative to propylene oxide which is a toxic reagent. Organic carbonates have the potential to be synthesized using atmospheric CO_2 [174]. Moreover, organic carbonates are considered green solvents because of their benign chemical nature, ease of separation and high boiling

points [174]. The chemical reaction of propylene carbonate was understood using ^{31}P NMR and 2D NMR. Based on the analysis of ^{31}P NMR, both the aliphatic and aromatic hydroxyl groups reacted with propylene carbonate, leading to the formation of an extended chain with terminal aliphatic hydroxyl groups. An illustration of the same with lignin has been shown in Fig 15. In the second step, these terminal aliphatic hydroxyl groups were esterified with maleic anhydride, resulting in the formation of terminal carboxylic acid groups. These carboxylic acid groups could then undergo further polymerization through polycondensation with various diamines. The oxypropylation of lignin was performed at 170 °C, causing the elimination of carbonate groups as CO_2 [161] as illustrated in the reaction scheme Fig. 15.Complete conversion of all aromatic hydroxyl groups was achieved within 1 hour, as confirmed by spectroscopic analysis using ^{31}P NMR.

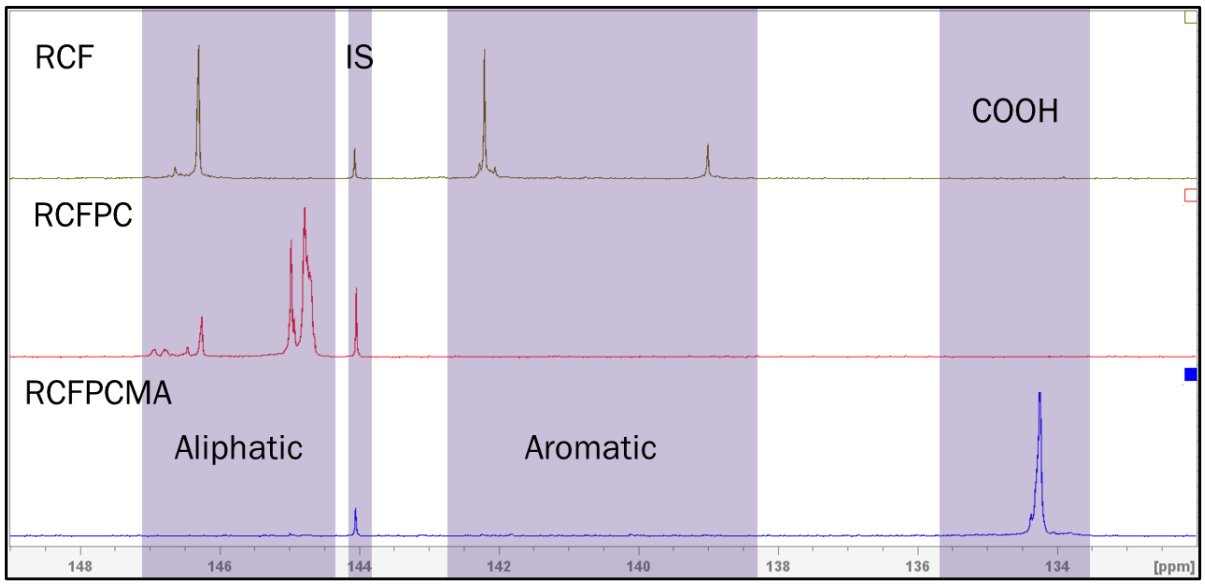

Figure 16 ^{31}P NMR Spectra for RCF, RCFPC, and RCFPCMA

A two-step strategy was employed to convert aromatic hydroxyl groups into aliphatic hydroxyl groups. In the second step, maleic anhydride was reacted with RCFPC at 130°C, resulting in the complete conversion of all hydroxyl groups to carboxylic acid groups. Initially, a direct reaction of RCF with maleic anhydride was attempted to

functionalize the lignin with carboxylic acid groups. However, unlike propylene carbonate, maleic anhydride did not react with the aromatic hydroxyl groups at temperatures up to 170°C. The results for this have been highlighted in Fig S1 that showed unreacted aromatic groups at 142 ppm and 138 ppm. Without conversion of aliphatic hydroxyl groups, it would be difficult to have bifunctional monomers for further polymerization. The stacked NMR with RCF, RCFPC, and RCFPCMA has been shown in Fig. 16. The NMR spectrum of the RCF shows peaks corresponding to the aliphatic hydroxyl groups at 146-147 ppm and peaks corresponding to the aromatic hydroxyl groups at 139 and 142 ppm. The NMR spectra of RCFPC indicated that both aliphatic and aromatic hydroxyl groups reacted with propylene carbonate. The initial step of the reaction showed that all aromatic hydroxyl groups at 139 and 142 ppm extended the chain, leading to the formation of aliphatic hydroxyl groups at 145 ppm. Some pre-existing aliphatic hydroxyl groups also reacted with propylene carbonate. The signal around 145 ppm corresponded to hydroxyl groups from propylene carbonate, while the signal at 146-147 ppm corresponded to existing aliphatic hydroxyl groups on the lignin oil monomers and dimers. Previous studies on propylene carbonate functionalization on lignin showed similar behavior with aliphatic hydroxyl groups also participating in oxypropylation. Upon esterification of these newly generated aliphatic hydroxyl groups with maleic anhydride, a new peak at 134 ppm emerged as seen in the RCFPCMA spectra in Fig.16, signifying the esterification of all the aliphatic hydroxyl groups.

Table 8 Hydroxyl Content of lignin oil

Sample	**Aliphatic OH Content (mmol/g)**	**Aromatic OH Content (mmol/g)**	**Carboxylic Acid Content (mmol/g)**	**Total OH Content (mmol/g)**
RCF	3.0	3.1	0	6.1

RCFPC	4.6	0	0	4.6
RCFPCMA	0	0	3.6	3.6

These two steps of reactions led to a decrease in hydroxyl content as seen in Table 8. The hydroxyl content of the oil initially is 6.1 mmol/g which decreases over the functionalization steps. This decrease was based primarily on increased molecular weight and some condensation reactions in between lignin.

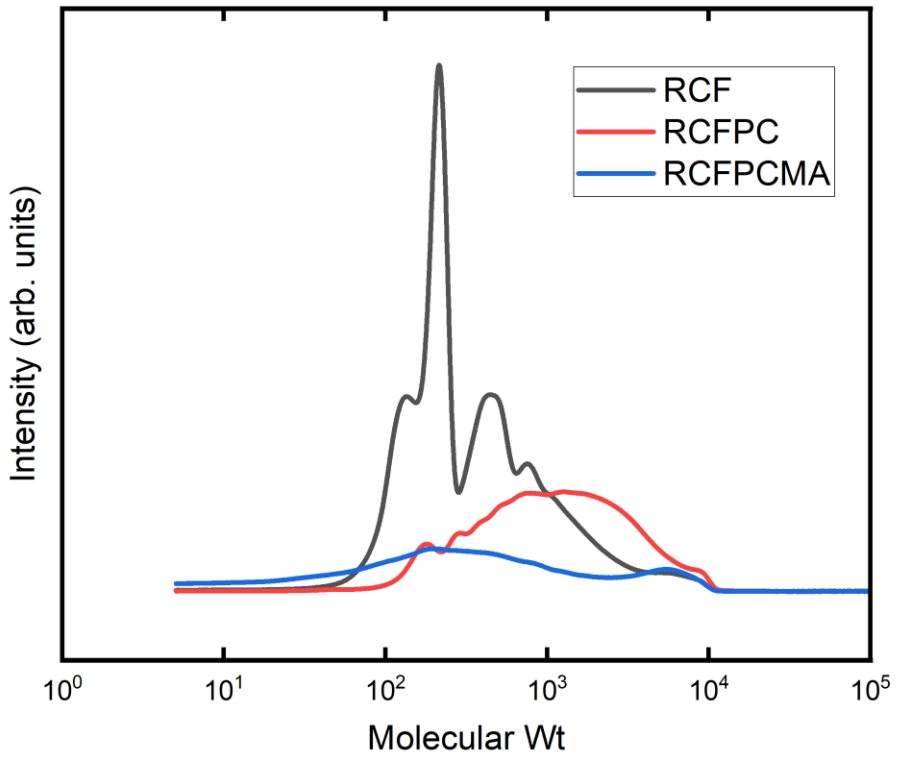

Figure 17 GPC chromatograms of the functionalized lignin oil

The condensation was further corroborated by the GPC chromatogram as seen in Fig 17. It showed that the molecular weight distribution in the final functionalized oil differed from that of the original oil due to condensation reactions. Initial RCF showed a sharp peak corresponding to the bifunctional monomer 4-propanolysringol and 4-

propanolguaiacol with a molecular weight of ~200. RCFPC showed a considerable increase in molecular weight compared to native RCF. Similar observations have been reported by Kuhnel et al [161] and during the functionalization of organosolv lignin and by Sternberg et al [55] during the functionalization of Kraft lignin. It is important to note that there are two peaks in the GPC chromatogram of RCFPCMA, suggesting some bond cleavage in the presence of maleic anhydride. Further studies are necessary for determining the structure of these cleaved molecular units. A secondary test using GC/MS (Fig. S2) was conducted to confirm the molecular weight of the monomer formed during reductive catalytic fractionation, and the results aligned with the findings from GPC and previous studies [60].

Table 9 Molecular Weight of the functionalized lignin oil

Sample	**M_n**	**M_w**	**PDI**
RCF	260	724	2.78
RCFPC	600	1784	2.98
RCFPCMA	167	1316	7.00

Thermal analysis of the oil indicated its heterogenous nature, consisting of a mixture of monomers, dimers, and oligomers. The glass transition temperature of the oil increased with each functionalization step, from -48°C to 0°C over the course of two steps further indicating an increase in hydrogen bonding due to etherified and esterified units acting as hydrogen bond acceptors.

2D NMR spectroscopy, specifically HSQC NMR, was employed to elucidate the chemical bond structures within functionalized lignin oil. The HSQC NMR technique facilitates the correlation between carbon and hydrogen atoms across different chemical environments, providing a detailed insight into the molecular structure of the lignin oil after functionalization.

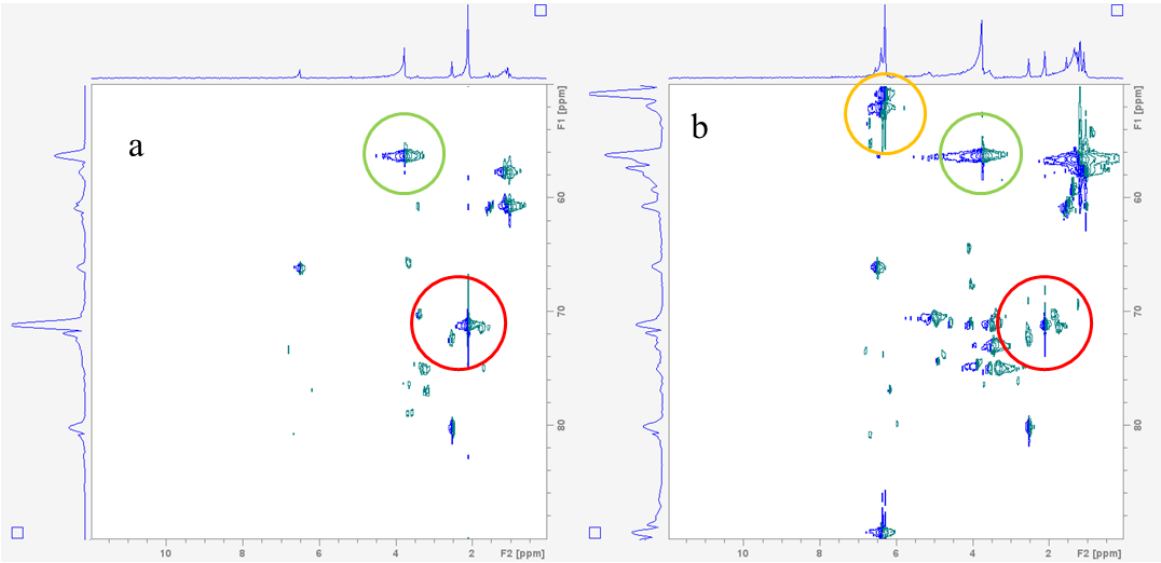

Figure 18 2D HSQC NMR Spectra of (a,c) RCFPC (b,d) RCFPCMA

The 2D NMR spectra focused on the region representing interunit aliphatic carbon-hydrogen pairs (δC/δH 50.0–90/0–12 ppm), was selected to investigate the presence of carbons adjacent to alcohol, ether, and aromatic methoxyl (Ar-OCH_3) groups. It was showcased and marked in Fig. 18. This area is particularly informative for identifying the chemical shifts associated with such functional groups in lignin.

Within the aliphatic region, areas highlighted in green in the spectra for both RCFPC and RCFPCMA corresponded to O-Me groups from the original lignin oil, indicating that these methoxyl groups remained unaltered during the functionalization process. This observation is consistent with previous 2D NMR analyses of lignin oil, reaffirming the stability of these groups under the conditions applied [53].

Furthermore, the appearance of new chemical activity, marked in red, pinpointed the formation of ether bonds, specifically highlighting the CH bonds adjacent to newly formed ether linkages resulting from the functionalization with propylene carbonate. Additionally, the spectra for RCFPCMA showcased further activity, delineated in yellow, which was attributed to the CH bonds in maleic anhydride that formed ester linkages with

the lignin oil. This additional activity confirms the successful attachment of maleic anhydride to the lignin structure through ester bond formation.

4.3.2 Polymerization with various diamines

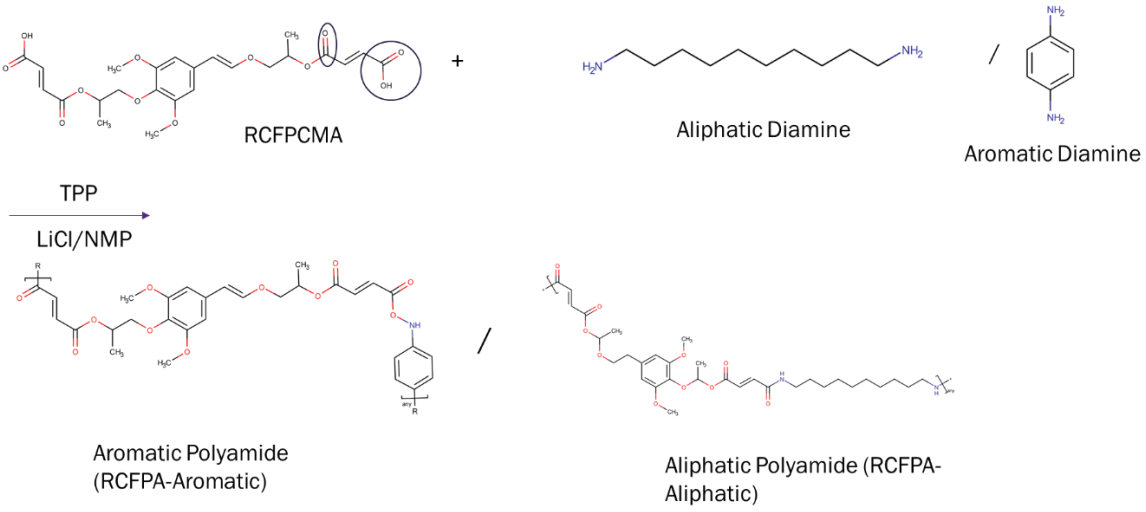

In this study, polymerization of the functionalized lignin oil was conducted using a polycondensation method with different diamines. The polymerization was carried out in a solvent-based environment following the Higashi method [175]. LiCl and pyridine were added to the solvent to aid in dissolving the polymer by forming a complex that enhances polymer solubility by hindering hydrogen bonding of aromatic rings. TPP served as the catalyst that activated the acid group for polymerization. The Higashi method was chosen for its non-toxic synthesis procedure that avoids the use of acid chlorides. The resulting polyamides had a brown color, and the polymerization process was optimized to achieve desired thermal properties in the final polymer. A solventless – catalyst free polymerization process was also attempted to see the alternative greener synthesis method. The temperature of polymerization ranged from 110-180°C, and the reaction time varied from 6-24 hours. Lower temperatures were found suitable for polymerization with aromatic

diamines, while higher temperatures were required for polymerization with aliphatic diamines.

The synthesized polymers were insoluble in most organic solvents and hence FTIR analysis was primarily used to characterize the polymerization by confirming the presence of amide linkages. The polymerization process led to increased viscosity of the mixture and the evolution of water, which needed to be removed for the polymer to achieve high molecular weight. The reaction was carried out under a vacuum to continuously eliminate water vapor formed during the reaction. An equivalent molar ratio of the acid and amine groups was used to achieve the highest possible molecular weight in polycondensation reactions.

With longer reaction times, parts of the polymer started precipitating out of the solvent. After polymerization, the polymer was washed with water and methanol to dissolve catalysts and unreacted monomers. The final polymer was not soluble in traditional organic solvents like DMSO, NMP, DCM, THF, and Chloroform. However, the polymers derived from DAD were soluble in a mixture of DCM and formic acid, which is a characteristic feature of other commercially available aliphatic polyamides. RCFPA-Aromatic was not soluble in any solvent, preventing NMR characterization. FTIR analysis was conducted to gain insights into the polymerization reaction, and the FTIR graph was divided into two regions for detailed analysis.

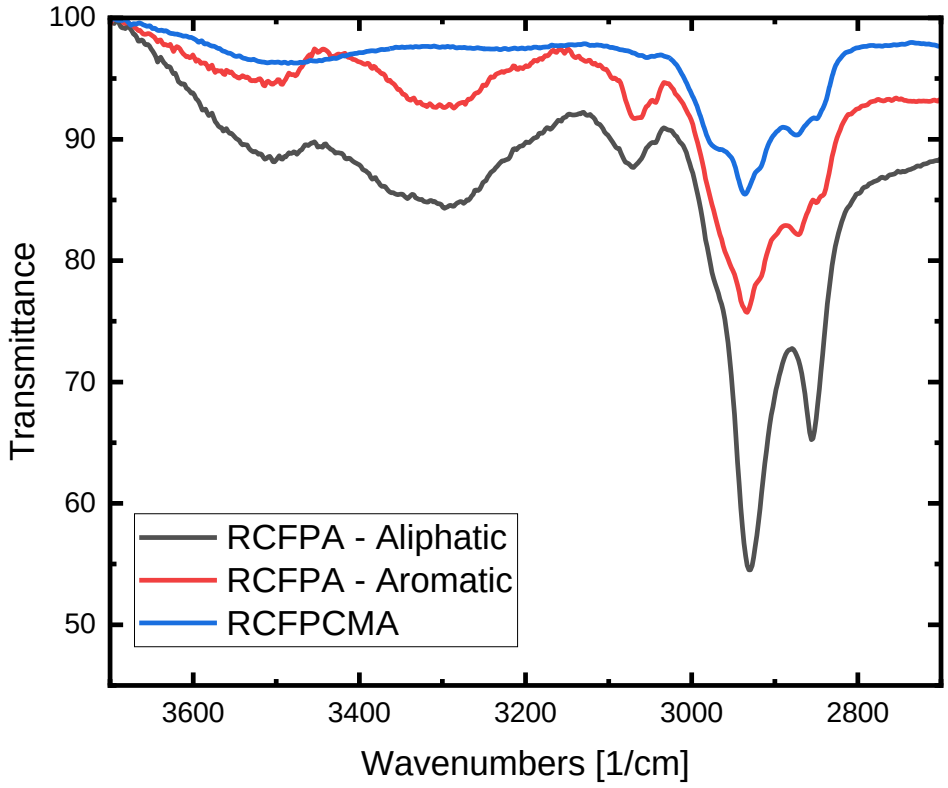

Figure 19 FTIR Spectra of the various polymers compared with functionalized lignin oil with a focus on 2500-4000 cm^{-1}

The IR spectrum shown in Fig. 19 displayed characteristics of strong CH linkages due to their aliphatic nature. This was evident in the peaks at 2800-2950 cm^{-1}, which were distinctively different for RCFPA-PPD compared RCFPA-DAD. Additionally, the OH peak in between 3400-3600 cm^{-1} reduced in intensity after polymerization and a peak corresponding to the NH vibrations showed up in between 3400-3200 cm^{-1}. This confirmed the polymerization of the functionalized lignin oil with the aliphatic and aromatic diamines.

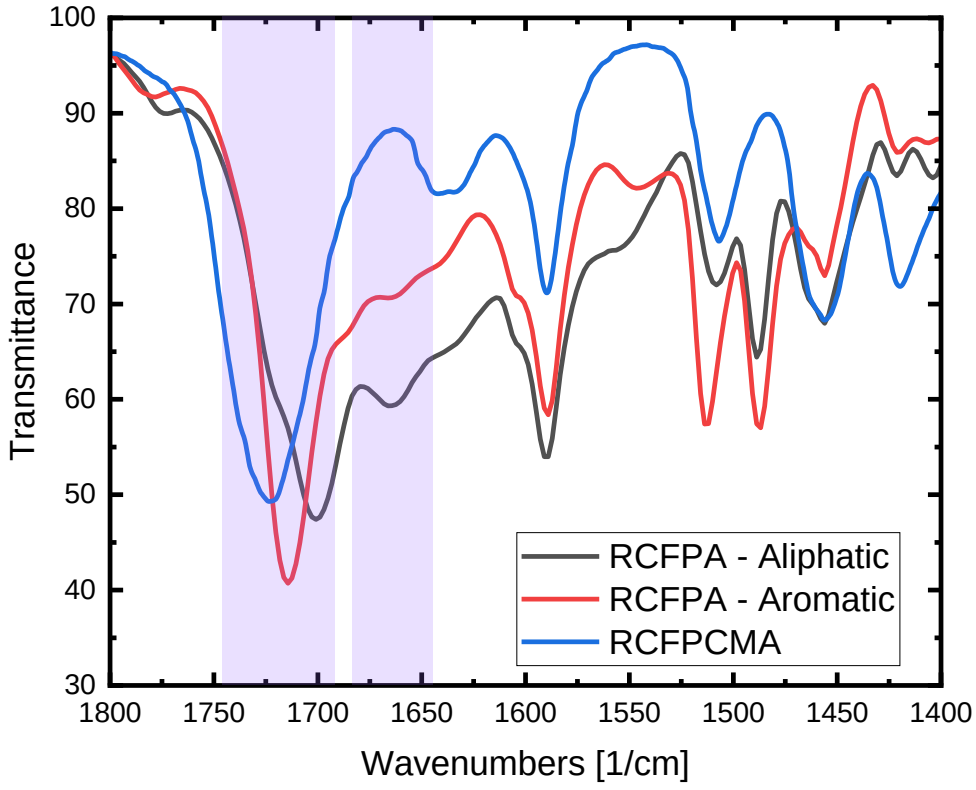

Figure 20. FTIR Spectra of the various polymers compared with functionalized lignin oil with a focus on 1400-1800 cm^{-1}

Upon closer examination of the FTIR spectrum in Fig. 20. the carboxylic acid carbonyl peak in the lignin oil appeared at 1721 cm^{-1}. This peak was of particular interest as it indicated the conversion of the acid group to an amide group. Amide group carbonyls are represented by peaks in the region between 1600-1700 cm^{-1}. The distinct carbonyl peaks in the final IR spectrum between 1700-1710 cm^{-1} for all the polyamides corresponded to the ester linkage in the modified lignin oil. The amide peak varied based on the diamine used: 1667 cm^{-1} for p-phenylene diamine polyamide, and 1655 cm^{-1} for Diaminodecane polyamide. This variation is expected, as conjugated and unconjugated amides exhibit different absorption peaks in an FTIR spectrum. The solventless synthesis

method led to the material solidifying within 1 hour of the reaction under vacuum and in an oil bath. FTIR analysis of the solventless polyamide synthesis revealed that the amine targeted the ester bond over the acid bond in RCFPCMA leading to reduction of the ester bond peak in the FTIR.

Thermally, the polyamides underwent analysis using Differential Scanning Calorimetry (DSC) and Thermogravimetric Analysis (TGA). The DSC data for the synthesized polyamides indicated that their glass transition temperatures varied significantly, presenting values considerably higher than those of the functionalized lignin oil. Notably, the DSC thermograms displayed neither melting nor crystallization behavior within the temperature range of -50°C to 200°C, as depicted in Fig. 21. This confirmed the amorphous nature of the synthesized polyamides. The amorphous nature can be attributed to branched chemical structures on lignin oil monomer and a mixture of chemical species being used to synthesize the polyamides. The analysis of the second cycle in the DSC thermograms provided insights into the glass transition temperatures of the polyamides, revealing that the aromatic polyamide exhibited a higher glass transition temperature in comparison to the aliphatic polyamide. This difference is attributed to the inherent rigidity of the sp^2-bonded aromatic rings, as opposed to the more flexible sp^3-bonded aliphatic carbon chains, thereby imparting increased rigidity to the polymer chains [176]. Moreover, aromatic rings can act as hydrogen bond acceptors, thereby causing there to be increased hydrogen bonding in the aromatic polyamide leading to an elevated T_g [177]. This observation aligns with findings from a previous study by Brianna and Kasko, which explored the use of various diamines with lignin-based monomers for polyester-amide synthesis, underscoring the impact of using a variety of diamines to synthesize lignin

derivable polyester-amides [74]. Moreover, the samples showed a broad glass transition spanning over 40 °C for both the samples. The values reported in the table are the mid-point values for the change in heat flow of the thermogram. The glass transition temperatures and the temperatures at 5% weight loss ($T_{5\%}$) are summarized in Table 8.

Table 10 Thermal Properties of the various polymers

Polyamide	**T_g DSC (°C)**	**$T_{5\%}$ (°C)**
RCFPA – Aromatic	45	220.47
RCFPA – Aliphatic	17	265.87

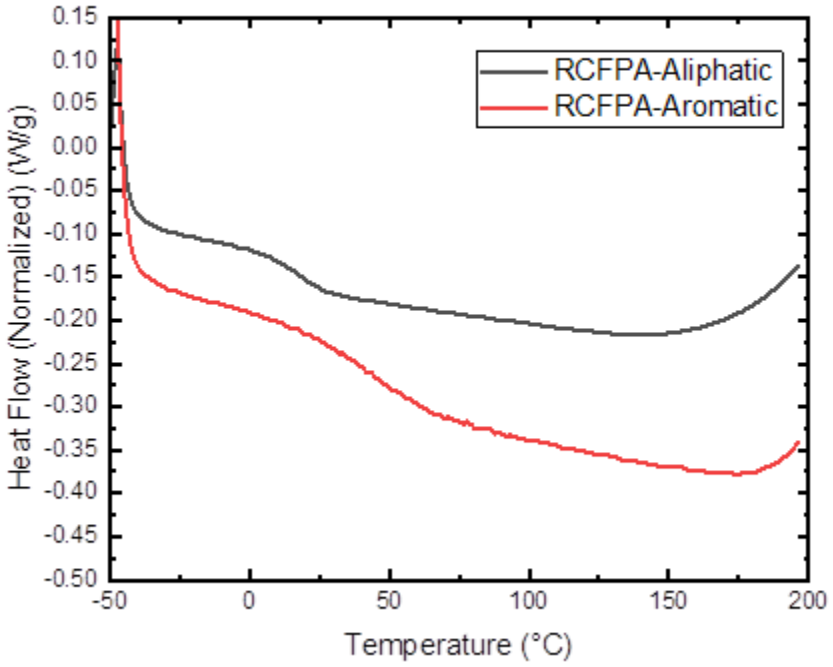

Figure 21 DSC Thermograms of the synthesized polyamides

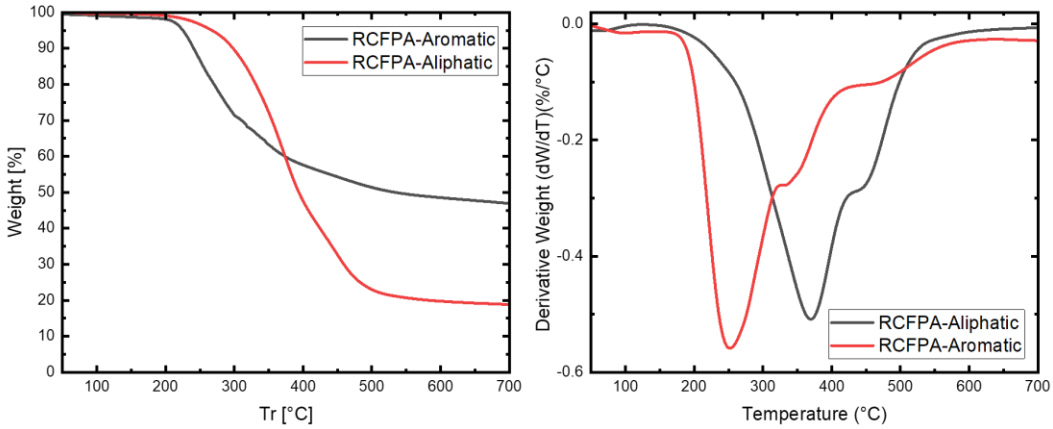

Figure 22 Thermal Degradation Curves of the Polyamides

The thermal degradation profiles of the polyamides, depicted in Fig. 22, demonstrated that the temperatures at 5% weight loss for all polyamides exceeded 220°C. However, the aliphatic polyamides exhibited some mass loss below 150°C, potentially due to the absorption of moisture from the atmosphere. Moreover, the aliphatic polymers began degrading at higher temperatures compared to the aromatic polymers, which could be explained by the higher molecular weight of the aliphatic polyamides. The degradation profiles of all polyamides exhibited a two-step degradation process, with the first step corresponding to the degradation of ester linkages and the second step to the degradation of amide linkages. Aromatic polyamides displayed a higher residual weight at the conclusion of the TGA cycles, attributed to the higher aromatic content which enhances thermal stability relative to aliphatic carbon chains. This behavior mirrors that observed in polyester-amides synthesized from lignin-based monomers, highlighting the thermal stability imparted by aromatic structures [178].

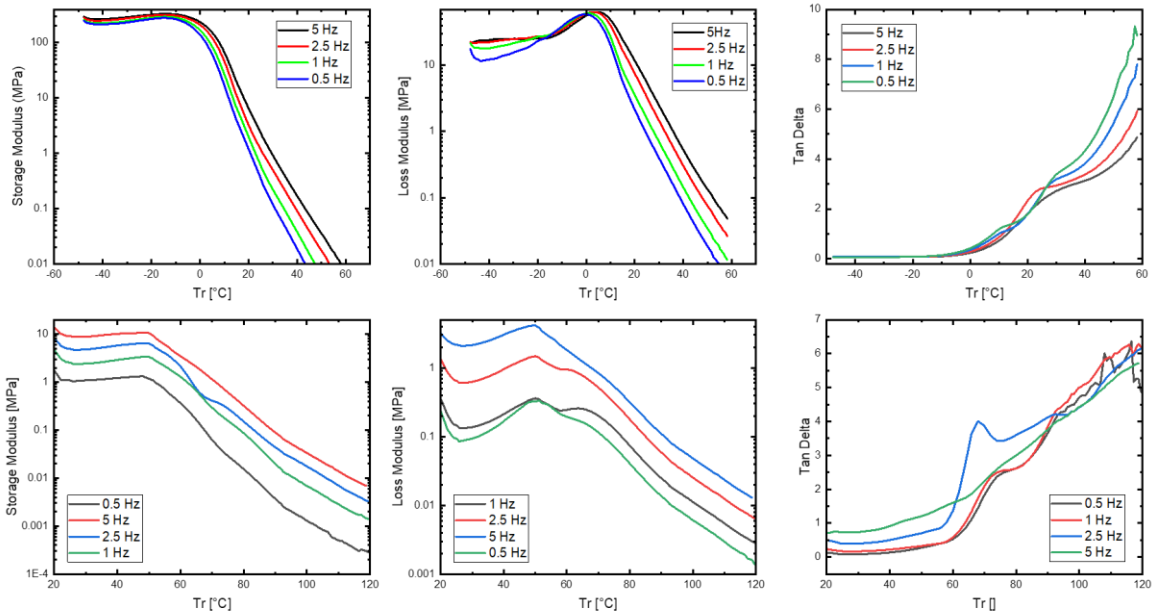

DMA was carried out to understand the viscoelastic behavior of the polymers. A shear fixture was used as it is the advised fixture for soft elastomeric materials [179,180]. An advantage of shear loading over other forms of loading is because materials do not undergo volume change under shear loading, only the shape changes. The displacement created under shear loading is straightforward to analyze as it is proportional to its distance from the plate [181]. The aliphatic polyamide exhibited a higher storage modulus than the aliphatic polyamide in the glassy state, DMA was conducted between -50 and 60 °C for RCFPA-Aliphatic and 20 to 120 °C for the RCFPA-Aromatic according to the degradation behavior shown by TGA and T_g observed in the DSC thermograms. Tan delta peaks were analyzed to verify the T_g values. For the aromatic polyamide, the T_g varied from 65 °C to 74 °C with decreasing frequencies. This was higher than the T_g from the DSC thermogram. Multiple frequencies were utilized for DMA characterization to reveal additional frequency dependent relaxations. Upon closer examination of the loss modulus curves for the aromatic polyester, multiple transitions could be observed in between 40 – 80 °C. These

could be a sign of polymer heterogeneity. Since the polymers were synthesized from lignin oil, which is a heterogenous material, it is possible for the material to have multiple relaxation transitions. Similarly for the aliphatic polyamide, multiple transitions were observed in between -20 – 20 °C. These are primarily associated with the aliphatic chain relaxation corresponding to the DAD used for polymerization. The peak of the tan delta curve for the aliphatic polyamide pointed to T_g values in between 11 – 23 °C. This was in line with what was observed from the DSC thermograms. Transitions associated with aliphatic chain relaxations are associated with lower temperatures compared to aromatic building blocks. The aromatic polyamide had a very low storage modulus making it unsuitable for real world applications. The storage modulus of the aliphatic polyamide pointed towards its use as an elastomer with a low glassy and rubbery state storage modulus.

4.4 Conclusion

A polyamide material incorporating lignin oil as one of the prepolymeric components was successfully synthesized using solvent-based chemistry. The lignin oil underwent chemical modification through simple solventless procedures, resulting in the introduction of extended carboxylic acid groups. It is important to note that production of lignin oil is an energy intensive process and for this study, the most repeatable method was chosen to prove the potential of lignin oil. Ethanol can be utilized instead of methanol to minimize toxic chemical utilization and lower temperature depolymerizations can be carried out with improved catalyst design. The obtained results were in line with previous attempts at lignin oxyalkylations and malleations. Molecular weight determination and chemical structure characterizations confirmed the successful synthesis of the prepolymeric material. Some evidence of bond cleavage in the RCFPCMA chromatogram

was observed. A higher molecular weight column for GPC followed by other 2D NMR (COSY, ROESY) would elucidate bond cleavage in detail. By combining the aromatic rigid and brittle structure of lignin with the flexible aliphatic structure of Diaminodecane, the resulting polymers exhibited desirable properties. Thermal analysis indicated a moderate glass transition temperature and an amorphous nature of the polymers. Moreover, the thermal degradation analysis revealed that the material exhibited an onset of degradation at temperatures exceeding 220°C, indicating its potential for real-life applications. To gather some insight into the viscoelastic behavior, DMA was carried out at varying frequencies. The aromatic polyamide showed considerably higher storage modulus compared to the aliphatic polyamide at the same temperature. The tan delta plot showed multiple relaxations associated with heterogeneity of the polymers.

4.5 Supplementary Information

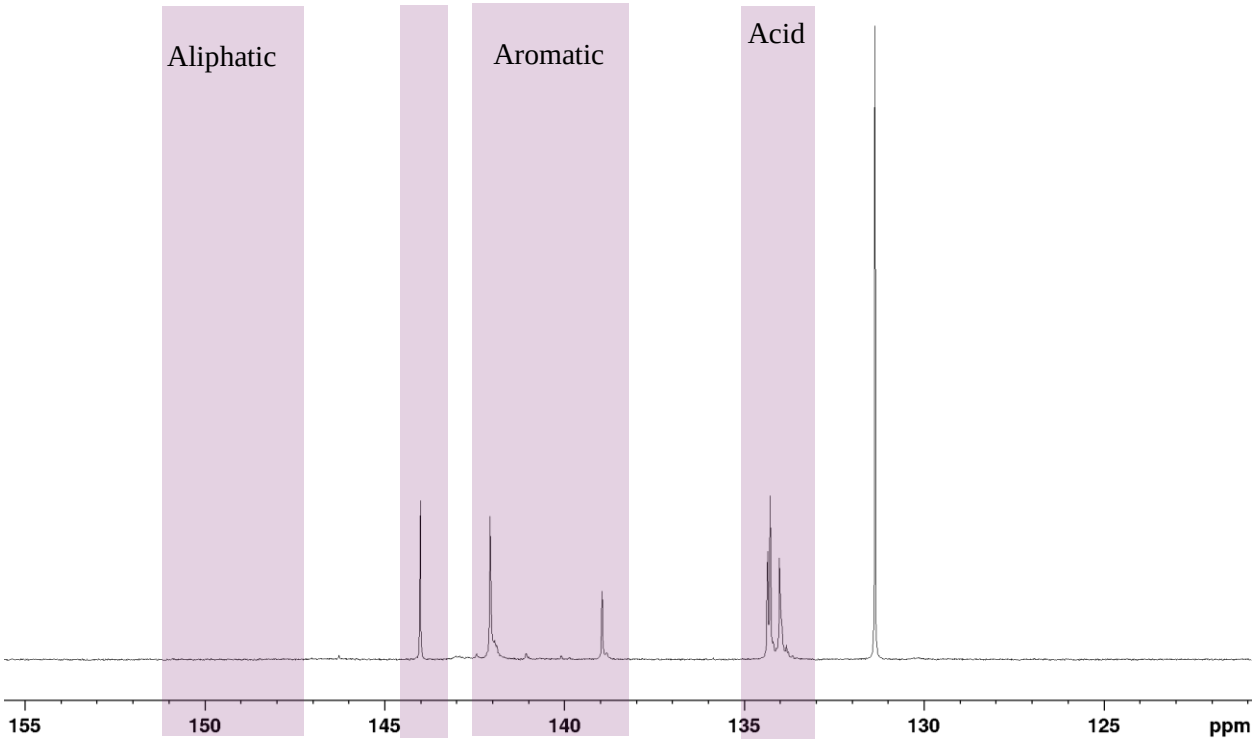

Figure S 1 ^{31}P NMR Spectra of RCF directly reacted with Maleic Anhydride

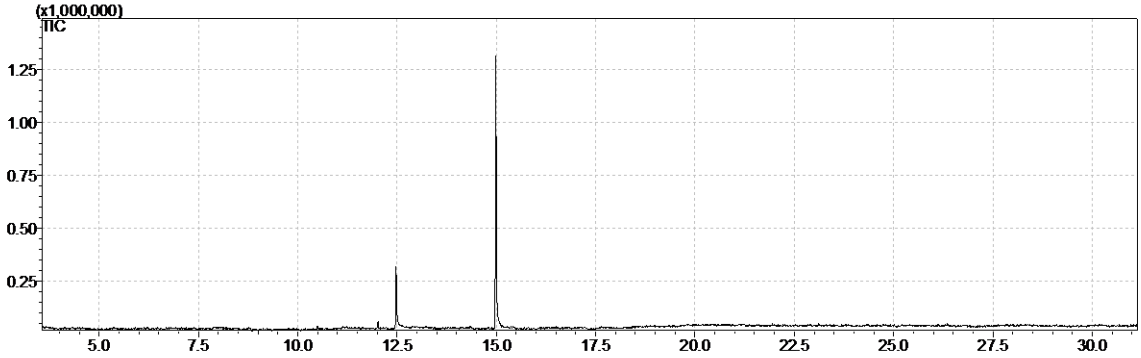

Figure S 2 GC Spectra of the Synthesized RCF confirming the synthesis of 2 monomers.

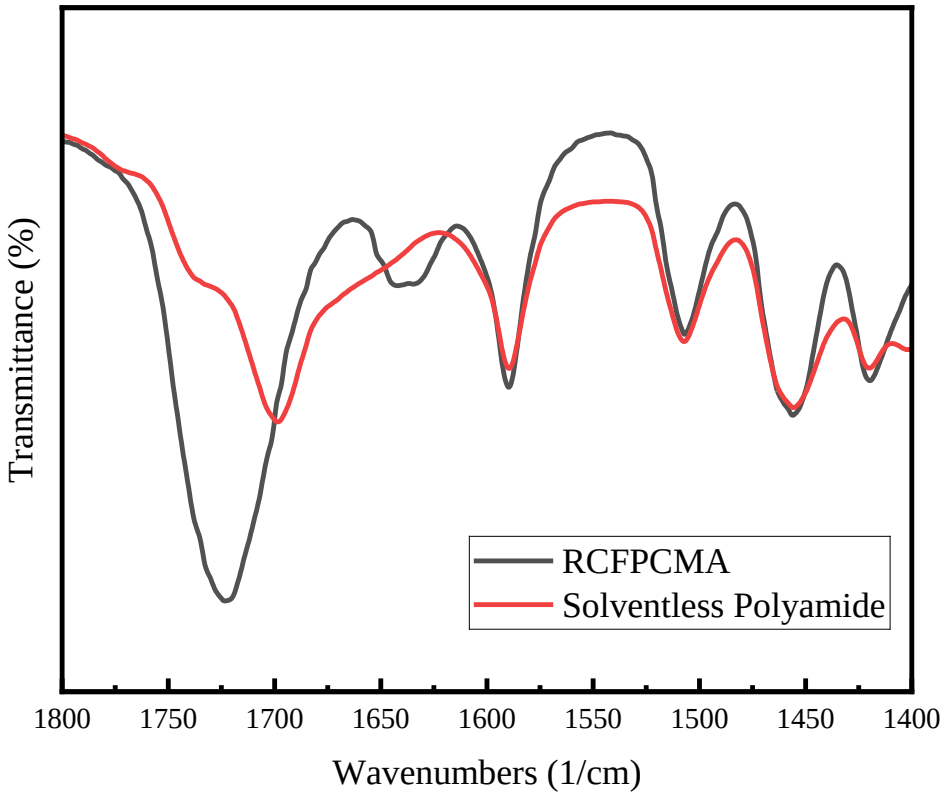

Figure S 3 FTIR Spectra of solventless polyamide synthesis

CHAPTER FIVE

UNSATURATED POLYESTERS FROM LIGNIN OIL

5.1 Introduction

Lignin, as the most abundant renewable source of aromatic biocarbon, has garnered significant interest from both academia and industry. The chemical structure of lignin is particularly intriguing to polymer scientists because it offers a renewable pathway to high-performance aromatic polymers. Chemically, lignin is a macromolecule adorned with hydroxyl groups, both aliphatic and aromatic. These groups have been exploited to incorporate various functionalities, including urethanes, epoxies, polyesters, vinyl groups, and even direct usage as formaldehyde resins. However, mechanically, the properties of lignin macromonomers do not align with those of commercial polymers, and polymers synthesized using lignin as a macromonomer fall short of global requirements. To address this, various methods have been developed for extracting and fractionating lignin, including organosolv, kraft pulping, sulfite process, soda, pyrolysis, and reductive catalytic fractionation, each with its own set of advantages and disadvantages that influence the final chemical structure of lignin.

Reductive catalytic fractionation has drawn particular interest from the research community as it aligns with the principles of "Lignin-first" biorefining. This method aims at the selective depolymerization of lignin while preserving cellulose and hemicellulose in lignocellulosic biomass, offering a scalable approach to an integrated biorefinery. The product of this process, lignin oil, comprises a mixture of monomers, dimers, and oligomers, which can be utilized individually or as a mixture in polymeric materials. The advantage of employing smaller building blocks, as opposed to larger lignin macromolecules, lies in

their increased reactivity and reduced resistance towards polymerization reactions. Small molecules derived from lignin have sparked interest among polymer scientists for the creation of thermosetting networks, given their abundance of polyfunctional molecules (molecules with more than two reactive/polymerization centers), making them suitable for synthesizing thermosetting networks. Polyurethanes and epoxies have predominantly been explored for thermosetting networks derived from lignin, with previous studies employing isocyanates for polyurethanes and epichlorohydrin for epoxies. Additionally, lignin oil has been utilized to create epoxy polymers, with some studies mixing it with BPA-based epoxy precursors to form thermosets. Furthermore, studies have investigated the creation of vinyl networks from lignin by incorporating vinyl groups and crosslinking them with styrene or other acrylates. However, the use of lignin in unsaturated polyesters remains largely unexplored, despite its conceptualization in 2005, with scant research on synthesizing unsaturated polyester resins from lignin.

The current study focuses on the functionalization of lignin oil, elucidating the chemical structure of the polymer resin, and examining the final properties of the cured polymers. Unlike previous chapters that used propylene carbonate, this study employs ethylene carbonate for functionalization due to its higher reactivity and the absence of a branched structure. Maleic anhydride, used in excess as a functionalization agent in previous chapters, is herein utilized as a polymerization diacid while incorporating vinyl units. These units act as crosslinking sites with various acrylates, leading to the formation of a polymeric thermoset network. The chemical structures of functionalization and polymerization were characterized using ^{31}P NMR and FTIR, while the unsaturated polyester's structure was analyzed using ^{1}H NMR and FTIR. The thermal properties of the

polymers were assessed using DSC and TGA, with preliminary studies on gel time and curing temperature conducted via rheology and DSC. Finally, the viscoelastic behavior of the polymers was evaluated using shear DMA.

5.2 Materials and Methods

5.2.1 Chemicals

Poplar wood was acquired from Home Depot. Methanol, acetone, 1,8-Diazabicyclo[5.4.0]undec-7-ene (DBU), hydroxyethyl acrylate (HEA), methyl methacrylate (MEA), and dichloromethane (DCM) were procured from Fisher Scientific. N-methyl-2-pyrrolidone (NMP), deuterated dimethyl sulfoxide (d-DMSO), deuterated chloroform (d-chloroform), ethylene carbonate, palladium on carbon (Pd/C), and maleic anhydride were sourced from Sigma Aldrich. Lignin oil (RCF) was generously supplied by the National Renewable Energy Laboratory (NREL) specifically for the preparation of samples intended for Dynamic Mechanical Analysis (DMA) testing.

5.2.2 Reductive Catalytic Fractionation of Wood

The conversion of poplar wood to sawdust was accomplished using an electric saw, followed by sieving through a 0.5 mm mesh to eliminate larger chips. The experimental setup included a 500 mL high-pressure batch reactor from Parr Instruments. For reactor preparation, 30 g of poplar wood, 3 g of palladium on carbon (Pd/C) catalyst, and 300 mL of methanol were combined in the reactor under a nitrogen atmosphere. The reactor was sealed, flushed three times with nitrogen gas at 10 bar to ensure an inert environment, and then pressurized with hydrogen to 30 bar at ambient temperature. Stirring was maintained at 750 rpm, and the mixture was heated to 250°C for about 30 minutes, with the reaction proceeding for 6 hours. Post-reaction, the reactor was cooled to room temperature and

depressurized. The reactor contents were thoroughly washed out with methanol to collect the products. The solid pulp was mixed with acetone for 3 hours, filtered, and the residue washed with additional acetone. This filtrate underwent a three-stage liquid-liquid extraction using dichloromethane (DCM) and water. The DCM phase with RCF lignin oil, was then dried at 80°C in an oven. Caution is advised throughout this procedure due to the use of highly flammable solvents and a catalyst mixture, necessitating strict safety measures.

5.2.3 Functionalization of RCF Lignin

One gram of RCF lignin oil was accurately measured and combined with ten equivalents of ethylene carbonate. As a catalyst, 0.01 equivalents of 1,8-Diazabicyclo[5.4.0]undec-7-ene (DBU) were introduced to the mixture. The reactants were subjected to a reaction process at 170°C under a nitrogen atmosphere, using a condenser setup, for a duration of 1 hour. Following the reaction, the product underwent a three-stage liquid-liquid extraction utilizing dichloromethane (DCM) and distilled water to separate the organic phase from the aqueous one. The organic phase, which contained the ethylene carbonate-functionalized RCF lignin oil (RCFEC), was then dried in an oven at 80°C overnight to remove any residual solvents.

5.2.4 Polymerization

One gram of RCFEC was reacted with one equivalent of maleic anhydride in the presence of 0.03 equivalents of Titanium(IV) butoxide ($Ti(OBu)_4$) as a catalyst. NMP served as the solvent for this polymerization process. The reaction was conducted at a temperature of 200°C for a duration of 24 hours. Following the polymerization, the product, referred to as RCFECUP, underwent a three-stage liquid-liquid extraction process using

DCM and distilled water to separate the organic phase. The organic phase containing RCFECUP was then dried in an oven at 80°C overnight to eliminate any remaining solvent.

5.2.5 Curing

RCFECUP was combined with a crosslinking monomer mixture consisting of 20% by weight of hydroxyethyl acrylate (HEA) and methyl methacrylate (MMA). The curing of this mixture was performed using a two-step process in an oven. Initially, the mixture underwent a first curing step at 110°C for a duration of 24 hours. This was followed by a hardening phase at 170°C for 4 hours to further solidify the polymer network. Benzoyl peroxide served as the curing agent throughout this process, initiating the polymerization and crosslinking reactions necessary for forming the final cured product.

5.2.6 FTIR Spectroscopy

Fourier transform infrared spectroscopy (FTIR, Thermo-Nicolet is50) was used to determine the chemical nature of the polymers and prepolymers. Spectra were collected in ATR mode from 4000 to 400 cm^{-1} at a resolution of 2 cm^{-1} with 64 scans. All FTIR spectra were baseline corrected using an adaptive baseline.

5.2.7 NMR Spectroscopy

^{31}P NMR spectroscopy was conducted to elucidate the phosphorylation status of lignin samples. The experiments utilized a Bruker Avance Neo III 300 MHz spectrometer, equipped with a phosphorus-optimized pulse program to ensure accurate quantification and resolution of phosphorus-containing species. An internal standard solution was prepared by dissolving cholesterol in a mixed solvent of pyridine and deuterated chloroform (CDCl3) at a ratio of 1.6:1 (v/v), achieving a concentration of 40 mg/ml. Using the same solvent mixture, a relaxation agent solution of chromium acetylacetonate was prepared at 10 mg/ml.

For the sample preparation, approximately 40 mg of lignin was precisely weighed and combined and dissolved in 500 µL of the solvent solution. To this, 100 µL of the internal standard solution and 50 µL of the relaxation agent solution were added. 100 µL of 2-chloro-4,4,5,5-tetramethyl-1,3,2-dioxaphospholane was added to the prepared solution. A standard phosphorus pulse program was employed, with the spectral acquisition consisting of 256 scans. ^{1}H-NMR measurements were carried out using d-DMSO as a solvent. Approximately 40 mg of polymer was dissolved in 0.75 ml d-DMSO. The ^{1}H spectra were obtained using a standard pulse program of 64 scans. The spectral width was set as Topspin 4.2 software was used for data processing and volume integration.

5.2.8 Thermal Analysis

Thermogravimetric analysis of the cured resins was performed while heating under N_2 using a TA instruments TGA 500. About 5 mg of the dried sample was heated at 10 °C/mi to 700 °C at a flow rate of 25 mL/min. TGA allows determination of the degradation temperature and simultaneously indicated the absence of residual solvents. Differential Scanning Calorimetry (DSC) measurements were performed on a DSC 250 (TA Instruments) by using a heat-cool-heat cycle from -50 to 200 °C. The glass transition temperatures were reported from the second heating cycle.

5.2.9 Dynamic Mechanical Analysis

DMA was conducted using a Mettler Toledo DMA (SDTA 861) instrument. The These discs were affixed to a shear fixture, and the sample thickness was determined by measuring the difference in the fixture's thickness before and after the samples were clamped. A dynamic force of 35 N was applied. The strain was set at 1%, corresponding to an amplitude of 6.1 µm. Temperature sweeps were conducted for the RCFPA-Aliphatic

samples over two distinct ranges: from -50°C to 60°C and from 20°C to 120°C. Additionally, the frequency of the sweeps was adjusted between 0.5 Hz and 5 Hz. Specifically, the storage modulus, loss modulus, and tan delta values, were plotted to assess the materials' mechanical behaviors over the specified temperature and frequency ranges.

5.3 Results and Discussion

5.3.1 Preparation of the unsaturated polyester resin –

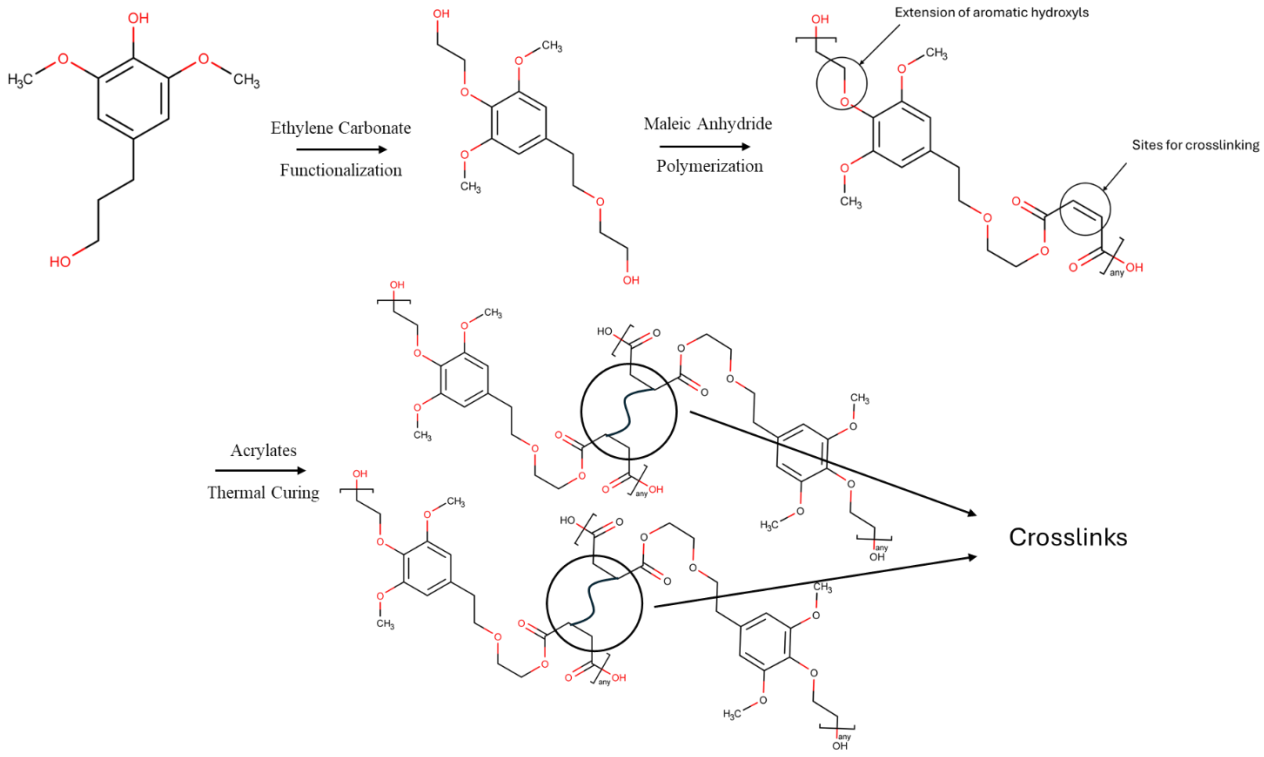

Figure 23 Representative Scheme of the Unsaturated Polyester

Unsaturated polyester resins from lignin oil were synthesized using a two-step process. In the first step, the hydroxyl groups were oxyethylated using ethylene carbonate. The reaction was studied in detail using ^{31}P NMR and FTIR. Ethylene carbonate is a greener alternative to ethylene oxide for the extension of aromatic hydroxyl groups using ether bonds. The reaction was carried out at 170 °C in order to minimize formation of linear carbonate linkages in between lignin monomers. There were a number of reasons as to why

ethylene carbonate was chosen over propylene carbonate as in the previous chapter. Propylene carbonate has an additional methyl group that promotes steric hindrance and reduces reactivity. Oxyalkylation has been shown to increase reactivity of lignin hydroxyl groups in numerous previous studies [163]. The drawbacks to organic carbonate based oxyalkylation is side reaction to form carbonates. Catalyst, temperature, and time choices for the reaction alleviate some of the concerns but not completely. In the case of propylene carbonate, the additional methyl group causes the terminal hydroxyl group to be a secondary aliphatic alcohol which has considerably lower reactivity than a primary aliphatic hydroxyl group. Additionally, during the crosslinking reaction, the methyl group can cause significant steric hindrance. The functionalization was carried out at 170 °C for 1 hour to incorporate aliphatic hydroxyl groups via an ether linkage.

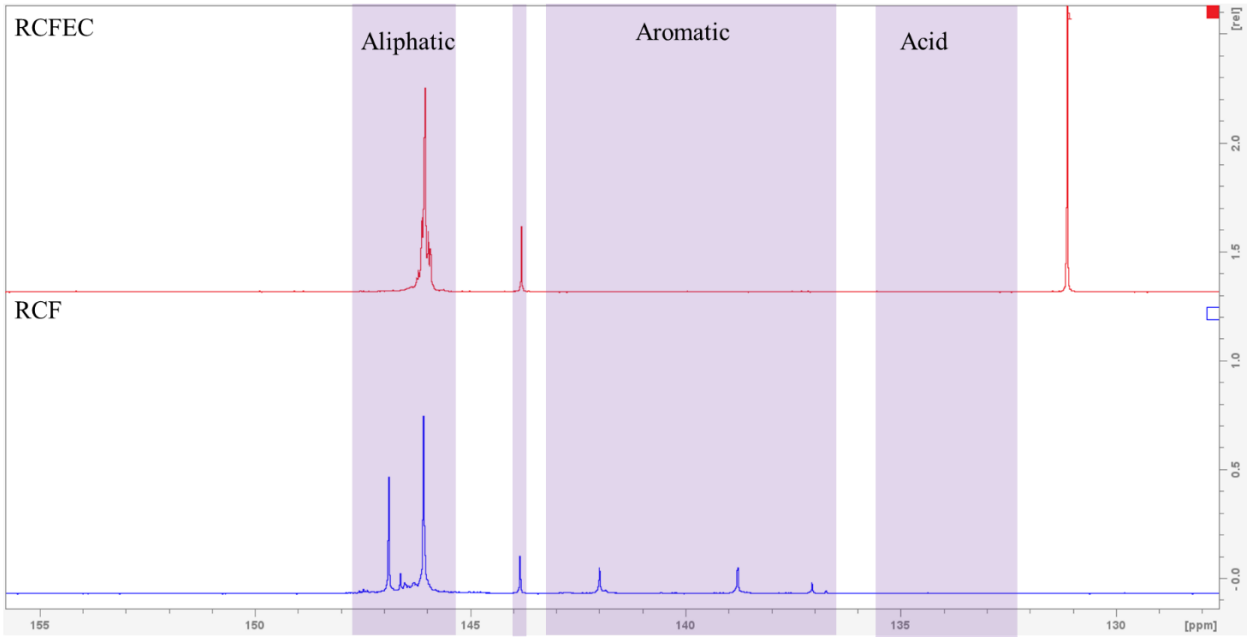

Figure 24 ^{31}P NMR Spectra of RCF (Bottom) and RCFEC (Top)

The reaction was understood using ^{31}P NMR which clearly showed the complete reaction of the aromatic hydroxyl groups to yield aliphatic hydroxyl groups. In a ^{31}P NMR the aliphatic, aromatic, and carboxylic acid hydroxyl groups resonate in specific regions.

In the region of 145-148 ppm, the lignin oil showed distinct peaks depending on the nature of the monomers. After oxyalkylation, due to near complete substitution of all hydroxyl groups, the NMR showed a distinct peak at 146.2 ppm. Kuhnel et al also showed similar results while functionalizing different kinds of lignin with ethylene carbonate [182]. This has one major implication that the functionality could be considered uniform, which would aid in optimization of polymerization reactions. A similar approach was used by Liu et al using ethylene carbonate on technical lignin [163].

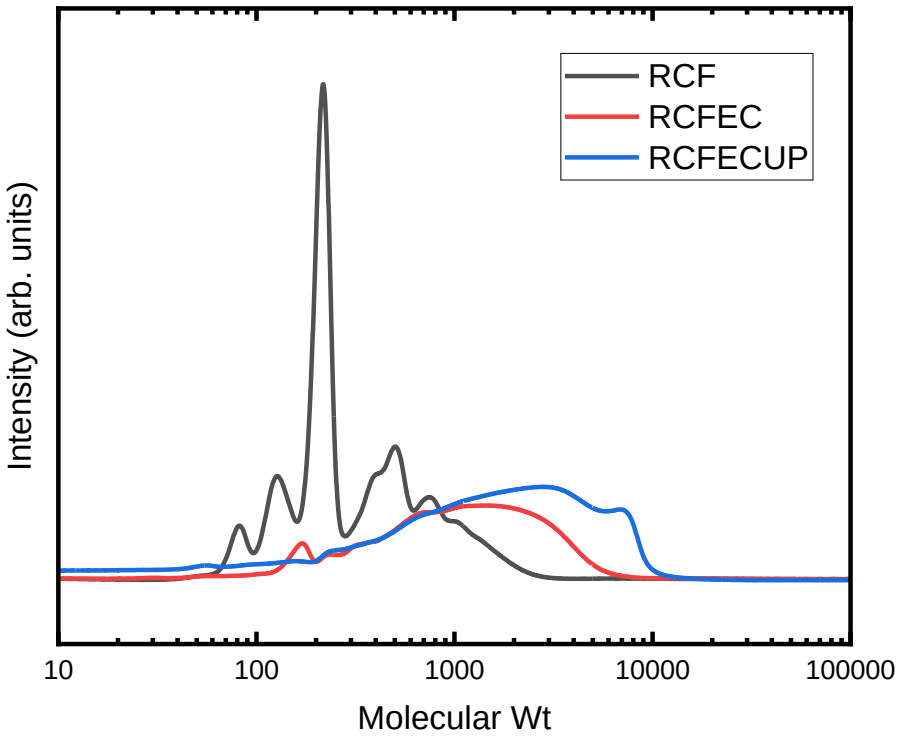

Figure 25 GPC Chromatograms for the functionalization of lignin oil

Initial hydroxyl content of the lignin oil was measured to be around 6.1 mmol/g. After functionalization with ethylene carbonate, the final hydroxyl content was around 3.11 mmol/g. The reduction in hydroxyl content was proportional to the increase in molecular weight determined from GPC. Other studies have attributed this to side reactions like linear

carbonate linkages as well as condensation in basic medium via the aromatic hydroxyl groups [182]. However, for the case of lignin oil, the primary reason was the increase in molecular weight of the lignin oil. Table 9 highlights the molecular weight distribution of the lignin oil, the functionalized lignin oil, and the unsaturated polyester resin.

Table 11 Molecular Weight Distribution for Lignin

Sample	M_n	M_w	PDI
RCF	259	471	1.82
RCFEC	567	1396	2.46
RCFECMA	470	2081	4.43

The oxyalkylated lignin oil was further polymerized with maleic anhydride. Anhydrides have a higher reactivity with aliphatic hydroxyl groups compared to acid groups. Maleic anhydride was chosen as the monomer as it has an unsaturated C=C double bond that can serve as a site for crosslinking. Previous studies on biobased unsaturated polyester resins utilized maleic acid and phthalic anhydride as the reactive monomers for polymerizations. The polymerization was carried out in NMP as a solvent with $Ti(OBu)_4$ as a catalyst. The polymerization was carried out at 200 C for 24 hours under a vacuum to remove moisture. The polymerization was understood using FTIR and ^1H NMR. The proton of interest in the ^1H was the proton from the unsaturated bond in maleic anhydride at 6.4 ppm. The ^1H NMR spectra shows a small peak associated with the C=C as highlighted in Fig 26. The spectrum also shows characteristic peaks from the aromatic region in lignin and ether bonds associated with lignin and RCFEC. Initial studies attempted a 2-step functionalization similar to the previous chapter followed by polycondensation with hexanediol. The polymer prepared using this method was insoluble in organic solvents as well as reactive dilutants. The product of solventless polycondensation using RCFEC and maleic anhydride was also insoluble in organic

solvents and reactive dilutants. A study on the curing of esterified lignin showed similar observations with the final polymer coating being insoluble in organic solvents [183]. It is hypothesized that the solvent based polycondensation inhibited network formation. The polymerization of RCFEC to RCFUP increased the T_g from -41 °C to -23 °C.

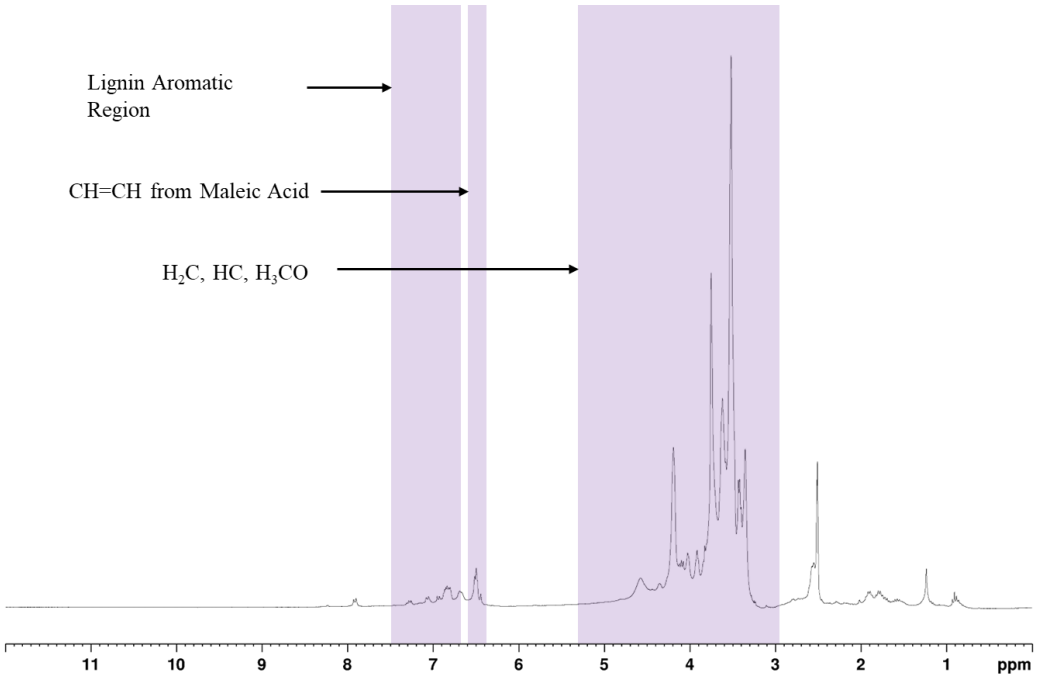

Figure 26 1H NMR Spectra of RCFECUP

5.3.2 Curing of the unsaturated polyester resins

The curing of the polyesters with crosslinkers was carried out using benzoyl peroxide as a free radical initiator. Benzoyl peroxide decomposes at 75 °C to yield free radicals which catalyze the curing process. A DSC was conducted to understand the curing temperature for the reaction system. An exothermic peak on the DSC scan revealed an optimum temperature of 110 °C for the curing of the system. A hardening step at 170 °C was also incorporated. The curing chemistry was understood using FTIR as the cured polymers were insoluble in organic solvents.

The FTIR spectra of the self - cured and crosslinked polyesters were shown in Fig 27. The spectra were divided into two regions of interest, first corresponding to the C=O carbonyls and C=C regions and the second corresponding to the OH and CH vibration regions. Analyzing the FTIR spectra of the CH region, it was seen that CH vibrations in between 2800 cm^{-1} to 3000 cm^{-1} increased in intensity for both the HEA cured polyester and the MMA cured polyester. This can be attributed to the thermal curing of C=C bonds to C-C during the curing process. A very slight increase was also observed when RCFECUP was self-cured using benzoyl peroxide. While observing the broad carbonyl peaks between 1800 cm^{-1} and 1700 cm^{-1}, the self-cured samples showed a peak shift signifying ester bond rearrangement during self-curing. The broad peak covers carbonyls from ester groups, acid groups, linear carbonate groups, and acid groups. The spectrum for RCFUP showed a broad peak representing linear carbonate groups and ester groups in between 1750 – 1700 cm^{-1}. The two prominent peaks in the cured samples in the FTIR in between 1750-1700 cm^{-1} correspond to a linear carbonate group at 1740 cm^{-1} and an ester group from the crosslinking acrylates. Another key feature of the region is the C=C bond stretching in between 1640-1680 cm^{-1}. The RCFECUP graph shows a peak corresponding to disubstituted C=C stretching. Upon self curing, the intensity of the peak reduces. And upon curing with the acrylate based crosslinkers, the peak disappears, confirming the curing reaction.

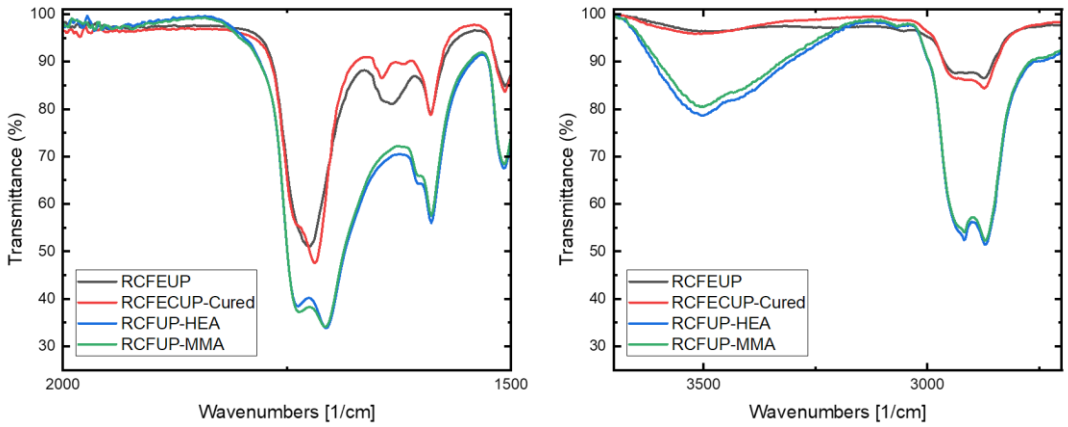

Figure 27 FTIR Spectra of the Polyesters of the carbonyl region (left) and hydroxyl region (right)

The completion of curing and the thermal properties of the polymers were further verified through DSC thermograms. DSC analysis revealed that the first heating curve of both cured samples did not exhibit any specific thermal activity, indicating that the curing process for the reactants was complete. The T_g for all samples were recorded between -20°C and -10°C, marking a slight elevation compared to the base RCFUP. This similarity in T_g across all samples can be attributed to the aliphatic extensions introduced during the oxyalkylation of the lignin oil. This phenomenon of relatively low Tg is consistent with observations from a study on the hydroxyethylation of lignin [163]. Additionally, no high-temperature transitions associated with lignin were detected, which is likely due to the highly depolymerized state of the lignin oil used in the study and low crosslink densities as observed from DMA studies.

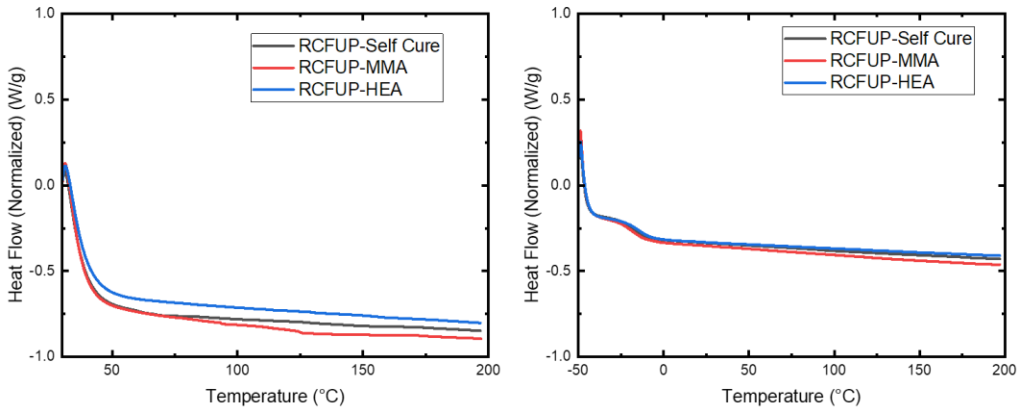

Figure 28 DSC Thermograms of Cured Esters (a) First Heating (b) Second Heating

The thermogravimetric analysis (TGA) curves of the cured polyesters, illustrated in Figure 29, revealed multistep degradation profiles with a significant degradation peak around 400°C. The curing process notably enhanced the thermal stability of the polyesters. The RCFUP polyester exhibited a $T_{5\%}$ of 220°C, which was slightly lower than the 235°C $T_{5\%}$ observed for the functionalized lignin oil. However, when these polyester resins underwent self-curing or were cured with acrylates, their thermal stability improved significantly, with the $T_{5\%}$ of all cured polyesters exceeding 280°C. This indicates that the cured materials possess the thermal resilience required for real-world applications.

The TGA data for the cured polyesters also highlighted two distinct steps in the degradation process. The initial step is attributed to the degradation of side groups attached to the lignin structure, while the subsequent main degradation step corresponds to the breakdown of the polymer backbone.

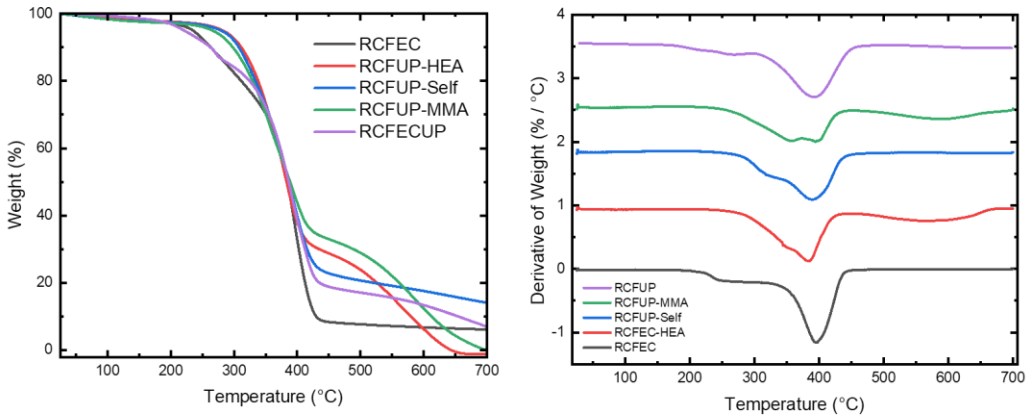

Figure 29 TGA Thermograms of the Polyesters (left) and Derivative of weight (right)

The DMA results for the cured polyesters were presented in Figure 30, displaying the storage modulus (G'), loss modulus (G''), and tan delta as functions of temperature. The frequency of the analysis was varied from 0.5 Hz to 5 Hz, ensuring that measurements were made within the linear viscoelastic range of the polymers. The resulting curves confirm the characteristics of a crosslinked material, exhibiting a transition from a glassy to a rubbery state, as indicated by the changes in the storage modulus. Specifically, polyesters crosslinked with methyl MMA demonstrated higher storage modulus values in the glassy state compared to those crosslinked with HEA. However, in the rubbery state, the distinction in storage modulus between the different crosslinkers was less pronounced.

The T_g of the polymers were derived from the peak of the tan delta curves, ranging between 3°C and 12°C. These T_g values were higher than those reported through DSC analysis. Additionally, the T_g values increased with the frequency of oscillation, illustrating the frequency dependence of the glass transition. This frequency dependence suggests that at higher frequencies, molecular motions may not adequately respond to the applied stress, leading to a shift of the tan delta peak to higher temperatures. Conversely, at lower frequencies, molecular motions can more readily adjust to the stress, resulting in a shift of

the peak to lower temperatures. Moreover, the tan delta curves did not reveal any additional relaxation phenomena within the tested temperature range, reinforcing the effectiveness of hydroxyethylation in enhancing the homogeneity of the final polymers.

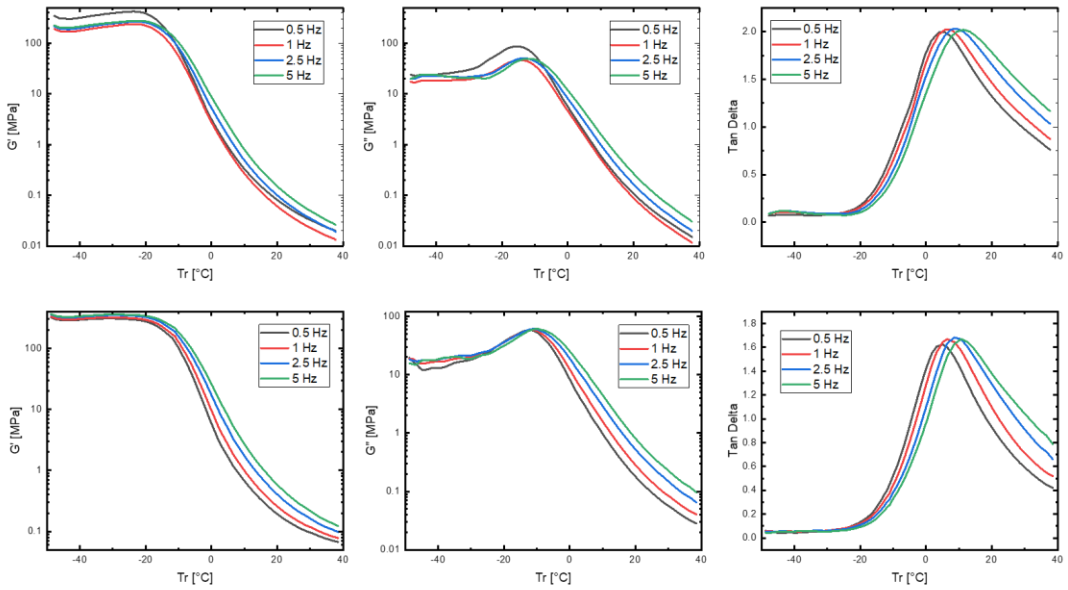

Figure 30 DMA Scans for the cured polyesters RCFUP-HEA (top) and RCFUP-MMA (bottom)

Crosslink density for the polymers was estimated from the rubbery plateau observed in the storage modulus (G') curves, a phase that follows the glass transition and is characterized by a relatively flat region on the graph. For RCFUPMMA, this plateau was noted at 35°C, and for RCFUPHEA, at 40°C. These densities were calculated employing a simplified Flory-Rehner equation:

$$\nu = \frac{G'}{3RT}$$

where: ν is the crosslink density (moles of crosslinks per unit volume), G′ is the storage modulus in the rubbery plateau region (in Pascals), R is the universal gas constant (8.314 J/mol·K), and T is the absolute temperature (in Kelvin) at which G′ is measured.

The storage modulus within the rubbery region displayed values ranging between 0.1 – 0.2 MPa, indicating not very high storage moduli. For the MMA crosslinked polyester, the crosslink density calculated was 15.742 moles/m^3, whereas for HEA, it was significantly lower at 3.63 moles/m^3. It is to be noted that the crosslink densities are relative in nature and further testing at higher temperature needs to be carried out to understand the behavior of the polyesters. A flat rubbery plateau at elevated temperatures would confirm crosslinking while a sloping rubbery region would indicate inadequate crosslinking and branched structure formation. The more efficient crosslinking in MMA can be attributed to its smaller molecular structure, which enhances its ability to crosslink, thereby improving the storage modulus in both the glassy and rubbery phases of the DMA analysis.

5.4 Conclusion

This study involved utilizing lignin oil to make unsaturated polyesters. These were synthesized using simple green chemical reactions using ethylene carbonate for hydroxyethylation followed by polymerization with maleic anhydride to incorporate cross linking sites. The chemistry of functionalization and polymerization were understood in detail using FTIR and NMR and GPC. These pointed towards successful hydroxyethylation and successful polymerization. These polymers were further thermally cured using acrylate based crosslinkers to improve the thermal properties of the polyesters. A significant improvement in thermal degradation behavior was observed while incorporating crosslinks in the polyester matrix. The high $T_{5\%}$ of 280 °C of the cured samples suggested potential for real world high thermal resistance applications. The DMA studies revealed the existence of a homogenous crosslinked structure with a distinct relaxation mode. The

storage modulus behavior in the glassy and the rubber regions pointed to a low crosslinking density for the RCFUPHEA compared to the RCFUPMMA.

CHAPTER SIX

CONCLUSION AND FUTURE WORK

6.1 Summary

The dissertation presented here addresses research gaps regarding the utilization of lignocellulosic biomass for the synthesis of fillers and polymers using the lignin first principles. The study presented here employs benign functionalization on lignin oil extracted by reductive catalytic functionalization and the utilization of cellulose nanocrystals as fillers in PHBV.

The dissertation demonstrated successful hybridization of cellulose nanocrystals using carbamation chemistry which as fillers improved the stiffness by up to 34%. The primary reason for this improvement was believed to be the nucleating nature of cellulose nanocrystals in the PHBV matrix. Morphological studies revealed uniform filler dispersion at lower concentrations and agglomeration at higher concentrations. Moreover, the first ever instance of batch foaming of PHBV using N_2 was demonstrated. Rheological studies revealed a considerably improved melt stiffness and storage modulus which inhibited the foaming of the composites. In summary, while the hybrid filler dispersed well within the matrix, the reinforcement ability was subpar and inhibited foaming of the composites. This study showed the potential of hybrid fillers being utilized to reinforce biobased polymers to improve their performance. Foaming using N_2 showed an alternative to CO_2 based foaming.

The latter part of the dissertation focused solely on the utilization of lignin oil. As stated earlier, utilizing lignin without further separation for polymeric materials can be largely beneficial. Lignin oil was functionalized using organic carbonates (propylene

carbonate and ethylene carbonate) which are touted as benign alternatives to propylene and ethylene oxides. Maleic acid, which is produced by oxidation of benzene but can be produced from lignocellulosic biomass was used to incorporate acid functionality onto the lignin oil. This acid functionality was leveraged by polymerization with diaminodecane to form aliphatic-aromatic polyamides. Diaminodecane also has a path to be synthesized from biobased sources. Aromatic-aromatic polyamides were also synthesized using p-Phenylenediamine. The polymerization was carried out using solvent based direct polycondensation as opposed to acid chloride based interfacial polymerization to avoid the use of harmful acid chlorides. The polymers showed amorphous thermoplastic behavior and good thermal resistance with a $T_{5\%}$ of at least 220 °C. The aliphatic polyamides showed higher thermal stability than the aromatic counterparts, possibly due to their higher molecular weight. DMA studies revealed heterogeneity in the polymer structure of both the aliphatic and aromatic polyamides owing to lignin side chains. In summary it was the first study that demonstrated lignin to be used as one of the prepolymeric material for polyamide synthesis. The study highlights the structure-property relationships of lignin oil and its corresponding polyamides. Moreover, this study highlighted the potential of green chemistry functionalization on lignin oil to make an amorphous thermoplastic material that could have potential applications in elastomeric materials.

Building on a similar concept of functionalized lignin oil, ethylene carbonate was used for the study involving the synthesis of unsaturated polyesters. Ethylene carbonate was chosen as the aliphatic hydroxyl groups at the end of the oxyalkylation are primary alcohols. These in turn lead to formation of thermally stable ester bonds compared to esters from secondary alcohols. This improvement in thermal stability was observed in the

polyesters synthesized from ethylene carbonate functionalized lignin oil. The polyesters showed exceptional thermal stability with a $T_{5\%}$ of at least 280 °C. The crosslinking of the polyester was evident in its viscoelastic behavior as observed using DMA. MMA showed a higher crosslink density compared to HEA owing to its smaller molecular size. Overall a simple reaction scheme was developed to form crosslinkable polyesters directly from lignin. This simple reaction scheme showed the potential of creating a new class of thermoset materials (Unsaturated Polyesters) from lignin and lignin oil with properties suitable for elastomeric applications with high temperature resistance.

While these studies focused on using benign pathways, there were a few harmful chemicals that were utilized and should be acknowledged and worked on avoiding in future studies. Cellulose nanocrystals were functionalized using toluene diisocyanate which is also acutely toxic and carcinogenic in nature. The aromatic polyamide was synthesized using p-Phenylene diamine which is an acutely toxic chemical. Dichloromethane, methanol, N-methyl pyrrolidone, which were used as solvents for lignin purification, extraction, and polymerization respectively have been reported to be carcinogenic and toxic. Hydroxyethyl acrylate used for curing is also acutely toxic and corrosive in nature.

6.2 Future Work

Expanding upon the current research, there are significant opportunities for advancing the use of lignocellulose in creating diverse condensation polymers. A promising direction for future research could involve utilizing cellulose pulp, derived from the reductive catalytic fractionation process, to manufacture cellulose nanocrystals. This proof of concept would highlight the potential applications of such materials.

From a chemical standpoint, the polymerization processes involving lignin oil warrant further investigation. Establishing a correlation between the structure and molecular weight of the different functionalized lignin oil constituents could dramatically enhance our understanding of the relationship between the chemical structure of synthesized polyamides and polyesters and their material properties. Additionally, a detailed chemical analysis of the inert and oxidative thermal decomposition products of these polymers could provide deeper insights into their chemical structures and potential avenues for optimization.

On the practical side, scaling up the production of these polymers is essential for a more comprehensive analysis of their mechanical properties, such as tensile strength, Young's modulus, and elongation at break. Understanding the fracture morphology of these amorphous and crosslinked polymers at a larger scale would offer valuable information about their potential applications and performance under stress.

Furthermore, integrating chemical recyclability into these polymers presents a critical challenge. Polyamides and polyesters, as condensation polymers, have demonstrated potential for recyclability through solvolysis reactions. Conducting a study to investigate the chemical nature of the solvolysis products of these polymers could pave the way for developing effective chemical recycling methods for lignin-based polymers. This research direction not only aligns with sustainability goals but also opens the door to circular economy practices in polymer science.

APPENDIX

Rights and Permissions

ELSEVIER LICENSE
TERMS AND CONDITIONS
Mar 07, 2024

This Agreement between Clemson University -- Kavan Sheth ("You") and Elsevier ("Elsevier") consists of your license details and the terms and conditions provided by Elsevier and Copyright Clearance Center.

License Number	5743550574346
License date	Mar 07, 2024
Licensed Content Publisher	Elsevier
Licensed Content Publication	Trends in Chemistry
Licensed Content Title	Lignin Functionalization for the Production of Novel Materials
Licensed Content Author	Stefania Bertella,Jeremy S. Luterbacher
Licensed Content Date	May 1, 2020
Licensed Content Volume	2
Licensed Content Issue	5
Licensed Content Pages	14
Start Page	440
End Page	453
Type of Use	reuse in a thesis/dissertation
Portion	figures/tables/illustrations
Number of figures/tables/illustrations	1
Format	electronic
Are you the author of this Elsevier article?	No
Will you be translating?	No
Title of new work	HARNESSING NATURE'S BUILDING BLOCKS: EXPLORING SUSTAINABLE BIOMASS FOR POLYMER AND COMPOSITE MATERIALS
Institution name	Clemson University
Expected presentation date	Mar 2024

Portions	Figure 1. Overview of the Structure of Lignocellulosic Biomass
Requestor Location	Clemson University 221 Fairforest Way Apt 6207 GREENVILLE, SC 29607 United States Attn: Clemson University
Publisher Tax ID	98-0397604
Total	0.00 USD

Terms and Conditions

This Agreement between Clemson University -- Kavan Sheth ("You") and The American Association for the Advancement of Science ("The American Association for the Advancement of Science") consists of your license details and the terms and conditions provided by The American Association for the Advancement of Science and Copyright Clearance Center.

License Number	5743551207204
License date	Mar 07, 2024
Licensed Content Publisher	The American Association for the Advancement of Science
Licensed Content Publication	Science
Licensed Content Title	Designing for a green chemistry future
Licensed Content Author	Julie B. Zimmerman, Paul T. Anastas, Hanno C. Erythropel, Walter Leitner
Licensed Content Date	Jan 24, 2020
Licensed Content Volume	367
Licensed Content Issue	6476
Volume number	367
Issue number	6476
Type of Use	Thesis / Dissertation
Requestor type	Scientist/individual at a research institution
Format	Electronic
Portion	Text Excerpt
Number of pages requested	1

Title of new work	HARNESSING NATURE'S BUILDING BLOCKS: EXPLORING SUSTAINABLE BIOMASS FOR POLYMER AND COMPOSITE MATERIALS
Institution name	Clemson University
Expected presentation date	Mar 2024
Portions	Figure 1. Characteristics of today's and tomorrow's chemical sectors
Requestor Location	Clemson University 221 Fairforest Way Apt 6207 GREENVILLE, SC 29607 United States Attn: Clemson University
Total	0.00 USD

SPRINGER NATURE LICENSE TERMS AND CONDITIONS

Mar 10, 2024

This Agreement between Clemson University -- Kavan Sheth ("You") and Springer Nature ("Springer Nature") consists of your license details and the terms and conditions provided by Springer Nature and Copyright Clearance Center.

License Number	5745650192481
License date	Mar 10, 2024
Licensed Content Publisher	Springer Nature
Licensed Content Publication	Springer eBook
Licensed Content Title	Chemical Composition and Structure of Natural Lignocellulose
Licensed Content Author	Hongzhang Chen
Licensed Content Date	Jan 1, 2014
Type of Use	Thesis/Dissertation
Requestor type	academic/university or research institute
Format	electronic
Portion	figures/tables/illustrations
Number of figures/tables/illustrations	1
Will you be translating?	no
Circulation/distribution	1 - 29

Author of this Springer Nature content	no
Title of new work	HARNESSING NATURE'S BUILDING BLOCKS: EXPLORING SUSTAINABLE BIOMASS FOR POLYMER AND COMPOSITE MATERIALS
Institution name	Clemson University
Expected presentation date	Mar 2024
Portions	Table 1
Requestor Location	Clemson University 221 Fairforest Way Apt 6207 GREENVILLE, SC 29607 United States Attn: Clemson University
Total	0.00 USD
Terms and Conditions	

WORKS CITED

[1] Nicholson SR, Rorrer NA, Carpenter AC, Beckham GT. Manufacturing energy and greenhouse gas emissions associated with plastics consumption. Joule 2021;5:673–86. https://doi.org/10.1016/j.joule.2020.12.027.

[2] MacArthur DE. Beyond plastic waste. Science (1979) 2017;358:843. https://doi.org/10.1126/science.aao6749.

[3] Leslie HA, van Velzen MJM, Brandsma SH, Vethaak AD, Garcia-Vallejo JJ, Lamoree MH. Discovery and quantification of plastic particle pollution in human blood. Environ Int 2022:107199. https://doi.org/10.1016/J.ENVINT.2022.107199.

[4] Sheldon RA. The E factor 25 years on: the rise of green chemistry and sustainability. Green Chemistry 2017;19:18–43. https://doi.org/10.1039/C6GC02157C.

[5] Payne J, McKeown P, Jones MD. A circular economy approach to plastic waste. Polym Degrad Stab 2019;165:170–81. https://doi.org/10.1016/j.polymdegradstab.2019.05.014.

[6] Rosenboom JG, Langer R, Traverso G. Bioplastics for a circular economy. Nature Reviews Materials 2022 7:2 2022;7:117–37. https://doi.org/10.1038/s41578-021-00407-8.

[7] PlasticsEurope. The Circular Economy for Plastics - A European Overview. PlasticsEurope 2019:1–36.

[8] Technologies Office B, Advance Manufacturing Office the. Plastics for a Circular Economy Workshop: Summary Report. 2019.

[9] DeVierno Kreuder A, House-Knight T, Whitford J, Ponnusamy E, Miller P, Jesse N, et al. A Method for Assessing Greener Alternatives between Chemical Products Following the 12 Principles of Green Chemistry. ACS Sustain Chem Eng 2017;5:2927–35. https://doi.org/10.1021/acssuschemeng.6b02399.

[10] Zimmerman JB, Anastas PT, Erythropel HC, Leitner W. Designing for a green chemistry future. vol. 367. 2020. https://doi.org/10.1126/science.aay3060.

[11] Cywar RM, Beckham GT. Producing performance-advantaged bioplastics. Nature Chemistry 2022 14:9 2022;14:967–9. https://doi.org/10.1038/s41557-022-01030-y.

[12] US EPA. National recycling strategy — Part one of a series on building a circular economy for all 2021.

[13] Zang H, Wang K, Zhang M, Xie R, Wang L, Chen EYX. Catalytic coupling of biomass-derived aldehydes into intermediates for biofuels and materials. Catal Sci Technol 2018;8:1777–98. https://doi.org/10.1039/c7cy02221b.

[14] Chundawat SPS, Beckham GT, Himmel ME, Dale BE. Deconstruction of lignocellulosic biomass to fuels and chemicals. Annu Rev Chem Biomol Eng 2011;2:121–45. https://doi.org/10.1146/annurev-chembioeng-061010-114205.

[15] Ragauskas AJ, Beckham GT, Biddy MJ, Chandra R, Chen F, Davis MF, et al. Lignin valorization: Improving lignin processing in the biorefinery. Science (1979) 2014;344. https://doi.org/10.1126/science.1246843.

[16] Renders T, Van den Bossche G, Vangeel T, Van Aelst K, Sels B. Reductive catalytic fractionation: state of the art of the lignin-first biorefinery. Curr Opin Biotechnol 2019;56:193–201. https://doi.org/10.1016/j.copbio.2018.12.005.

[17] Bertella S, Luterbacher JS. Lignin Functionalization for the Production of Novel Materials. Trends Chem 2020;2:440–53. https://doi.org/10.1016/j.trechm.2020.03.001.
[18] Wu X, Xie S, Zhang H, Zhang Q, Sels BF, Wang Y. Metal Sulfide Photocatalysts for Lignocellulose Valorization. Advanced Materials 2021;33:1–20. https://doi.org/10.1002/adma.202007129.
[19] Galkin M V., Samec JSM. Lignin Valorization through Catalytic Lignocellulose Fractionation: A Fundamental Platform for the Future Biorefinery. vol. 9. 2016. https://doi.org/10.1002/cssc.201600237.
[20] Van Den Bosch S, Renders T, Kennis S, Koelewijn SF, Van Den Bossche G, Vangeel T, et al. Integrating lignin valorization and bio-ethanol production: On the role of Ni-Al2O3 catalyst pellets during lignin-first fractionation. Green Chemistry 2017;19:3313–26. https://doi.org/10.1039/c7gc01324h.
[21] Okolie JA, Nanda S, Dalai AK, Kozinski JA. Chemistry and Specialty Industrial Applications of Lignocellulosic Biomass. Waste Biomass Valorization 2021;12:2145–69. https://doi.org/10.1007/S12649-020-01123-0.
[22] Abu-Omar MM, Barta K, Beckham GT, Luterbacher JS, Ralph J, Rinaldi R, et al. Guidelines for performing lignin-first biorefining. Energy Environ Sci 2021;14:262–92. https://doi.org/10.1039/d0ee02870c.
[23] Galkin M V., Samec JSM. Lignin Valorization through Catalytic Lignocellulose Fractionation: A Fundamental Platform for the Future Biorefinery. vol. 9. 2016. https://doi.org/10.1002/cssc.201600237.
[24] Chen H. Chemical Composition and Structure of Natural Lignocellulose. Biotechnology of Lignocellulose 2014:25–71. https://doi.org/10.1007/978-94-007-6898-7_2.
[25] Ralph J, Lapierre C, Boerjan W. Lignin structure and its engineering. Curr Opin Biotechnol 2019;56:240–9. https://doi.org/10.1016/J.COPBIO.2019.02.019.
[26] Feofilova EP, Mysyakina IS. Lignin: Chemical structure, biodegradation, and practical application (a review). Appl Biochem Microbiol 2016;52:573–81. https://doi.org/10.1134/S0003683816060053/METRICS.
[27] Chen H. Chemical Composition and Structure of Natural Lignocellulose. Biotechnology of Lignocellulose 2014:25–71. https://doi.org/10.1007/978-94-007-6898-7_2.
[28] Khan R, Jolly R, Fatima T, Shakir M. Extraction processes for deriving cellulose: A comprehensive review on green approaches. Polym Adv Technol 2022;33:2069–90. https://doi.org/10.1002/PAT.5678.
[29] Trache D, Tarchoun AF, Derradji M, Hamidon TS, Masruchin N, Brosse N, et al. Nanocellulose: From Fundamentals to Advanced Applications. Front Chem 2020;8:392. https://doi.org/10.3389/FCHEM.2020.00392.
[30] Thomas B, Raj MC, Athira BK, Rubiyah HM, Joy J, Moores A, et al. Nanocellulose, a Versatile Green Platform: From Biosources to Materials and Their Applications. Chem Rev 2018;118:11575–625. https://doi.org/10.1021/acs.chemrev.7b00627.
[31] Kim JH, Shim BS, Kim HS, Lee YJ, Min SK, Jang D, et al. Review of nanocellulose for sustainable future materials. International Journal of Precision Engineering and Manufacturing - Green Technology 2015;2:197–213. https://doi.org/10.1007/s40684-015-0024-9.

[32] Ghasemlou M, Daver F, Ivanova EP, Habibi Y, Adhikari B. Surface modifications of nanocellulose: From synthesis to high-performance nanocomposites. Prog Polym Sci 2021;119:101418. https://doi.org/10.1016/j.progpolymsci.2021.101418.
[33] Rana AK, Frollini E, Thakur VK. Cellulose nanocrystals: Pretreatments, preparation strategies, and surface functionalization. Int J Biol Macromol 2021;182:1554–81. https://doi.org/10.1016/J.IJBIOMAC.2021.05.119.
[34] Xu J, Wu Z, Wu Q, Kuang Y. Acetylated cellulose nanocrystals with high-crystallinity obtained by one-step reaction from the traditional acetylation of cellulose. Carbohydr Polym 2020;229:115553. https://doi.org/10.1016/J.CARBPOL.2019.115553.
[35] Zhang X, Wang L, Dong S, Zhang X, Wu Q, Zhao L, et al. Nanocellulose 3, 5-Dimethylphenylcarbamate Derivative Coated Chiral Stationary Phase: Preparation and Enantioseparation Performance. Chirality 2016;28:376–81. https://doi.org/10.1002/CHIR.22578.
[36] Abushammala H. On the para/ortho reactivity of isocyanate groups during the carbamation of cellulose nanocrystals using 2,4-toluene diisocyanate. Polymers (Basel) 2019;11:1–12. https://doi.org/10.3390/polym11071164.
[37] Abushammala H, Mao J. A review of the surface modification of cellulose and nanocellulose using aliphatic and aromatic mono- And di-isocyanates. Molecules 2019;24. https://doi.org/10.3390/molecules24152782.
[38] Cellante L, Costa R, Monaco I, Cenacchi G, Locatelli E. One-step esterification of nanocellulose in a Brønsted acid ionic liquid for delivery to glioblastoma cancer cells. New Journal of Chemistry 2018;42:5237–42. https://doi.org/10.1039/C7NJ04633B.
[39] Leszczyńska A, Radzik P, Szefer E, Mičušík M, Omastová M, Pielichowski K. Surface Modification of Cellulose Nanocrystals with Succinic Anhydride. Polymers 2019, Vol 11, Page 866 2019;11:866. https://doi.org/10.3390/POLYM11050866.
[40] Shen Y, Li X, Lan Y, Zu M, Liu X, Huang H, et al. Enhancing magnetic resonance imaging of bio-based nano-contrast via anchoring manganese on rod-shaped cellulose nanocrystals. Cellulose 2021;28:2905–16. https://doi.org/10.1007/S10570-021-03693-1/METRICS.
[41] Wu C, Zhang X, Wang X, Gao Q, Li X. Surface modification of cellulose nanocrystal using succinic anhydride and its effects on poly(butylene succinate) based composites. Cellulose 2019;26:3167–81. https://doi.org/10.1007/S10570-019-02292-5/METRICS.
[42] Zainuddin S, Fahim A, Shoieb S, Syed F, Hosur M V., Li D, et al. Morphological and mechanical behavior of chemically treated jute-PHBV bio-nanocomposites reinforced with silane grafted halloysite nanotubes. J Appl Polym Sci 2016;133. https://doi.org/10.1002/app.43994.
[43] Zheng T, Clemons CM, Pilla S. Grafting PEG on cellulose nanocrystals via polydopamine chemistry and the effects of PEG graft length on the mechanical performance of composite film. Carbohydr Polym 2021;271:118405. https://doi.org/10.1016/j.carbpol.2021.118405.
[44] Chen J, Yang R, Ou J, Tang C, Xiang M, Wu D, et al. Functionalized cellulose nanocrystals as the performance regulators of poly(β-hydroxybutyrate-co-valerate)

biocomposites. Carbohydr Polym 2020;242. https://doi.org/10.1016/J.CARBPOL.2020.116399.
[45] Bellani CF, Pollet E, Hebraud A, Pereira F V., Schlatter G, Avérous L, et al. Morphological, thermal, and mechanical properties of poly(ε-caprolactone)/poly(ε-caprolactone)-grafted-cellulose nanocrystals mats produced by electrospinning. J Appl Polym Sci 2016;133. https://doi.org/10.1002/APP.43445.
[46] Zheng T, Zhang Z, Shukla S, Agnihotri S, Clemons CM, Pilla S. PHBV-graft-GMA via reactive extrusion and its use in PHBV/nanocellulose crystal composites. Carbohydr Polym 2019;205:27–34. https://doi.org/10.1016/j.carbpol.2018.10.014.
[47] Yu HY, Qin ZY. Surface grafting of cellulose nanocrystals with poly(3-hydroxybutyrate-co- 3-hydroxyvalerate). Carbohydr Polym 2014;101:471–8. https://doi.org/10.1016/J.CARBPOL.2013.09.048.
[48] Han X, Han Y, Jin Y, Wang Z, Tian H, Huang J, et al. Microcrystalline cellulose grafted hyperbranched polyester with roll comb structure for synergistic toughening and strengthening of microbial PHBV/bio-based polyester elastomer composites. Int J Biol Macromol 2023;242. https://doi.org/10.1016/J.IJBIOMAC.2023.124608.
[49] Yu HY, Qin ZY, Yan CF, Yao JM. Green nanocomposites based on functionalized cellulose nanocrystals: A study on the relationship between interfacial interaction and property enhancement. ACS Sustain Chem Eng 2014;2:875–86. https://doi.org/10.1021/SC400499G.
[50] Li F, Yu HY, Wang YY, Zhou Y, Zhang H, Yao JM, et al. Natural Biodegradable Poly(3-hydroxybutyrate- co-3-hydroxyvalerate) Nanocomposites with Multifunctional Cellulose Nanocrystals/Graphene Oxide Hybrids for High-Performance Food Packaging. J Agric Food Chem 2019;67:10954–67. https://doi.org/10.1021/ACS.JAFC.9B03110.
[51] Li F, Abdalkarim SYH, Yu HY, Zhu J, Zhou Y, Guan Y. Bifunctional Reinforcement of Green Biopolymer Packaging Nanocomposites with Natural Cellulose Nanocrystal-Rosin Hybrids. ACS Appl Bio Mater 2020;3:1944–54. https://doi.org/10.1021/ACSABM.9B01100.
[52] Laurichesse S, Avérous L. Chemical modification of lignins: Towards biobased polymers. Prog Polym Sci 2014;39:1266–90. https://doi.org/10.1016/J.PROGPOLYMSCI.2013.11.004.
[53] Van Aelst K, Van Sinay E, Vangeel T, Cooreman E, Van Den Bossche G, Renders T, et al. Reductive catalytic fractionation of pine wood: Elucidating and quantifying the molecular structures in the lignin oil. Chem Sci 2020;11:11498–508. https://doi.org/10.1039/d0sc04182c.
[54] Duval A, Vidal D, Sarbu A, René W, Avérous L. Scalable single-step synthesis of lignin-based liquid polyols with ethylene carbonate for polyurethane foams. Mater Today Chem 2022;24. https://doi.org/10.1016/j.mtchem.2022.100793.
[55] Sternberg J, Pilla S. Materials for the biorefinery: High bio-content, shape memory Kraft lignin-derived non-isocyanate polyurethane foams using a non-toxic protocol. Green Chemistry 2020;22:6922–35. https://doi.org/10.1039/d0gc01659d.
[56] Van Aelst K, Van Sinay E, Vangeel T, Zhang Y, Renders T, Van den Bosch S, et al. Low molecular weight and highly functional RCF lignin products as a full bisphenol a replacer in bio-based epoxy resins. Chemical Communications 2021;57:5642–5. https://doi.org/10.1039/d1cc02263f.

[57] Feghali E, Van De Pas DJ, Torr KM. Toward Bio-Based Epoxy Thermoset Polymers from Depolymerized Native Lignins Produced at the Pilot Scale. Biomacromolecules 2020;21:1548–59. https://doi.org/10.1021/ACS.BIOMAC.0C00108/ASSET/IMAGES/LARGE/BM0C00108_0008.JPEG.
[58] Gioia C, Colonna M, Tagami A, Medina L, Sevastyanova O, Berglund LA, et al. Lignin-Based Epoxy Resins: Unravelling the Relationship between Structure and Material Properties. Biomacromolecules 2020;21:1920–8. https://doi.org/10.1021/acs.biomac.0c00057.
[59] Guo ZX, Gandini A. Polyesters from lignin—2. The copolyesterification of kraft lignin and polyethylene glycols with dicarboxylic acid chlorides. Eur Polym J 1991;27:1177–80. https://doi.org/10.1016/0014-3057(91)90053-Q.
[60] Van Den Bosch S, Schutyser W, Koelewijn SF, Renders T, Courtin CM, Sels BF. Tuning the lignin oil OH-content with Ru and Pd catalysts during lignin hydrogenolysis on birch wood. Chemical Communications 2015;51:13158–61. https://doi.org/10.1039/c5cc04025f.
[61] Upton BM, Kasko AM. Strategies for the conversion of lignin to high-value polymeric materials: Review and perspective. Chem Rev 2016;116:2275–306. https://doi.org/10.1021/ACS.CHEMREV.5B00345/ASSET/IMAGES/LARGE/CR-2015-003454_0003.JPEG.
[62] Ma K, Chen G, Wang W, Zhang A, Zhong Y, Zhang Y, et al. Partially bio-based aromatic polyimides derived from 2,5-furandicarboxylic acid with high thermal and mechanical properties. J Polym Sci A Polym Chem 2018;56:1058–66. https://doi.org/10.1002/POLA.28982.
[63] Nurhamiyah Y, Irvine G, Themistou E, Chen B. Novel Biobased Polyamide Thermoplastic Elastomer with Medium Hardness. Macromol Chem Phys 2021;222:2100218. https://doi.org/10.1002/MACP.202100218.
[64] Ahmadi R, Ullah A. Synthesis and Characterization of Unsaturated Biobased-Polyamides from Plant Oil. ACS Sustain Chem Eng 2020;8:8049–58. https://doi.org/10.1021/ACSSUSCHEMENG.0C02692/SUPPL_FILE/SC0C02692_SI_001.PDF.
[65] Cureton LST, Napadensky E, Annunziato C, La Scala JJ. The effect of furan molecular units on the glass transition and thermal degradation temperatures of polyamides. J Appl Polym Sci 2017;134:45514. https://doi.org/10.1002/APP.45514.
[66] Xie S, Yang J, Wang X, Yang J. Synthesis of fully biobased semi-aromatic furan polyamides with high performance through facile green synthesis process. Eur Polym J 2022;162:110932. https://doi.org/10.1016/J.EURPOLYMJ.2021.110932.
[67] Yin Q, Xu B, Qin Y, Zhao J, Cheng J, Zhang J. Biobased Linear and Crystallizable Polyhydroxy(amide-urethane)s from Diglycerol Bis(cyclic carbonate) and the Polyamides of Dimer Fatty Acids. ACS Appl Polym Mater 2022;4:2116–31. https://doi.org/10.1021/ACSAPM.1C01933/SUPPL_FILE/AP1C01933_SI_001.PDF.
[68] Ali DK. Synthesis and Characterization of Novel Biobased Ion-Exchange Bisfuran Polyamides Prepared by Interfacial Polycondensation of Bisfuran Diamine Monomer and Sustainable Dicarboxylic Acid Derivatives. J Polym Environ 2022;30:4102–13. https://doi.org/10.1007/S10924-022-02496-0/FIGURES/7.

[69] Mao L, Pan L, Ma B, He Y. Synthesis and Characterization of Bio-Based Amorphous Polyamide From Dimethyl furan-2,5-dicarboxylate. J Polym Environ 2022;30:1072–9. https://doi.org/10.1007/S10924-021-02265-5/TABLES/3.
[70] Yagura K, Enomoto Y, Iwata T. Synthesis of fully divanillic acid-based aromatic polyamides and their thermal and mechanical properties. Polymer (Guildf) 2022;256:125222. https://doi.org/10.1016/J.POLYMER.2022.125222.
[71] He J, Song L, Wang Z. The conversion of castor oil to a series of functional polyamides inspired by natural silks. Ind Crops Prod 2022;181:114852. https://doi.org/10.1016/J.INDCROP.2022.114852.
[72] Mirzakhanian Z, Hasani M, Faghihi K. Synthesis of Bio-Based Polyamide/Acid-Functionalized Multiwalled Carbon Nanotube Nanocomposites Using Vanillin. Https://DoiOrg/101080/0360255920171381252 2017;57:1367–76. https://doi.org/10.1080/03602559.2017.1381252.
[73] Yagura K, Zhang Y, Enomoto Y, Iwata T. Synthesis of highly thermally stable divanillic acid-derived polyamides and their mechanical properties. Polymer (Guildf) 2021;228:123907. https://doi.org/10.1016/J.POLYMER.2021.123907.
[74] Upton BM, Kasko AM. Biodegradable Aromatic-Aliphatic Poly(ester-amides) from Monolignol-Based Ester Dimers. ACS Sustain Chem Eng 2018;6:3659–68. https://doi.org/10.1021/ACSSUSCHEMENG.7B03784/ASSET/IMAGES/LARGE/SC-2017-037843_0003.JPEG.
[75] Upton BM, Kasko AM. Biomass-Derived Poly(ether-amide)s Incorporating Hydroxycinnamates. Biomacromolecules 2019;20:758–66. https://doi.org/10.1021/ACS.BIOMAC.9B00044/ASSET/IMAGES/LARGE/BM-2019-00044N_0005.JPEG.
[76] Luo K, Wang Y, Yu J, Zhu J, Hu Z. Semi-bio-based aromatic polyamides from 2,5-furandicarboxylic acid: Toward high-performance polymers from renewable resources. RSC Adv 2016;6:87013–20. https://doi.org/10.1039/C6RA15797A.
[77] Wilsens CHRM, Noordover BAJ, Rastogi S. Aromatic thermotropic polyesters based on 2,5-furandicarboxylic acid and vanillic acid. Polymer (Guildf) 2014;55:2432–9. https://doi.org/10.1016/j.polymer.2014.03.033.
[78] Sternberg J, Pilla S. Thermoplastic Polymer from Lignin: Creating an Extended Polyamide Network through Reactive Kraft Lignin Derivatives. ACS Omega 2023;8:40110–8. https://doi.org/10.1021/ACSOMEGA.3C01259/ASSET/IMAGES/LARGE/AO3C01259_0005.JPEG.
[79] Guo Z -X, Gandini A, Pla F. Polyesters from lignin. 1. The reaction of kraft lignin with dicarboxylic acid chlorides. Polym Int 1992;27:17–22. https://doi.org/10.1002/PI.4990270104.
[80] Matsushita Y, Toyoki Inomata ·, Takagi Y, Hasegawa T, Fukushima K, Matsushita Y, et al. Conversion of sulfuric acid lignin generated during bioethanol production from lignocellulosic materials into polyesters with ε-caprolactone. Journal of Wood Science 2011 57:3 2011;57:214–8. https://doi.org/10.1007/S10086-010-1158-6.
[81] Arza CR, Wang P, Linares-Pastén J, Zhang B. Synthesis, thermal, rheological characteristics, and enzymatic degradation of aliphatic polyesters with lignin-based aromatic pendant groups. J Polym Sci A Polym Chem 2019;57:2314–23. https://doi.org/10.1002/POLA.29534.

[82] Winfield D, Ring J, Horn J, White EM, Locklin J. Semi-aromatic biobased polyesters derived from lignin and cyclic carbonates. Green Chemistry 2021;23:9658–68. https://doi.org/10.1039/D1GC03135J.
[83] Ren T, Chen Q, Zhao C, Zheng Q, Xie H, North M. Introducing the Tishchenko reaction into sustainable polymer chemistry. Green Chemistry 2020;22:1542–7. https://doi.org/10.1039/C9GC03926K.
[84] van Schijndel J, Molendijk D, van Beurden K, Vermeulen R, Noël T, Meuldijk J. Repeatable molecularly recyclable semi-aromatic polyesters derived from lignin. Journal of Polymer Science 2020;58:1655–63. https://doi.org/10.1002/POL.20200088.
[85] Curia S, Biundo A, Fischer I, Braunschmid V, Gübitz GM, Stanzione JF. Towards Sustainable High-Performance Thermoplastics: Synthesis, Characterization, and Enzymatic Hydrolysis of Bisguaiacol-Based Polyesters. ChemSusChem 2018;11:2529–39. https://doi.org/10.1002/CSSC.201801059.
[86] Enomoto Y, Iwata T. Synthesis of biphenyl polyesters derived from divanillic acid, and their thermal and mechanical properties. Polymer (Guildf) 2020;193. https://doi.org/10.1016/J.POLYMER.2020.122330.
[87] Zhang Y, Enomoto Y, Iwata T. Synthesis of homo- and copolyesters containing divanillic acid, 1,4-cyclohexanedimethanol, and alkanediols and their thermal and mechanical properties. Polym Degrad Stab 2021;192. https://doi.org/10.1016/J.POLYMDEGRADSTAB.2021.109706.
[88] Fujieda K, Enomoto Y, Zhang Y, Iwata T. Synthesis and characterization of novel potentially biodegradable aromatic polyesters consisting of divanillic acids with free phenolic hydroxyl groups. Polymer (Guildf) 2022;257. https://doi.org/10.1016/J.POLYMER.2022.125241.
[89] Fujieda K, Enomoto Y, Huang Q, Iwata T. Synthesis and enzymatic biodegradation of co-polyesters consisting of divanillic acid with free hydroxyl groups. Polymer (Guildf) 2023;268. https://doi.org/10.1016/J.POLYMER.2023.125685.
[90] Hanson KG, Lin CH, Abu-Omar MM. Preparation and properties of renewable polyesters based on lignin-derived bisphenol. Polymer (Guildf) 2021;233:124202. https://doi.org/10.1016/J.POLYMER.2021.124202.
[91] Xu Y, Odelius K, Hakkarainen M. Recyclable and Flexible Polyester Thermosets Derived from Microwave-Processed Lignin. ACS Appl Polym Mater 2020;2:1917–24. https://doi.org/10.1021/ACSAPM.0C00130/ASSET/IMAGES/LARGE/AP0C00130_0006.JPEG.
[92] Evtugin D V., Gandini A. Polyesters based on oxygen-organosolv lignin. Acta Polymerica 1996;47:344–50. https://doi.org/10.1002/ACTP.1996.010470805.
[93] Hanson KG, Lin CH, Abu-Omar MM. Crosslinking of renewable polyesters with epoxides to form bio-based epoxy thermosets. Polymer (Guildf) 2022;238:124363. https://doi.org/10.1016/J.POLYMER.2021.124363.
[94] Bonini C, D'Auria M, Emanuele L, Ferri R, Pucciariello R, Sabia AR. Polyurethanes and polyesters from lignin. J Appl Polym Sci 2005;98:1451–6. https://doi.org/10.1002/APP.22277.
[95] Dong W, Peng H, Zhang R, He C, Gu Y, Yang Q, et al. Ultra-Tough Vanillin-Based Polyester Hot-Melt Adhesive through Multiple Oxygenated Groups. ACS Appl

Polym Mater 2023;5:10010–20. https://doi.org/10.1021/ACSAPM.3C01878/ASSET/IMAGES/LARGE/AP3C01878_0008.JPEG.
[96] Llevot A, Grau E, Carlotti S, Grelier S, Cramail H. Renewable (semi)aromatic polyesters from symmetrical vanillin-based dimers. Polym Chem 2015;6:6058–66. https://doi.org/10.1039/C5PY00824G.
[97] Gandini A, Belgacem MN, Guo Z-X, Montanari S. Lignins as Macromonomers for Polyesters and Polyurethanes. Chemical Modification, Properties, and Usage of Lignin, Boston, MA: Springer US; 2002, p. 57–80. https://doi.org/10.1007/978-1-4615-0643-0_4.
[98] Xanthopoulou E, Terzopoulou Z, Zamboulis A, Papadopoulos L, Tsongas K, Tzetzis D, et al. Poly(propylene vanillate): A Sustainable Lignin-Based Semicrystalline Engineering Polyester. ACS Sustain Chem Eng 2021;9:1383–97. https://doi.org/10.1021/ACSSUSCHEMENG.0C08346.
[99] Zhang Y, Enomoto Y, Iwata T. Synthesis and characterization of biphenyl polyesters derived from divanillic acid and cyclic diols. Polymer (Guildf) 2020;203. https://doi.org/10.1016/J.POLYMER.2020.122751.
[100] Alaerts L, Augustinus M, Van Acker K. Impact of bio-based plastics on current recycling of plastics. Sustainability (Switzerland) 2018;10. https://doi.org/10.3390/su10051487.
[101] Global bioplastic production capacities by material 2022 | Statista n.d. https://www.statista.com/statistics/678775/production-capacity-distribution-of-bioplastics-worldwide-by-material/ (accessed June 22, 2023).
[102] Yu HY, Qin ZY, Liu YN, Chen L, Liu N, Zhou Z. Simultaneous improvement of mechanical properties and thermal stability of bacterial polyester by cellulose nanocrystals. Carbohydr Polym 2012;89:971–8. https://doi.org/10.1016/j.carbpol.2012.04.053.
[103] Market – European Bioplastics e.V. n.d. https://www.european-bioplastics.org/market/ (accessed June 22, 2023).
[104] Rivera-Briso AL, Serrano-Aroca Á. Poly(3-Hydroxybutyrate-co-3-Hydroxyvalerate): Enhancement strategies for advanced applications. Polymers (Basel) 2018;10:1–28. https://doi.org/10.3390/polym10070732.
[105] Yu H, Sun B, Zhang D, Chen G, Yang X, Yao J. Reinforcement of biodegradable poly(3-hydroxybutyrate-co-3-hydroxyvalerate) with cellulose nanocrystal/silver nanohybrids as bifunctional nanofillers. J Mater Chem B 2014;2:8479–89. https://doi.org/10.1039/c4tb01372g.
[106] Do Amaral Montanheiroa TL, Cristóvan FH, Machado JPB, Tada DB, Durán N, Lemes AP. Effect of MWCNT functionalization on thermal and electrical properties of PHBV/MWCNT nanocomposites. J Mater Res 2014;760:55–65. https://doi.org/10.1557/jmr.2014.303.
[107] Sridhar V, Lee I, Chun HH, Park H. Graphene reinforced biodegradable poly(3-hydroxybutyrate-co-4-hydroxybutyrate) nano-composites. Express Polym Lett 2013;7:320–8. https://doi.org/10.3144/expresspolymlett.2013.29.
[108] Yu HY, Qin ZY, Sun B, Yang XG, Yao JM. Reinforcement of transparent poly(3-hydroxybutyrate-co-3-hydroxyvalerate) by incorporation of functionalized carbon

nanotubes as a novel bionanocomposite for food packaging. Compos Sci Technol 2014;94:96–104. https://doi.org/10.1016/J.COMPSCITECH.2014.01.018.
[109] Barkoula NM, Garkhail SK, Peijs T. Biodegradable composites based on flax/polyhydroxybutyrate and its copolymer with hydroxyvalerate. Ind Crops Prod 2010;31:34–42. https://doi.org/10.1016/j.indcrop.2009.08.005.
[110] Srubar W V., Pilla S, Wright ZC, Ryan CA, Greene JP, Frank CW, et al. Mechanisms and impact of fiber-matrix compatibilization techniques on the material characterization of PHBV/oak wood flour engineered biobased composites. Compos Sci Technol 2012;72:708–15. https://doi.org/10.1016/j.compscitech.2012.01.021.
[111] Luo S, Netravali AN. Mechanical and thermal properties of environment-friendly "green" composites made from pineapple leaf fibers and poly(hydroxybutyrate-co-valerate) resin. Polym Compos 1999;20:367–78. https://doi.org/10.1002/pc.10363.
[112] Keller A. Compounding and mechanical properties of biodegradable hemp fibre composites. Compos Sci Technol 2003;63:1307–16. https://doi.org/10.1016/S0266-3538(03)00102-7.
[113] Gwon JG, Cho HJ, Chun SJ, Lee S, Wu Q, Li MC, et al. Mechanical and thermal properties of toluene diisocyanate-modified cellulose nanocrystal nanocomposites using semi-crystalline poly(lactic acid) as a base matrix. RSC Adv 2016;6:73879–86. https://doi.org/10.1039/c6ra10993d.
[114] Weiss CK, Isogai A, Konwarh R. Nanocellulose: From Fundamentals to Advanced Applications. Frontiers in Chemistry | WwwFrontiersinOrg 2020;1:392. https://doi.org/10.3389/fchem.2020.00392.
[115] Patil T V., Patel DK, Dutta SD, Ganguly K, Santra TS, Lim KT. Nanocellulose, a versatile platform: From the delivery of active molecules to tissue engineering applications. Bioact Mater 2022;9:566. https://doi.org/10.1016/J.BIOACTMAT.2021.07.006.
[116] Zheng T, Clemons CM, Pilla S. Comparative Study of Direct Compounding, Coupling Agent-Aided and Initiator-Aided Reactive Extrusion to Prepare Cellulose Nanocrystal/PHBV (CNC/PHBV) Nanocomposite. ACS Sustain Chem Eng 2020;8:814–22. https://doi.org/10.1021/acssuschemeng.9b04867.
[117] Girouard NM, Xu S, Schueneman GT, Shofner ML, Meredith JC. Site-Selective Modification of Cellulose Nanocrystals with Isophorone Diisocyanate and Formation of Polyurethane-CNC Composites. ACS Appl Mater Interfaces 2016;8:1458–67. https://doi.org/10.1021/acsami.5b10723.
[118] Montanheiro TL do A, Montagna LS, Patrulea V, Jordan O, Borchard G, Ribas RG, et al. Enhanced water uptake of PHBV scaffolds with functionalized cellulose nanocrystals. Polym Test 2019;79:106079. https://doi.org/10.1016/j.polymertesting.2019.106079.
[119] Li K, Mcgrady D, Zhao X, Ker D, Tekinalp H, He X, et al. Surface-modified and oven-dried microfibrillated cellulose reinforced biocomposites: Cellulose network enabled high performance. Carbohydr Polym 2021;256:117525. https://doi.org/10.1016/j.carbpol.2020.117525.
[120] Gwon JG, Cho HJ, Chun SJ, Lee S, Wu Q, Lee SY. Physiochemical, optical and mechanical properties of poly(lactic acid) nanocomposites filled with toluene

diisocyanate grafted cellulose nanocrystals. RSC Adv 2016;6:9438–45. https://doi.org/10.1039/C5RA26337A.
[121] Yu HY, Qin ZY, Zhou Z. Cellulose nanocrystals as green fillers to improve crystallization and hydrophilic property of poly(3-hydroxybutyrate-co-3-hydroxyvalerate). Progress in Natural Science: Materials International 2011;21:478–84. https://doi.org/10.1016/S1002-0071(12)60086-0.
[122] Yu HY, Qin ZY, Liu L, Yang XG, Zhou Y, Yao JM. Comparison of the reinforcing effects for cellulose nanocrystals obtained by sulfuric and hydrochloric acid hydrolysis on the mechanical and thermal properties of bacterial polyester. Compos Sci Technol 2013;87:22–8. https://doi.org/10.1016/J.COMPSCITECH.2013.07.024.
[123] Yu HY, Qin ZY. Surface grafting of cellulose nanocrystals with poly(3-hydroxybutyrate-co- 3-hydroxyvalerate). Carbohydr Polym 2014;101:471–8. https://doi.org/10.1016/j.carbpol.2013.09.048.
[124] Javadi A, Srithep Y, Clemons CC, Turng LS, Gong S. Processing of poly(hydroxybutyrate-co-hydroxyvalerate)-based bionanocomposite foams using supercritical fluids. J Mater Res 2012;27:1506–17. https://doi.org/10.1557/jmr.2012.74.
[125] Wu Y, Jin Y, Huang J, Tian H, Weng Y. Toughening of poly(3-hydroxybutyrate-co-3-hydroxyvalerate) by phenyl terminated hyperbranched polyesters with higher thermal stability. J Appl Polym Sci 2022;139. https://doi.org/10.1002/app.51551.
[126] Li F, Yu HY, Li Y, Hussain Abdalkarim SY, Zhu J, Zhou Y. "Soft-rigid" synergistic reinforcement of PHBV composites with functionalized cellulose nanocrystals and amorphous recycled polycarbonate. Compos B Eng 2021;206:108542. https://doi.org/10.1016/j.compositesb.2020.108542.
[127] Javadi A, Srithep Y, Pilla S, Clemons CC, Gong S, Turng LS. Microcellular poly(hydroxybutyrate-co-hydroxyvalerate)-hyperbranched polymer-nanoclay nanocomposites. Polym Eng Sci 2011;51:1815–26. https://doi.org/10.1002/pen.21972.
[128] Pradeep SA, Shukla S, Brown N, Pilla S. Thermoplastics Foams. Lightweight and Sustainable Materials for Automotive Applications 2017:369–400. https://doi.org/10.1201/9781315152967-11.
[129] Tiwary P, Park CB, Kontopoulou M. Transition from microcellular to nanocellular PLA foams by controlling viscosity, branching and crystallization. Eur Polym J 2017;91:283–96. https://doi.org/10.1016/j.eurpolymj.2017.04.010.
[130] Srithep Y, Ellingham T, Peng J, Sabo R, Clemons C, Turng LS, et al. Melt compounding of poly (3-hydroxybutyrate-co-3-hydroxyvalerate)/ nanofibrillated cellulose nanocomposites. Polym Degrad Stab 2013;98:1439–49. https://doi.org/10.1016/j.polymdegradstab.2013.05.006.
[131] Xu JK, Zhang L, Li DL, Bao JB, Wang ZB. Foaming of Poly(3-hydroxybutyrate-co-3-hydroxyvalerate) with Supercritical Carbon Dioxide: Foaming Performance and Crystallization Behavior. ACS Omega 2020;5:9839–45. https://doi.org/10.1021/acsomega.9b04501.
[132] Lee JWS, Park CB. Use of nitrogen as a blowing agent for the production of fine-celled high-density polyethylene foams. Macromol Mater Eng 2006;291:1233–44. https://doi.org/10.1002/mame.200600203.

[133] Foster EJ, Moon RJ, Agarwal UP, Bortner MJ, Bras J, Camarero-Espinosa S, et al. Current characterization methods for cellulose nanomaterials. Chem Soc Rev 2018;47:2609–79. https://doi.org/10.1039/C6CS00895J.
[134] Barham PJ, Keller A, Otun EL, Holmes PA. Crystallization and morphology of a bacterial thermoplastic: poly-3-hydroxybutyrate. J Mater Sci 1984;19:2781–94. https://doi.org/10.1007/BF01026954.
[135] Abushammala H. A Simple Method for the Quantification of Free Isocyanates on the Surface of Cellulose Nanocrystals upon Carbamation using Toluene Diisocyanate. Surfaces 2019;2:444–54. https://doi.org/10.3390/surfaces2020032.
[136] Woei Chieng B, Huey Lee S, Azowa Ibrahim N, Yee Then Y, Ying Loo Y. Isolation and Characterization of Cellulose Nanocrystals from Oil Palm Mesocarp Fiber 2017. https://doi.org/10.3390/polym9080355.
[137] Abushammala H, Mao J. A Review of the Surface Modification of Cellulose. Molecules 2019;24:1–18.
[138] Yu HY, Yao JM. Reinforcing properties of bacterial polyester with different cellulose nanocrystals via modulating hydrogen bonds. Compos Sci Technol 2016;136:53–60. https://doi.org/10.1016/j.compscitech.2016.10.004.
[139] Coates J. Interpretation of Infrared Spectra, A Practical Approach. Encyclopedia of Analytical Chemistry, 2006. https://doi.org/10.1002/9780470027318.a5606.
[140] Che K, Lyu P, Wan F, Ma M. Investigations on aging behavior and mechanism of polyurea coating in marine atmosphere. Materials 2019;12. https://doi.org/10.3390/ma12213636.
[141] Ariffin H, Nishida H, Shirai Y, Hassan MA. Highly selective transformation of poly[(R)-3-hydroxybutyric acid] into trans-crotonic acid by catalytic thermal degradation. Polym Degrad Stab 2010;95:1375–81. https://doi.org/10.1016/J.POLYMDEGRADSTAB.2010.01.018.
[142] Panaitescu DM, Trusca R, Gabor AR, Nicolae CA, Casarica A. Biocomposite foams based on polyhydroxyalkanoate and nanocellulose: Morphological and thermo-mechanical characterization. Int J Biol Macromol 2020;164:1867–78. https://doi.org/10.1016/J.IJBIOMAC.2020.07.273.
[143] Gallego R, Arteaga JF, Valencia C, Franco JM. Rheology and thermal degradation of isocyanate-functionalized methyl cellulose-based oleogels. Carbohydr Polym 2013;98:152–60. https://doi.org/10.1016/J.CARBPOL.2013.04.104.
[144] Oyeoka HC, Ewulonu CM, Nwuzor IC, Obele CM, Nwabanne JT. Packaging and degradability properties of polyvinyl alcohol/gelatin nanocomposite films filled water hyacinth cellulose nanocrystals. Journal of Bioresources and Bioproducts 2021;6:168–85. https://doi.org/10.1016/J.JOBAB.2021.02.009.
[145] Sridhar V, Lee I, Chun HH, Park H. Graphene reinforced biodegradable poly(3-hydroxybutyrate-co-4-hydroxybutyrate) nano-composites. Express Polym Lett 2013;7:320–8. https://doi.org/10.3144/EXPRESSPOLYMLETT.2013.29.
[146] Jun D, Guomin Z, Mingzhu P, Leilei Z, Dagang L, Rui Z. Crystallization and mechanical properties of reinforced PHBV composites using melt compounding: Effect of CNCs and CNFs. Carbohydr Polym 2017;168:255–62. https://doi.org/10.1016/J.CARBPOL.2017.03.076.
[147] Kuang T, Li K, Chen B, Peng X. Poly (propylene carbonate)-based in situ nanofibrillar biocomposites with enhanced miscibility, dynamic mechanical

properties, rheological behavior and extrusion foaming ability. Compos B Eng 2017;123:112–23. https://doi.org/10.1016/J.COMPOSITESB.2017.05.015.
[148] Ten E, Bahr DF, Li B, Jiang L, Wolcott MP. Effects of cellulose nanowhiskers on mechanical, dielectric, and rheological properties of poly(3-hydroxybutyrate-co-3-hydroxyvalerate)/cellulose nanowhisker composites. Ind Eng Chem Res 2012;51:2941–51. https://doi.org/10.1021/IE2023367/ASSET/IMAGES/IE-2011-023367_M008.GIF.
[149] Geyer R, Jambeck JR, Law KL. Production, use, and fate of all plastics ever made. Sci Adv 2017;3:25–9. https://doi.org/10.1126/sciadv.1700782.
[150] Cywar RM, Rorrer NA, Hoyt CB, Beckham GT, Chen EYX. Bio-based polymers with performance-advantaged properties. Nat Rev Mat 2022;7:83–103. https://doi.org/10.1038/s41578-021-00363-3.
[151] Chung H, Washburn NR. Chemistry of lignin-based materials. Green Mater 2013;1:137–60. https://doi.org/10.1680/gmat.12.00009.
[152] Schutyser W, Renders T, Van Den Bosch S, Koelewijn SF, Beckham GT, Sels BF. Chemicals from lignin: An interplay of lignocellulose fractionation, depolymerisation, and upgrading. Chem Soc Rev 2018;47:852–908. https://doi.org/10.1039/c7cs00566k.
[153] Linger JG, Vardon DR, Guarnieri MT, Karp EM, Hunsinger GB, Franden MA, et al. Lignin valorization through integrated biological funneling and chemical catalysis. Proc Natl Acad Sci U S A 2014;111:12013–8. https://doi.org/10.1073/pnas.1410657111.
[154] Stone ML, Anderson EM, Meek KM, Reed M, Katahira R, Chen F, et al. Reductive Catalytic Fractionation of C-Lignin. ACS Sustain Chem Eng 2018;6:11211–8. https://doi.org/10.1021/acssuschemeng.8b02741.
[155] Pu Y, Jiang N, Ragauskas AJ. Ionic Liquid as a Green Solvent for Lignin. Journal of Wood Chemistry and Technology 2007;27:23–33. https://doi.org/10.1080/02773810701282330.
[156] Patwardhan PR, Brown RC, Shanks BH. Understanding the fast pyrolysis of lignin. ChemSusChem 2011;4:1629–36. https://doi.org/10.1002/cssc.201100133.
[157] Llevot A, Grau E, Carlotti S, Grelier S, Cramail H. From Lignin-derived Aromatic Compounds to Novel Biobased Polymers. Macromol Rapid Commun 2016;37:9–28. https://doi.org/10.1002/marc.201500474.
[158] Naseem A, Tabasum S, Mahmood K, Zuber M, Ali M, Noreen A. International Journal of Biological Macromolecules Lignin-derivatives based polymers , blends and composites : A review. Int J Biol Macromol 2016;93:296–313. https://doi.org/10.1016/j.ijbiomac.2016.08.030.
[159] Zhang Y, Wang H, Eberhardt TL, Gu Q, Pan H. Preparation of carboxylated lignin-based epoxy resin with excellent mechanical properties. Eur Polym J 2021;150. https://doi.org/10.1016/j.eurpolymj.2021.110389.
[160] Kühnel I, Podschun J, Saake B, Lehnen R. Synthesis of lignin polyols via oxyalkylation with propylene carbonate. Holzforschung 2015;69:531–8. https://doi.org/10.1515/hf-2014-0068.
[161] Kühnel I, Saake B, Lehnen R. Oxyalkylation of lignin with propylene carbonate: Influence of reaction parameters on the ensuing bio-based polyols. Ind Crops Prod 2017;101:75–83. https://doi.org/10.1016/j.indcrop.2017.03.002.

[162] Sternberg J, Sequerth O, Pilla S. Green chemistry design in polymers derived from lignin: review and perspective. Prog Polym Sci 2021;113. https://doi.org/10.1016/j.progpolymsci.2020.101344.
[163] Liu LY, Cho M, Sathitsuksanoh N, Chowdhury S, Renneckar S. Uniform Chemical Functionality of Technical Lignin Using Ethylene Carbonate for Hydroxyethylation and Subsequent Greener Esterification. ACS Sustain Chem Eng 2018;6:12251–60. https://doi.org/10.1021/ACSSUSCHEMENG.8B02649/ASSET/IMAGES/LARGE/SC-2018-02649X_0005.JPEG.
[164] Sternberg J, Pilla S. Chemical recycling of a lignin-based non-isocyanate polyurethane foam. Nature Sustainability 2023 6:3 2023;6:316–24. https://doi.org/10.1038/s41893-022-01022-3.
[165] Balakshin MY, Capanema EA, Chang HM. Recent Advances in the Isolation and Analysis of Lignins and Lignin–Carbohydrate Complexes. Characterization of Lignocellulosic Materials 2009:148–70. https://doi.org/10.1002/9781444305425.CH9.
[166] Bass GF, Epps TH. Recent developments towards performance-enhancing lignin-based polymers. Polym Chem 2021;12:4130–58. https://doi.org/10.1039/D1PY00694K.
[167] Mahajan JS, O'Dea RM, Norris JB, Korley LSTJ, Epps TH. Aromatics from Lignocellulosic Biomass: A Platform for High-Performance Thermosets. ACS Sustain Chem Eng 2020;8:15072–96. https://doi.org/10.1021/acssuschemeng.0c04817.
[168] Yagura K, Enomoto Y, Iwata T. Synthesis of fully divanillic acid-based aromatic polyamides and their thermal and mechanical properties. Polymer (Guildf) 2022;256:125222. https://doi.org/10.1016/J.POLYMER.2022.125222.
[169] Yagura K, Zhang Y, Enomoto Y, Iwata T. Synthesis of highly thermally stable divanillic acid-derived polyamides and their mechanical properties. Polymer (Guildf) 2021;228:123907. https://doi.org/10.1016/j.polymer.2021.123907.
[170] Feghali E, Van De Pas DJ, Parrott AJ, Torr KM. Biobased Epoxy Thermoset Polymers from Depolymerized Native Hardwood Lignin. ACS Macro Lett 2020;9:1155–60. https://doi.org/10.1021/ACSMACROLETT.0C00424/ASSET/IMAGES/LARGE/MZ0C00424_0003.JPEG.
[171] Van De Pas DJ, Torr KM. Biobased Epoxy Resins from Deconstructed Native Softwood Lignin. Biomacromolecules 2017;18:2640–8. https://doi.org/10.1021/ACS.BIOMAC.7B00767/ASSET/IMAGES/LARGE/BM-2017-007672_0008.JPEG.
[172] Quinsaat JEQ, Feghali E, Van De Pas DJ, Vendamme R, Torr KM. Preparation of Mechanically Robust Bio-Based Polyurethane Foams Using Depolymerized Native Lignin. ACS Appl Polym Mater 2021;3:5845–56. https://doi.org/10.1021/ACSAPM.1C01081/ASSET/IMAGES/LARGE/AP1C01081_0008.JPEG.
[173] Anderson EM, Stone ML, Katahira R, Reed M, Muchero W, Ramirez KJ, et al. Differences in S/G ratio in natural poplar variants do not predict catalytic depolymerization monomer yields. Nat Commun 2019;10:1–10. https://doi.org/10.1038/s41467-019-09986-1.

[174] Schäffner B, Schäffner F, Verevkin SP, Börner A. Organic carbonates as solvents in synthesis and catalysis. Chem Rev 2010;110:4554–81. https://doi.org/10.1021/CR900393D/ASSET/IMAGES/MEDIUM/CR-2009-00393D_0046.GIF.
[175] Higashi F, Goto M, Kakinoki H. Synthesis of polyamides by a new direct polycondensation reaction using triphenyl phosphite and lithium chloride. Journal of Polymer Science: Polymer Chemistry Edition 1980;18:1711–7. https://doi.org/10.1002/POL.1980.170180606.
[176] Chantawansri TL, Yeh IC, Hsieh AJ. Investigating the glass transition temperature at the atom-level in select model polyamides: A molecular dynamics study. Polymer (Guildf) 2015;81:50–61. https://doi.org/10.1016/J.POLYMER.2015.09.069.
[177] Levitt M, Perutz MF. Aromatic rings act as hydrogen bond acceptors. J Mol Biol 1988;201:751–4. https://doi.org/10.1016/0022-2836(88)90471-8.
[178] Upton BM, Kasko AM. Biodegradable Aromatic−Aliphatic Poly(ester−amides) from Monolignol-Based Ester Dimers 2018. https://doi.org/10.1021/acssuschemeng.7b03784.
[179] Artiaga R, García A. Fundamentals of DMA 2005.
[180] Dynamic Mechanical Analysis Basic Theory & Applications Training TA Instruments-Waters LLC RSA-G2 DMA 850 DMA 3200 n.d.
[181] Menard KP, Menard NR. Dynamic Mechanical Analysis. CRC Press; 2020. https://doi.org/10.1201/9780429190308.
[182] Kühnel I, Saake B, Lehnen R. Comparison of different cyclic organic carbonates in the oxyalkylation of various types of lignin. React Funct Polym 2017;120:83–91. https://doi.org/10.1016/J.REACTFUNCTPOLYM.2017.09.011.
[183] Scarica C, Suriano R, Levi M, Turri S, Griffini G. Lignin Functionalized with Succinic Anhydride as Building Block for Biobased Thermosetting Polyester Coatings. ACS Sustain Chem Eng 2018;6:3392–401. https://doi.org/10.1021/ACSSUSCHEMENG.7B03583/ASSET/IMAGES/LARGE/SC-2017-03583R_0005.JPEG.